

American Aires Inc.  
Research and Development department  
**美國 Aires 公司研發部門**

REPORT 報告

R&D: Calculation of the strength and intensity of the electromagnetic field in the interaction of electromagnetic radiation at a frequency of 28 GHz (WiFi 5G) with an Aires C20S5G resonator (microprocessor), which is used in the Aires Crystal (2019 model)

**研發：計算在頻率為 28 GHz (WiFi 5G) 的電磁輻射與用於 Aires Crystal (2019 年型號) 的 Aires C20S5G 共振器（微處理器）相互作用時電磁場之強度與強度分佈**

Project manager: 專案經理：  
I. Serov

Responsible researcher: 負責研究者：  
K. Korshunov

Researchers: 研究人員：  
I. Soltovskaya  
T. Shamko

Consultants: 顧問：  
Prof. Dr. of Technical Sciences A. Kopyltsov

**技術科學博士 A. Kopyltsov**

Prof. Department of Physics Dr. A. Jukna

**物理系教授、博士 A. Jukna**

TABLE OF CONTENTS 目錄

Introduction. 引言。

Physical model. 物理模型。

Mathematical model. 數學模型。

Calculation parameters. 計算參數。

Algorithm for the calculation.

**計算演算法。**

Results and discussion. 結果與討論。

Conclusion. 結論。

Bibliography. 參考書目。

Appendix 1. Topology of the resonator (microprocessor) Aires C20S5G.

**附錄一。諧振器（微處理器）Aires C20S5G 的拓撲結構。**

Appendix 2. Hardware and software.

**附錄二。硬體與軟體。**

Appendix 3. Animation. **附錄 3。動畫片。**

INTRODUCTION 引言

In connection with the prospect of the use of next-generation 5G mobile networks ( 6 GHz and 28 GHz ), a fundamentally new microprocessor was developed. It can effectively differentiate the harmful effects of 5G networks' electromagnetic radiation on humans. 28 GHz EM radiation is in the frequency range approved in the US and Europe for 5G networks.

針對下一代 5G 行動網路（6 GHz 與 28 GHz）之使用前景，開發出一款全新的微處理器。它有效區分 5G 網路電磁輻射對人體的有害影響。28 GHz 電磁輻射屬於美國與歐洲核准用於 5G 網路的頻率範圍。

To simulate the processes occurring in the interaction of Aires resonators (microprocessors), which are manufactured using Micro-Electro-Mechanical Systems (MEMS) technology, with electromagnetic radiation, physical models of such interaction, as well as algorithms and computer programs based on them, were developed.

為了模擬以微機電系統（MEMS）技術製造的 Aires 共振器（微處理器）與電磁輻射相互作用時所發生的過程，開發了此類相互作用的物理模型，以及基於這些模型的演算法與電腦程式。

This software development was necessary, because the various software packages available on the market generally consider interactions in the context of classical physics. However, a number of studies have shown that the processes taking place in this case can only be explained by accounting for the counter wave interaction on the surface of the resonator and the numerous derivative resonances that result from these processes. Existing packages do not take these factors into consideration.

此軟體開發是必要的，因為市面上各種軟體套件通常僅在經典物理的框架下考量交互作用。然而，多項研究顯示，此情形下所發生的過程只能透過考慮在共振器表面上的反向波交互作用以及由此產生的大量衍生諧振來解釋。現有的套件並未將這些因素納入考量。

The following experiment with the Aires resonator (microprocessor) showed the possibility of using it in a new class of devices used in medicine, energy conservation, and protecting humans from man-made electromagnetic radiation.

對 Aires 共振器（微處理器）進行的下列實驗顯示，將其應用於一類新型裝置是可行的，此類裝置可用於醫療、節能以及保護人類免受人為電磁輻射的傷害。

This report discusses the interaction of electromagnetic radiation at a frequency of 28 GHz with an Aires resonator (microprocessor) with the C2oS5G topology (Appendix 1), which is used in the Aires Crystal (2019 model). The calculations were made on hardware using software (Appendix 2).

本報告討論了頻率為 28 GHz 的電磁輻射與具有 C2oS5G 拓撲（附錄 1）的 Aires 共振器（微處理器）之間的相互作用，該共振器用於 Aires Crystal（2019 型號）。計算是在硬體上使用軟體進行的（附錄 2）。

In order to most closely approximate specific technical problems: the design of the simulated element, the range of electromagnetic radiation corresponding to the frequency of a WiFi router ( 28 GHz ) and other modern mobile communication devices, the following physical model was considered in the simulation.

為了最貼近特定技術問題：模擬元件的設計、對應 WiFi 路由器（28 GHz）及其他現代行動通訊裝置頻率範圍的電磁輻射，本次模擬中考慮了以下物理模型。

1. PHYSICAL MODEL 1. 物理模型

Aires resonators (microprocessors) are self-affine circular diffraction gratings with a fractalization factor of 2 and a number of fractalization axes corresponding to the number of the topological circuit (from 8 to 32 ).

Aires 諧振器（微處理器）是自相似的圓形繞射光柵，具有 2 的分形化因子，且分形化軸的數量對應於拓撲電路的編號（從 8 到 32）。

Characteristics of the Aires C2oS5G microprocessor

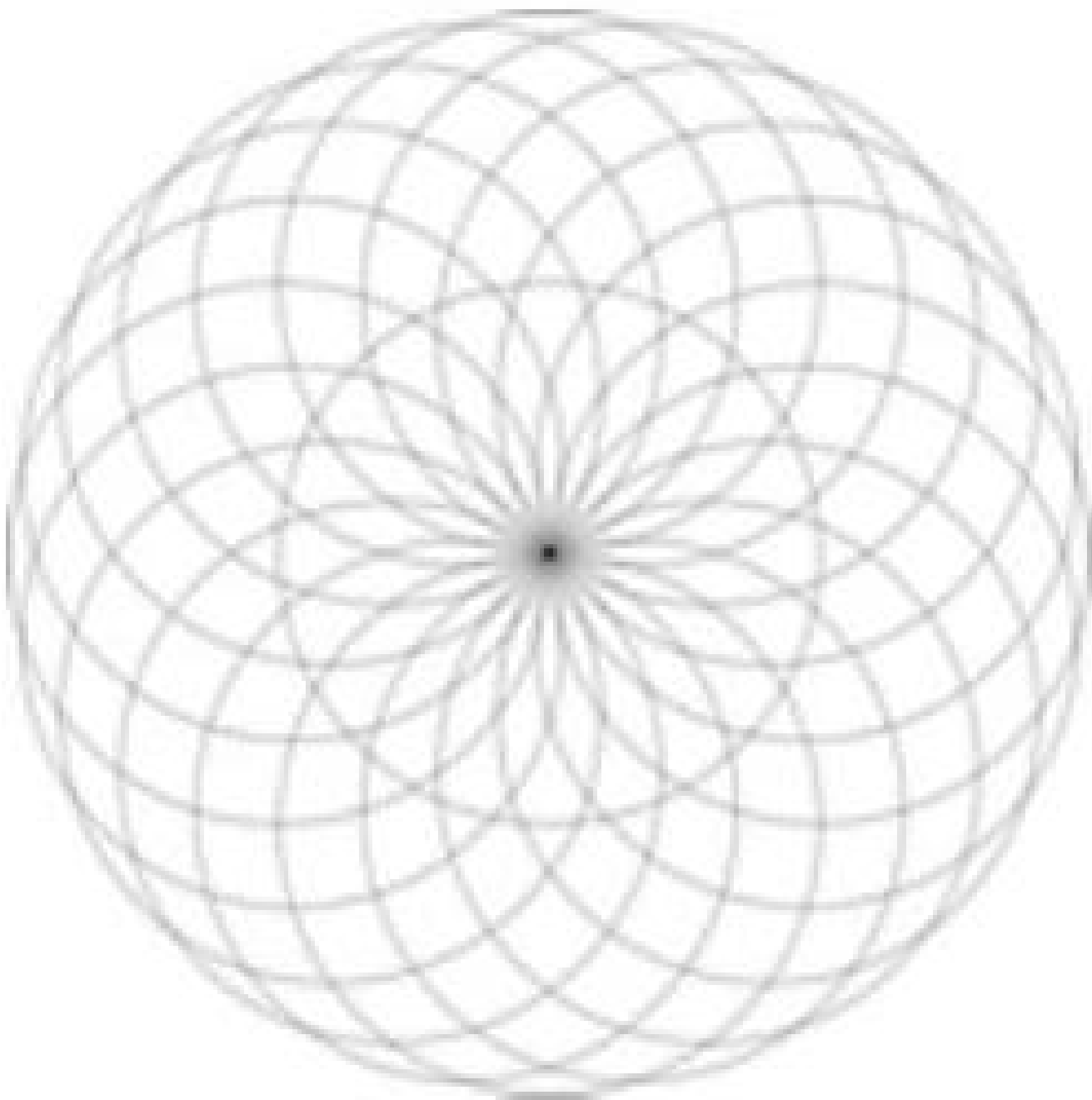
Aires C2oS5G 微處理器的特性

Number of fractalization axes: 20

分形化軸數：20

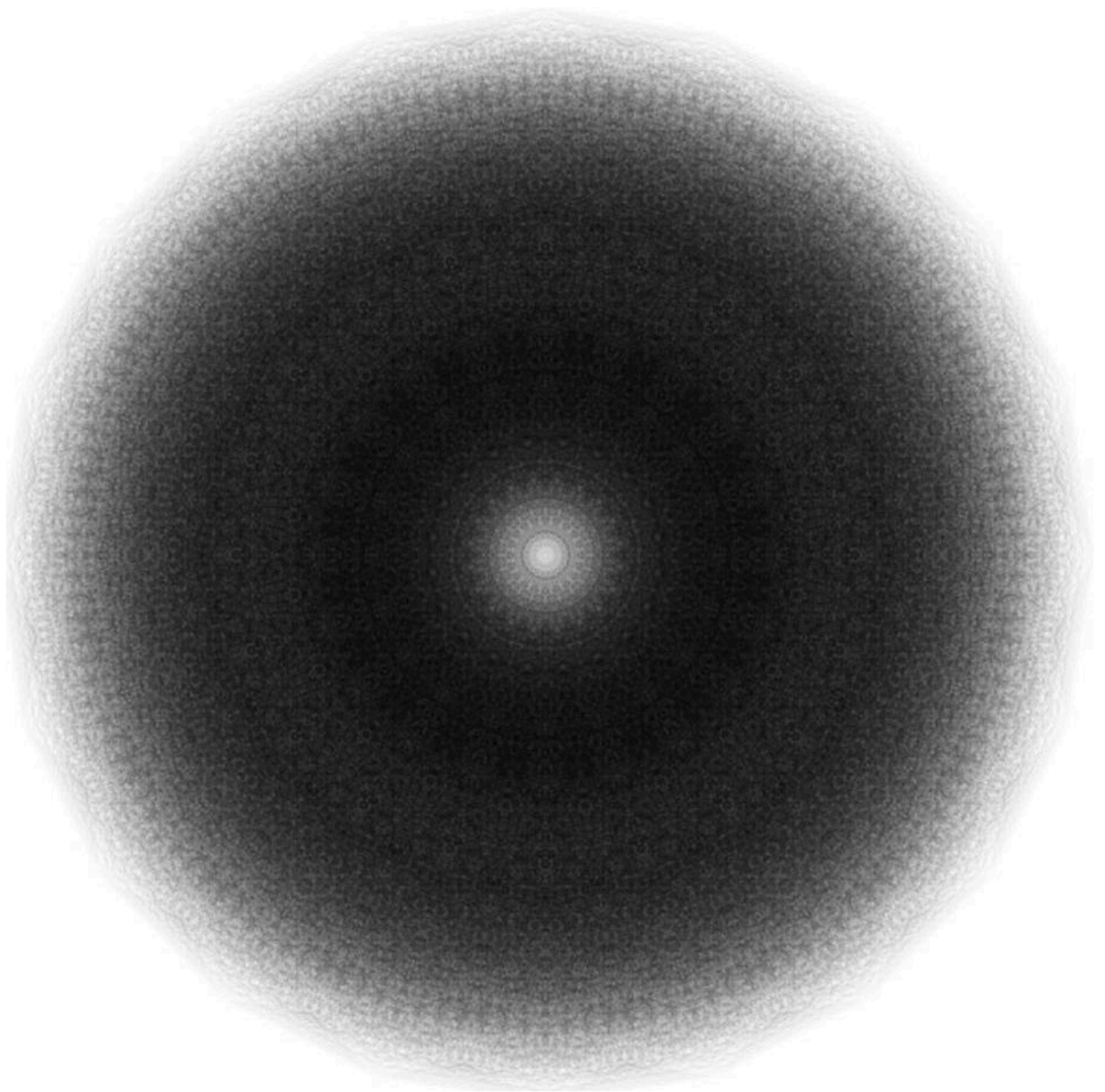
5 steps (levels) of fractalization:

5 個分形化步驟（層級）：



\captionsetup{labelformat=empty}  
Figure 1: Basic module,  $D = 0.925 * 10^{-3}$  m

圖 1：基本模組， $D = 0.925 * 10^{-3}$  m



\captionsetup{labelformat=empty}  
Figure 2: General view of the circuit,  $D = 7.4 * 10^{-3} \text{ m}$

圖 2：電路總體視圖， $D = 7.4 * 10^{-3} \text{ m}$

Fig. 1. Topology of the Aires C2oS5G resonator (microprocessor), which is a flat cut through the center of the self-affine hypersphere

圖 1. Aires C2oS5G 駐振器（微處理器）的拓樸結構，為自相似超球體中心的平面切面

Number of rings (slit resonators): 4084101  
Slit parameters (width / height):  $0.2 * 10^{-6} \text{ m} / 0.6 * 10^{-6} \text{ m}$ .

狹縫參數（寬 / 高）： $0.2 * 10^{-6} \text{ m} / 0.6 * 10^{-6} \text{ m}$  .

The radial axes of fractalization are arranged in pairs strictly by the diameters of the circuit, thereby forming a counter resonant interaction corresponding to the formula (1), which describes the equilibrium principle of a hypercomplex interaction system based on the deepest spatial-temporal amplitude-frequency harmonization of wave fronts, which



correlates with the stationary Schrödinger equation for a quantum system (superposition principle), which defines the arising wave function as a vector sum of all wave functions of elements of the system.

The phenomenon occurs in the case of wave interactions of opposite functions, when the agents participating in the interaction are maximally harmonized among themselves in terms of amplitudes, frequencies, phases (focal point of the system) and the spatial interaction diagram.

This process makes it possible to locally accumulate, register, and use the highest potential.

When presenting the base unit of the system as  $B_0(x_1, x_2, \dots, x_n)$ , and the functions of the fractal mapping (for example, scaling and shifting) through  $F(B_0)$ , the iterative process of the formation of the fractal structure, which reflects the hierarchical principle of the symmetry of the structural organization of the counter interaction system, can generally be described as:

$$F_k(B_0) = \sum_{i=1}^{k-1} F_i(B_0)$$

The level of contradictions within any arbitrarily taken hypercomplex system, if obtaining a functionally active and maximally stable design is required, should tend to zero, defining the principle of universal multi-level coordination (coherence).

The statement applies to both a three-dimensional "X, Y, Z" system, and to a self-affine hyperspherical form that has an infinite number of structural components of different dimensionality that tend to absolute symmetry, according to Noether's theorem.

$$\sum_{i=1}^n \frac{\partial L}{\partial \dot{x}_i} \delta_i = \text{constant}$$

For the case of the reciprocal vector interaction, the equation can be written as:

對於互易向量交互的情況，方程可寫為：

$$X^n + Y^n + Z^n + \dots + N^n \rightarrow 0$$

This expression implies the simultaneous solution of all equations comprising the given spatial hypercomplex. The number of these equations is equal to the number of interactions that define the process under consideration.

此表達式意味著需同步求解構成該空間超複數的所有方程。這些方程的個數等同於定義所考察過程的交互數量。

In the case of interaction of system-wide hyper-objects of different fractal dimensions with respect to a common "zero" center (a phase transition to the next quantum fractalization zone), the equation takes the form:

$$\sum_{k=1}^n X^k + \sum_{k=1}^n Y^k + \sum_{k=1}^n Z^k + \dots + \sum_{k=1}^n N^k \rightarrow 0$$

where o is the focal point (center point) of the circuit, which is a singularity zone where the potential density tends to infinity and its amplitude approaches zero.

其中 o 為電路的焦點（中心點），此處為一個奇異點區域，勢密度趨於無限而其振幅接近於零。

The resonators' topological circuits have the properties of the self-affine analogs of fractal antennas [4-6]. A fractal antenna is an antenna whose active part has the form of a self-similar curve or any other figure similarly divided or consisting of similar segments.

The specific properties of the Aires resonator (microprocessor) as a fractal ring diffraction grating are broadband interaction with external electromagnetic radiation and a high degree of signal amplification due to the summation of currents and the resulting iterative resonance effect as an integral superposition of subresonant processes. Thus, the resonator may be considered an analog of a fractal antenna.

**Aires 共振器（微處理器）**作為分形環繞衍射光柵的特殊性質包括與外來電磁輻射的寬頻互作用，以及由於電流的相加與由此產生的迭代共振效應，作為次共振過程整體疊加而導致的高信號放大程度。因此，該共振器可被視為分形天線的類比。

The total length of the rings forming the resonator's self-affine matrix as a conductor is composed of the sums of circumferences that form its topological circuit and determines the lower boundary of the frequency range of the

resonator’s interaction with incident electromagnetic radiation (Table 1).

構成共振器自相似矩陣的環之總長度，作為導體由構成其拓撲回路的圓周總和組成，並決定共振器與入射電磁輻射互作用頻率範圍的下界（表 1）。

Table 1: Table 1. 表 1：表 1。  
\\captionsetup{labelformat=empty}

Microprocessor model	C2o85G
Ring diameter	462.5*10 <sup>-6</sup> m
Number of rings 環數量	4084101
Length of the conductor (antenna) 導體（天線）長度	5931.14 m
Lower threshold of interaction frequency 互作用頻率下限	50.58*10 <sup>3</sup> Hz

Because the Gabor-Denisyuk hologram theory says that any wave superposition has the same properties as the regular system that generated it, we can consider the wave superposition (hologram) arising from the material regular circuit (Fig. 1) as the first derivative, which has the corresponding properties of the base grating that gave rise to it.

In turn, the first derivative, which is a regular system of maxima and minima of the field strength, acts as a secondary diffraction grating and, by interacting with the radiation incident on the system, forms the next level of a similar wave superposition, which can be called the second derivative. In the same way, the system of maxima and minima of the field strength of the second derivative generates a new superposition or a third derivative, which always represents deep interference, i.e. it includes the interaction of waves, half-waves, and quarter-waves, thus forming a three-level system of resonant interconnections.

In the end, the result of this process as the fourth derivative is the process of harmonizing the different types of external radiation through the structure of the second derivative giving rise to this process (superposition from a regular fractal base), which in this case acts as a universal filter initiating a direct and inverse Fourier transform. Thus, there is a differentiation of the initial wave flow ( 28 GHz ) into eigen harmonics with the subsequent formation of a matrix of electromagnetic superpositions that is spatially-temporally harmonized with respect to the amplitudes and frequencies.

The Aires resonator (microprocessor) is a type-n monocrystalline silicon substrate with a crystallographic plane of 100 (Miller index), with dimensions of 7.6 \* 10<sup>-3</sup> m × 7.6 \* 10<sup>-3</sup> m and a thickness of 0.5 \* 10<sup>-3</sup> m, whose surface has an absolutely symmetric fractal system of annular slits with a rectangular cross section with a width of 0.2 \* 10<sup>-6</sup> m and depth 0.6\*10<sup>-6</sup> m, forming a regular selfaffine structure that obeys the laws of self-similarity and scale invariance (Appendix 1).

The incident radiation’s interaction with the silicon substrate produces polarization and a surface wave.

入射輻射與矽基板的相互作用會產生極化和表面波。

According to modern scientific knowledge, everything is electromagnetic in nature. A material’s crystal lattice is a certain ordered, periodic field structure. Erwin Schrödinger, an Austrian Nobel laureate and one of the founders of quantum physics, was the first to express this idea. In turn, any material structure creates a periodic electromagnetic field (superposition) and is maintained by this same field. Moreover, the perfect structures initiate a maximally coherent response that is strictly systematized in terms of amplitudes, frequencies, phases, and the interaction diagram.

根據現代科學的認知，一切本質上都是電磁性的。物質的晶格是一種有序的、週期性的場結構。奧地利諾貝爾獎得主暨量子物理創始人之一的厄溫·薛丁格（Erwin Schrödinger）最早表達了這一觀點。反過來，任何物質結構都會產生一個週期性的電磁場（疊加），並由這同一個場來維持。而且，完美的結構會引發一種最大程度相干的回應，該回應在幅度、頻率、相位以及作用圖譜上都具有嚴格的系統性。

Hence we can draw the following conclusion: since the silicon substrate has an appropriate crystal lattice whose domains can be regarded as a regular system of conductors representing a fractal complex, the total length of such domains will determine the wavelength and the frequency range of the object’s response to external electromagnetic radiation. Of course, this phenomenon requires additional research.

因此我們可以得出如下結論：由於矽基材具有相應的晶格，其晶區可被視為一個由導體組成的規則系統，代表一個分形複合體，這些晶區的總長度將決定該物體對外來電磁輻射的響應波長與頻率範圍。當然，這一現象還需進一步研究。

When the resonator interacts with the radiation incident on its surface, a surface wave appears and is reflected from the surface with absorption in the slits, which leads to a redistribution of the characteristics of the electromagnetic field. The resonator's slit structure can be considered as a regular topology of the surface of a self-affine silicon wafer (substrate). Both the distribution of the electric field strength above the resonator surface and the distribution of the field's energy flux density (intensity) were modeled.

## 2. MATHEMATICAL MODEL

In the modeling, it is assumed that the charge carriers are concentrated in the slits. Thus, the potential density and, accordingly, the calculated intensity within the slit will depend on its geometry. In our case, since the slit width  $b = 0.2 \cdot 10^{-6}$  m and the slit depth  $glu = 0.6 \cdot 10^{-6}$  m, when an electromagnetic wave passes through the resonator surface during interaction with a slit, we consider two variants of wave propagation: movement over the slit (path  $l_1$ ) and motion along the slit (path  $l_2$ ):

在建模中，假定電荷載子集中於裂縫中。因此，電位密度，從而裂縫內的計算強度，將取決於其幾何形狀。在我們的情況中，由於裂縫寬度  $b = 0.2 \cdot 10^{-6}$  m 及裂縫深度  $glu = 0.6 \cdot 10^{-6}$  m，當電磁波在與裂縫相互作用時通過共振器表面，我們考慮兩種波的傳播變體：越過裂縫的運動（路徑  $l_1$ ）與沿裂縫的運動（路徑  $l_2$ ）。

$$l_1 = b = 0.2 \cdot 10^{-6} \text{ m},$$

$$l_2 = b + 2 \cdot glu = 7b = 7 \cdot 0.2 = 1.4 \cdot 10^{-6} \text{ m}.$$

Thus, the path difference is:

因此，路徑差為：

$$\Delta l = l_2 - l_1 = 7b - b = 6b = 6 \cdot 0.2 = 1.2 \cdot 10^{-6} \text{ m}.$$

If the initial strength on the surface of the resonator has a gain of 1, then it can reach a maximum of 6 in the slits. To calculate the strength, a gain coefficient  $K_l = 2 \div 6$  depending on the density of the resonator's topological circuit, i.e. in low density areas of the circuit  $K_l = 2$ , in high density zones  $K_l = 6$ .

$$E_0 \setminus = E_0 \cdot K_l,$$

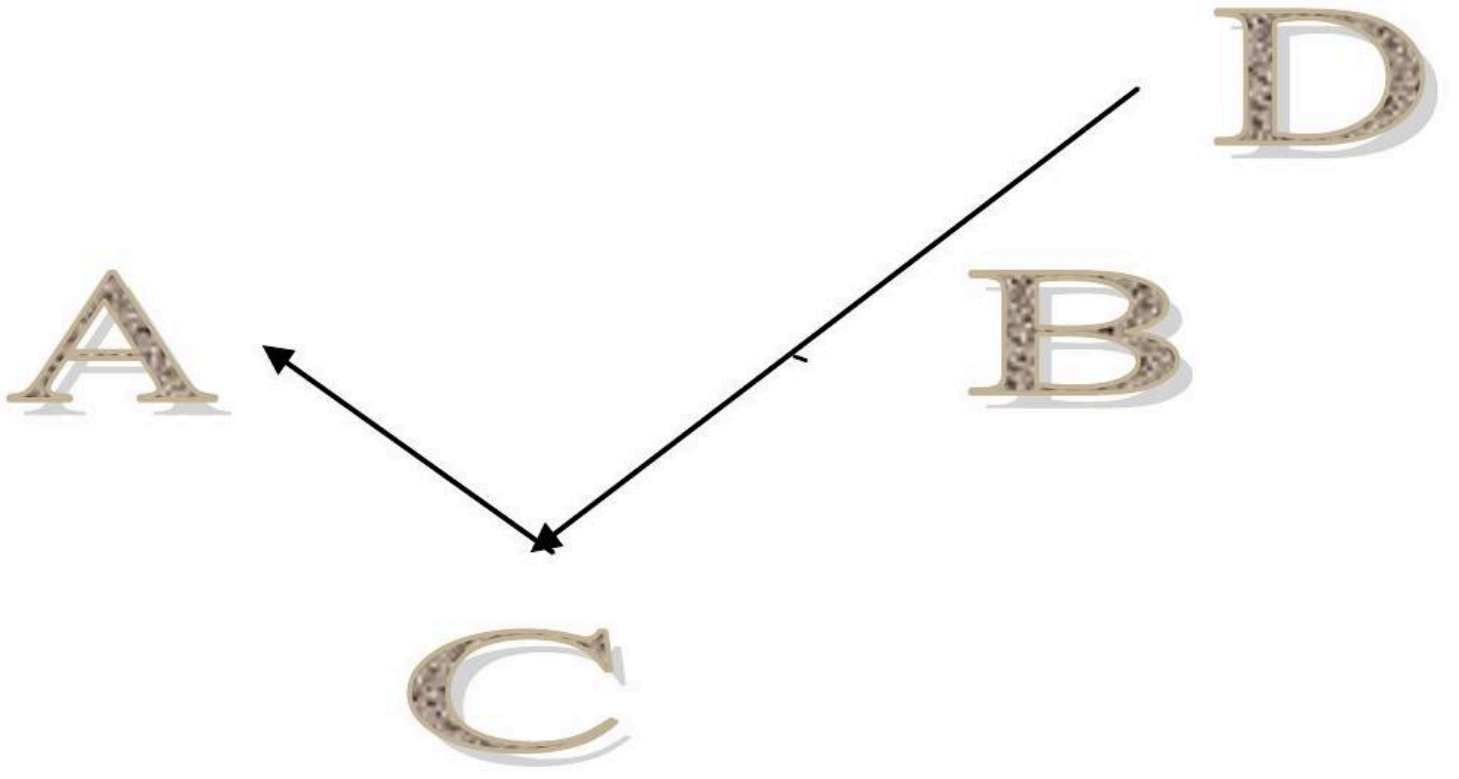
where  $E_0$  is the initial (background) electric field strength,  $E_0$  is the electric field strength, including the gain.

其中  $E_0$  為初始（背景）電場強度， $E_0$  為包含增益的電場強度。

To describe the current calculation model, it is assumed that the source radiation falls on the AIRES resonator (microprocessor) uniformly from all sides. Thus, we have a radiation source in the form of a hemisphere with radius  $R$ , which is significantly greater than the diameter of the resonator.

為了描述當前的計算模型，假定來源輻射從各個方向均勻落在 AIRES 共振器（微處理器）上。因此，我們有一個半徑為  $R$  的半球形輻射源，其半徑遠大於共振器的直徑。

The radiation is distributed along the DCA trajectory (Fig. 2). Point D is on the sphere with radius  $R$ . Point C is on the resonator wafer. Point A is on the receiver (the space above the resonator wafer), and the strength of electric field  $E$  is determined at this point. Point C has 2 possible locations - in the slit and on the surface of the resonator. If point C is on the surface, then the incident radiation at point C is reflected (the angle of incidence is equal to the angle of reflection). If point C is in the slit, then the incident radiation at point is absorbed.



\captionsetup{labelformat=empty}  
Figure 3: Fig. 2. Trajectory of the incident radiation DCA. ↻

The smooth surface of the resonator is broken into square cells with side  $h$  and point C successively (in a cycle) traverses every node in this twodimensional grating. The receiver is the three-dimensional space around the resonator, divided into cubic cells with side  $h$  and point A successively (in a cycle) traverses every node in this three-dimensional grating. At each time  $t$ , the coordinates of points A (on the receiver) and C (on the resonator) are assumed to be known.

共振器的光滑表面被分割成邊長為  $h$  的方形格子，點 C 按順序（循環地）遍歷此二維格狀結構中的每一個節點。接收器是環繞共振器的三維空間，劃分為邊長為  $h$  的立方格子，點 A 按順序（循環地）遍歷此三維格狀結構中的每一個節點。在每一時刻  $t$ ，假定已知接收器上點 A 及共振器上點 C 的坐標。

We assume that we know the intensity of the incident radiation  $E_0$  and the frequency of the radiation  $\omega$  at point D (radiation source).

我們假設已知在點 D（輻射源）處的入射輻射強度  $E_0$  與輻射頻率  $\omega$ 。

We need to find: the strength of electric field  $E$  at point A (receiver).

我們需要求得：在點 A（接收器）處的電場強度  $E$ 。

If the coordinates of points A  $(x_A, y_A, z_A)$  and C  $(x_C, y_C, z_C)$  are known, then the coordinates of point B  $(x_B, y_B, z_B)$  can be determined using the following formulas:

若已知點 A  $(x_A, y_A, z_A)$  與 C  $(x_C, y_C, z_C)$  的座標，則可使用以下公式來確定點 B  $(x_B, y_B, z_B)$  的座標：

$$x_B = 2x_C - x_A$$

$$y_B = 2y_C - y_A$$

$$z_B = z_A$$

Point B is symmetric to point A in the DCA plane relative to the normal to the resonator's surface at point C.

點 B 與點 A 在 DCA 平面內相對於點 C 處共振器表面法線呈對稱。

Equation for the line segment BC :

線段 BC 的方程式：

$$\frac{x - x_C}{x_B - x_C} = \frac{y - y_C}{y_B - y_C} = \frac{z - z_C}{z_B - z_C}$$

Equation for the line segment AC : 

$$\frac{x - x_C}{x_A - x_C} = \frac{y - y_C}{y_A - y_C} = \frac{z - z_C}{z_A - z_C}$$

Distance between points A and C :

**點 A 與點 C 之間的距離 :**

$$L1 = \sqrt{(x_A - x_C)^2 + (y_A - y_C)^2 + (z_A - z_C)^2}$$

Coordinates of vector CA: 

$$x_{CA} = x_A - x_C$$

$$y_{CA} = y_A - y_C$$

$$z_{CA} = z_A - z_C$$

Direction cosines of vector CA 

$$\cos(CA_x) = x_{CA}/L1$$

$$\cos(CA_y) = y_{CA}/L1$$

$$\cos(CA_z) = z_{CA}/L1$$

Equation for sphere with radius  $R$  with center at  $(x_0, y_0, z_0)$  (coordinates of the center of the resonator):

**以中心為  $(x_0, y_0, z_0)$  、半徑為  $R$  的球之方程（共振器中心的座標） :**

$$(x - x_0)^2 + (y - y_0)^2 + (z - z_0)^2 = R^2$$

The coordinates of point D  $(x_D, y_D, z_D)$ , the intersection of line segment BC and the sphere with radius  $R$ , are determined from the following system of equations:

**點 D  $(x_D, y_D, z_D)$ （線段 BC 與半徑為  $R$  的球的交點）的座標由下列方程組決定 :**

$$\frac{x - x_C}{x_B - x_C} = \frac{y - y_C}{y_B - y_C} = \frac{z - z_C}{z_B - z_C}$$

$$(x - x_0)^2 + (y - y_0)^2 + (z - z_0)^2 = R^2$$

Distance between points C and D :

**點 C 與點 D 之間的距離 :**

$$L2 = \sqrt{(x_D - x_C)^2 + (y_D - y_C)^2 + (z_D - z_C)^2}$$

The length of the DCA is equal

**DCA 的長度等於**

$$L = L1 + L2$$

The sphere with radius  $R$  radiates a monochromatic wave with frequency  $\omega$  and wavelength  $\lambda = \frac{2\pi V_C}{\omega}$  and speed of light  $V_C$  .

**半徑為  $R$  的球體發射頻率為  $\omega$  、波長為  $\lambda = \frac{2\pi V_C}{\omega}$  、光速為  $V_C$  的單色波。**

At time  $t$ , the strength of the electric field (created by the DCA beam) at point A is equal to

**在時間  $t$  , 位於 A 點的電場強度（由 DCA 光束產生）等於**

$$E = E_0 \cos \left( \omega \left( t - \frac{L}{V_C} \right) \right)$$

where  $E_0$  is strength of the incident radiation.

其中  $E_0$  為入射輻射的強度。

The projections of  $E$  (created by beam DCA) on axes X, Y and Z at point A at time  $t$  are equal to:

由光束 DCA 在時間  $t$  於點 A 在軸 X, Y 與 Z 上所產生的  $E$  的投影等於：

$$E_x = E \cos(CA_x), E_y = E \cos(CA_y), E_z = E \cos(CA_z)$$

The projections of  $E$  (created by the resonator) on axes X, Y and Z at point A at time  $t$  are equal to the amount of the projections of  $E$  (created by

由諧振器在時間  $t$  於點 A 在軸 X, Y 與 Z 上所產生的  $E$  的投影等於由  $E$  (由

beams DCA), where point C passes each node of the square cells into which the resonator is divided:

光束 DCA 所產生) 之投影的總和，其中點 C 通過諧振器分割成的方格單元的每一個節點：

$$E_x^{\text{resonator}} = \sum_{\text{resonator}} E_x, E_y^{\text{resonator}} = \sum_{\text{resonator}} E_y, E_z^{\text{resonator}} = \sum_{\text{resonator}} E_z.$$

The strength of electric field  $E$  (created by the resonator) at point A at time  $t$  is equal to

在時間  $t$  於點 A 由諧振器所產生之電場強度  $E$  等於

$$E_A^{\text{resonator}} = \sqrt{(E_x^{\text{resonator}})^2 + (E_y^{\text{resonator}})^2 + (E_z^{\text{resonator}})^2}$$

Given time change  $\Delta t$ , we can calculate the strength of electric field  $E$  at any point of the receiver at any point in time.

給定時間變化  $\Delta t$ ，我們可以計算接收器任意點在任意時間的電場強度  $E$ 。

The results are output as 4-dimensional matrices (the coordinates of the point at which  $E$  is calculated, and the time):

結果以四維矩陣輸出（計算  $E$  的點的座標，以及時間）：

$$E_A^{\text{resonator}}, E_x^{\text{resonator}}, E_y^{\text{resonator}}, E_z^{\text{resonator}}.$$

To following formula is used to account for diffraction:

為了考慮繞射，使用下列公式：

$$\frac{I_\beta}{I_0} = \frac{\sin^2\left(\frac{\pi b}{\lambda} \sin \beta\right)}{\left(\frac{\pi b}{\lambda} \sin \beta\right)^2}$$

where  $I_\beta$  is the intensity of waves propagating at an angle  $\beta$ ,  $I_0$  is the intensity of waves propagating at an angle  $\beta = 0$ ,  $b$  is the width of the slit,  $\beta$  is the angle,  $\lambda$  is the wavelength. Because the intensity of the wave is proportional to the square of the amplitude,

其中  $I_\beta$  為以角度  $\beta$ ,  $I_0$  傳播的波的強度， $\beta = 0$ ,  $b$  為以角度  $\beta$  傳播的波的強度， $\lambda$  為狹縫的寬度，{5} 為角度，{6} 為波長。由於波的強度與振幅的平方成正比，

$$\frac{I_\beta}{I_0} = \frac{E_\beta^2}{E_0^2} = \frac{\sin^2\left(\frac{\pi b}{\lambda} \sin \beta\right)}{\left(\frac{\pi b}{\lambda} \sin \beta\right)^2},$$
$$E_\beta = E_0 \frac{\sin\left(\frac{\pi b}{\lambda} \sin \beta\right)}{\frac{\pi b}{\lambda} \sin \beta}.$$

Thus, in the end in general we have a vector  $E$  :

因此，最終總體上我們得到一個向量  $E$ ：

$$E = E_{otr} + E_{dif},$$



where  $E_{\text{otr}}$  is due to reflection,  $E_{\text{diffr}}$  is due to diffraction (in the case of narrow slits).

### 3. CALCULATION PARAMETERS

#### 3. 計算參數

The topological circuit of the Aires resonator (microprocessor) is considered a self-affine annular diffraction grating made in the form of slits with the following dimensions:  $0.2 * 10^{-6} \text{ m} \times 0.6 * 10^{-6} \text{ m}$  ( $0.2\mu \text{ m} \times 0.6\mu \text{ m}$ , width and depth).

**Aires 共振器（微處理器）的拓撲電路被視為一個自相似環狀衍射光柵，製成狹縫的形式，具有以下尺寸：**  
 $0.2 * 10^{-6} \text{ m} \times 0.6 * 10^{-6} \text{ m}$  ( $0.2\mu \text{ m} \times 0.6\mu \text{ m}$ ，寬度和深度)。

Resonator dimensions:  $7.6 * 10^{-3} \text{ m} \times 7.6 * 10^{-3} \text{ m} \times 0.5 * 10^{-3} \text{ m}$  ( $7.6 \text{ mm} \times 7.6 \text{ mm} \times 0.5 \text{ mm}$ ).

The resonator interacts with the radiation of the WiFi-source (router) in the form of a large-diameter hemisphere (the diameter of a sphere larger than the wafer dimensions). The distance from the source to the resonator is 10 m.

The surface of the resonator reflects radiation (absorption is not considered), but the slits absorb (reflection in the slits is not considered).

**諧振器表面會反射輻射（不考慮吸收），但裂縫會吸收（不考慮裂縫內的反射）。**

Parameters of the incident radiation:

**入射輻射的參數：**

strength  $E_0 = 50 \text{ V/m}$ ; (manufacturer data)

frequency  $\omega = 2.4\text{GHz}$ , 頻率  $\omega = 2.4\text{GHz}$ 。

field strength  $E \sim \omega^2 = (28\text{GHz})^2 \sim 784 \text{ (V/m)}$ ;

flux density  $I \sim \omega^4 = (28\text{GHz})^4 \sim 61.47 \text{ (W/m}^2\text{)}$ .

The resonator surface is divided into square cells in increments of  $h = 24 * 10^{-6} \text{ m}$  ( $24\mu \text{ m}$ ). The resulting radiation is calculated in the space above the resonator, at the nodes of a cubic lattice with step  $h$ .

The electromagnetic radiation interacts with the resonator for  $t = 1 \text{ s}$ .

**電磁輻射與諧振器相互作用的時間為  $t = 1 \text{ s}$ 。**

The time spent on the calculations is 120 machine-hours.

**計算所花費的時間為 120 機器小時。**

### 4. ALGORITHM FOR THE CALCULATION

#### 4. 計算演算法

The algorithm for the calculation generally looks like this:

**計算演算法大致如下：**

The Aires resonator (microprocessor) with the C2oS5G topology (Appendix 1) is taken to be at the center of the cubic matrix. To reduce the required resources, the calculations are performed for the upper half of the cubic matrix with a determination of the estimated electric field strength at each node of the lattice, and then the results are mirrored to the lower half. As a result, we obtain a matrix that is symmetric with respect to the plane on which the resonator is placed, and a cubic matrix of the results of the initial strength calculation E - “Derivative 1”.

At this stage, an additional gradation of the lattice is introduced to the cubic matrix of the 1st derivative with a 2-fold decrease in the spatial increment  $h$  ( $24 * 10^{-6} \text{ m} \rightarrow 12 * 10^{-6} \text{ m}$ ), which makes it possible to identify internal structural relationships. The results are stored in the strength matrix E “Derivative 2”.

At this stage, an additional gradation of the lattice is introduced to the cubic matrix of the 1st derivative with a 2-fold decrease in the spatial increment  $h$  ( $12 * 10^{-6} \text{ m} \rightarrow 6 * 10^{-6} \text{ m}$ ) again, which makes it possible to identify internal structural relationships. The results are stored in the strength matrix E “Derivative 3”.

Next, “Derivative 3” with a center at the origin (center of the resonator) and radius  $R_1$  (radius of the topological circuit) is projected by distance  $R_1$  along 102 radii (the number of axes of fractalization of the spatial resonator whose 2D profile is the specimen with the C2oS5G topology under study), and at the nodes of the lattice we sum the results (103 spheres). In the end, we obtain calculated values of the superposition, fractalized along 102 axes, that determines the spatial distribution of the electric field strength, geometrically comprising a sphere of radius  $R_2 = 2 * R_1$ , which we denote as “Derivative 4”.

## 5. RESULTS AND DISCUSSION

### 5. 結果與討論

For the most complete and adequate understanding of the processes, the model was initially considered and calculations of the incident electromagnetic radiation's interaction with the resonator surface and the diffraction response that was induced on it. The resonator is a ring with a radius of  $462.5 \times 10^{-6}$  m with given slit parameters (depth  $-0.2 \times 10^{-6}$  m, width  $-0.6 \times 10^{-6}$  m), which is the basic symmetric structural element of the topology of the Aires C2oS5G resonator (microprocessor). The results are shown in Fig. 3.

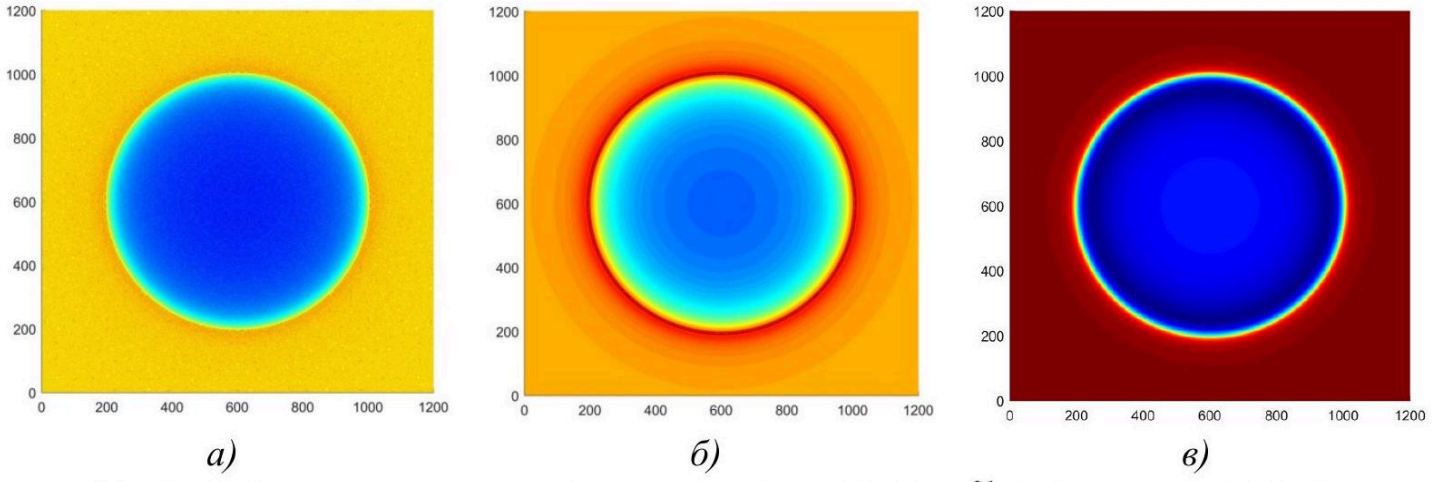


Figure 4: Fig. 3. Diffraction response on the 1s ring: a)  $\nu = 2.4 \times 10^{21}$  Hz (gamma radiation), b)  $\nu = 5.5 \times 10^{15}$  Hz (green spectrum of the Sun), c)  $\nu = 2.4 \times 10^9$  Hz (Wi-Fi radiation)

As can be seen from Fig. 3, the interaction produces an annular spectrogram. In the case of gamma radiation, a regular fractal structure is formed inside the ring as a result of integral interaction of waves (superposition), and outside - analogous to natural objects (Fig. 4).

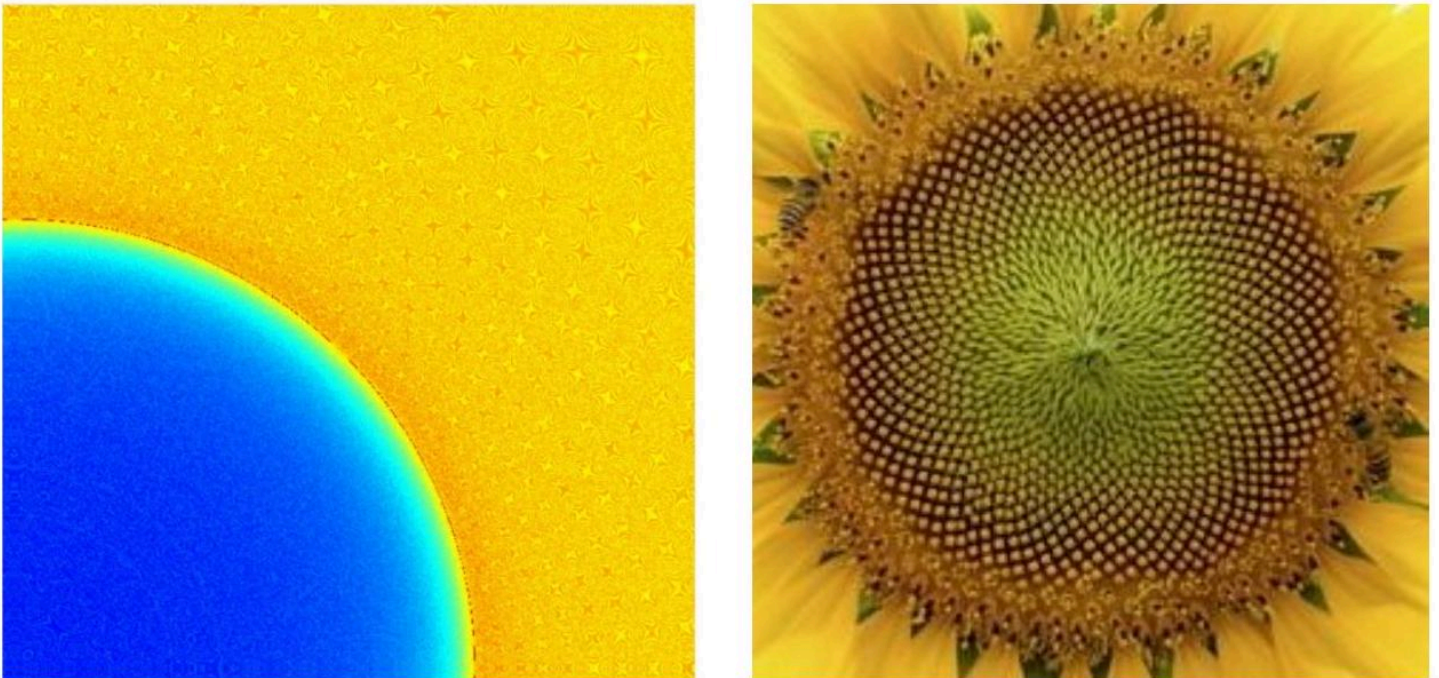


Figure 5: Fig. 4. Fragment of the image from Fig. 3a) and a photo of a sunflower

The ring shape has a specific feature in that, since its surface is curved and has a focal point located at the center of the ring, an impulse striking the interior begins to move along a trajectory that intersects this point and, upon reaching the opposite surface of the ring, is reflected and returned, again intersecting the focal point.


Thus, the appearance of an absolutely adequate counter function begins resonant self-generation of the potential with the transformation of the wave spectrum in the form of "Fresnel rings".

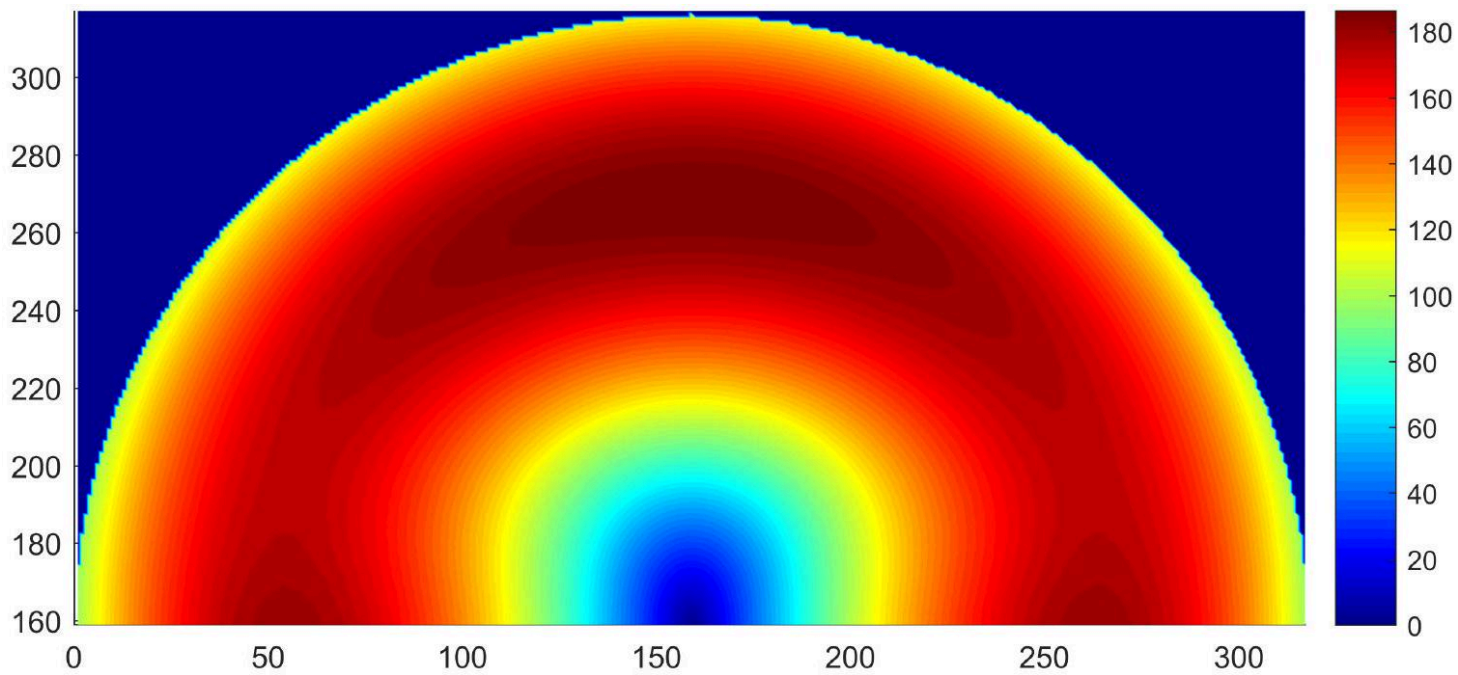


In turn, electrons begin to move along the annular slit, which provokes the formation of an opposing wave stream, and when their phases coincide, a standing wave is formed.

反過來，電子開始沿著環形縫隙運動，這促使一股相反的波流形成，當它們的相位重合時，便形成駐波。

The 1st step of the calculation is “Derivative 1”. 

In accordance with the algorithm, the calculations were performed in 4 stages. The result of the first stage is a matrix of the strength of the electric field  $E$  over the resonator (Fig. 5). 



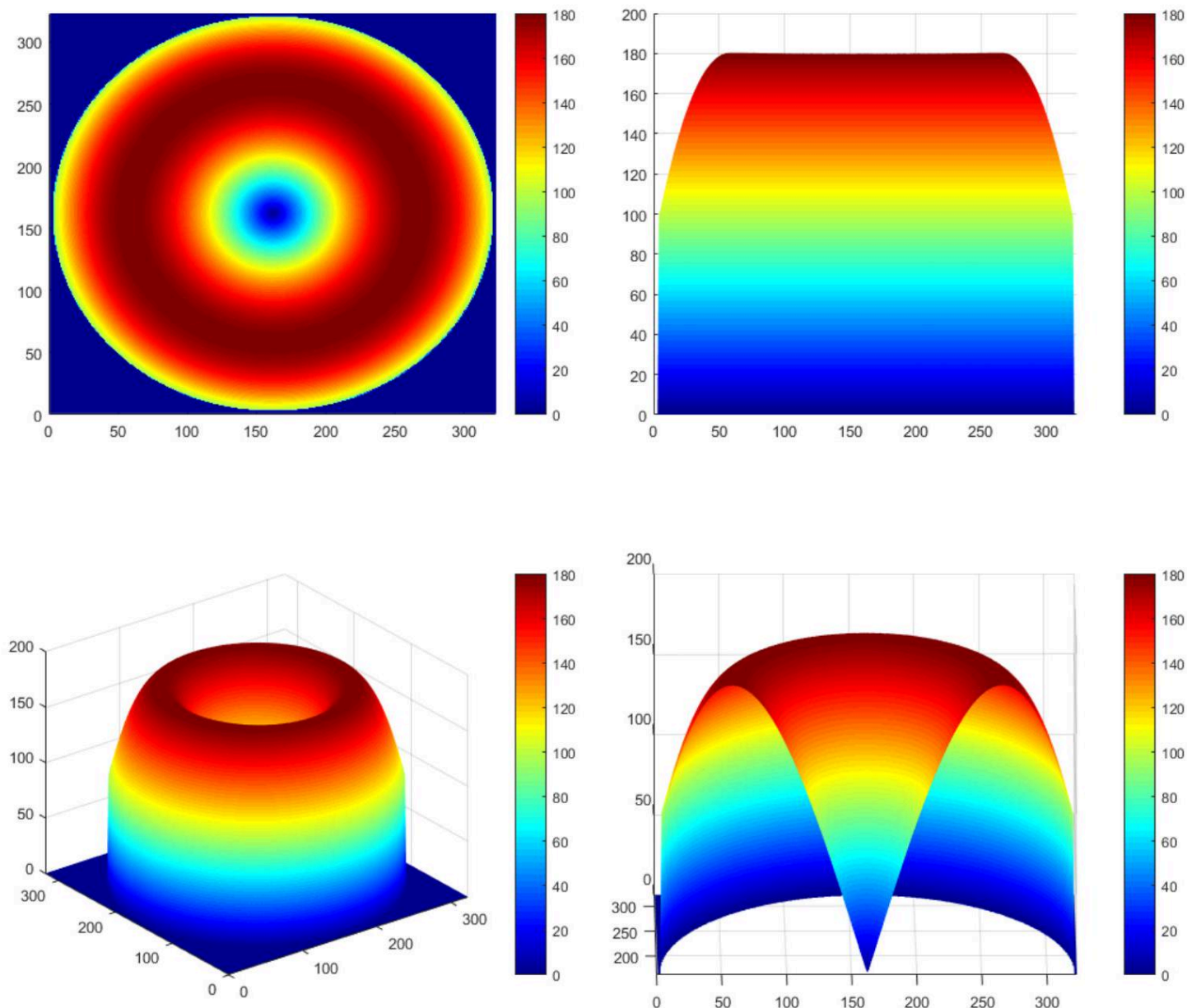
\captionsetup{labelformat=empty}

Figure 6: Fig.5. The distribution of the field strength  $E(V/m)$  over the resonator in the 1st stage of calculations (vertical section through the center)

圖 6：圖 5。第一階段計算中共振器上場強  $E(V/m)$  的分佈（通過中心的垂直剖面）

The distribution of the electric field strength occurs symmetrically from the center of the resonator, where  $E = 1.37( V/m)$ , to the edges, where the strength reaches  $E = 180.37( V/m)$  (Fig. 6).

電場強度的分佈從共振器中心處的  $E = 1.37( V/m)$  對稱地向邊緣延伸，在邊緣處場強達到  $E = 180.37( V/m)$ （圖 6）。



\captionsetup{labelformat=empty}

Figure 7: Fig. 6. The distribution of the field strength  $E$  over the resonator in the 1st stage of calculations (horizontal section at a height of  $h = 24 * 10^{-6}$  m), range  $E = 1.37 \div 180.37$ ( V/m)

圖 7：圖 6。第一階段計算中共振器上場強  $E$  的分佈（高度為  $h = 24 * 10^{-6}$  m 的水平剖面），範圍  $E = 1.37 \div 180.37$ ( V/m)

The 2nd step of the calculation is “Derivative 2”.

第二步計算為「導數 2」。

After introducing an additional gradation to the existing lattice, a cubic matrix of field strength was obtained with an increase in the maximum strength amplitude to a value of  $E = 252.18$ ( V/m) relative to the initial matrix obtained at stage 1 of the calculation (Fig. 7-9).

在對既有格點引入額外細分後，得到了一個場強的立方矩陣，最大強度振幅相較於計算第 1 階段所得的初始矩陣增加至  $E = 252.18$ ( V/m)（圖 7-9）。



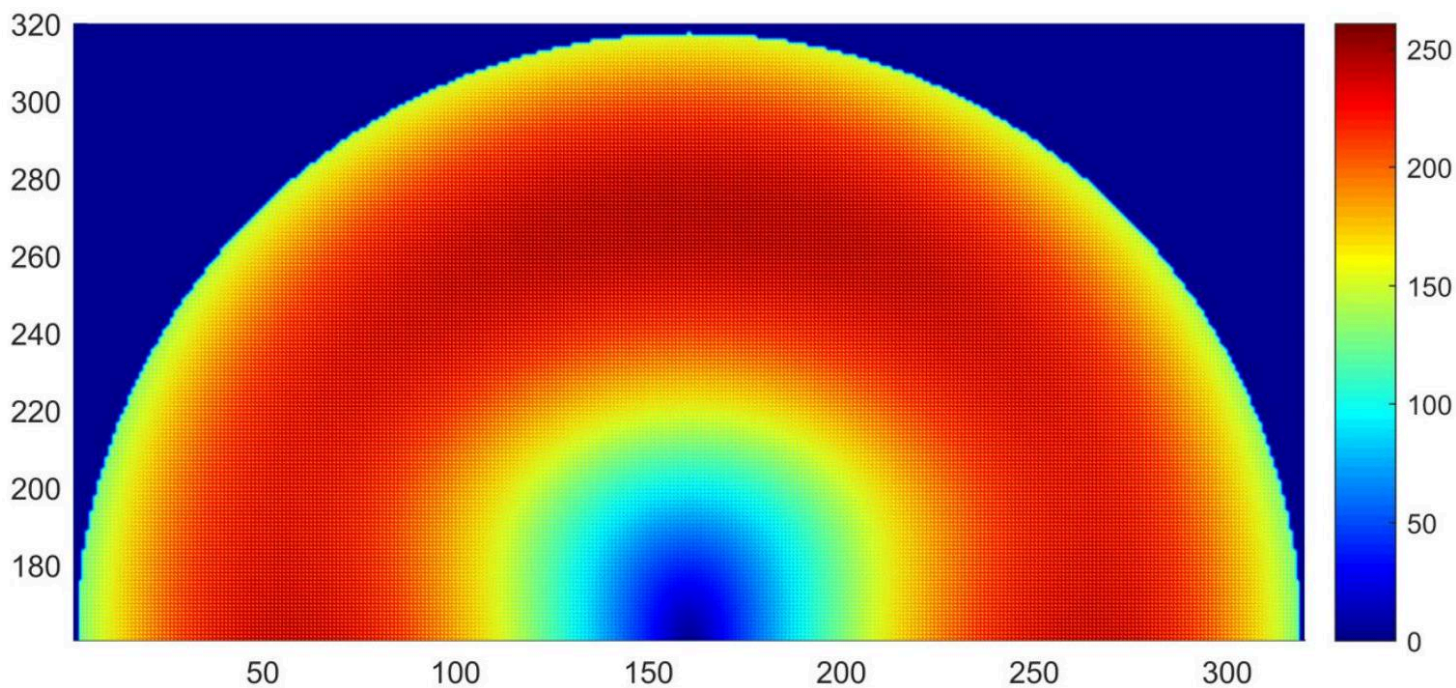


Figure 8: Fig.7. The distribution of the field strength  $E(V/m)$  over the resonator in the 2nd stage of calculations (vertical section through the center)

圖 8：圖 7。第 2 階段計算中共振器上場強  $E(V/m)$  的分佈（通過中心的垂直截面）

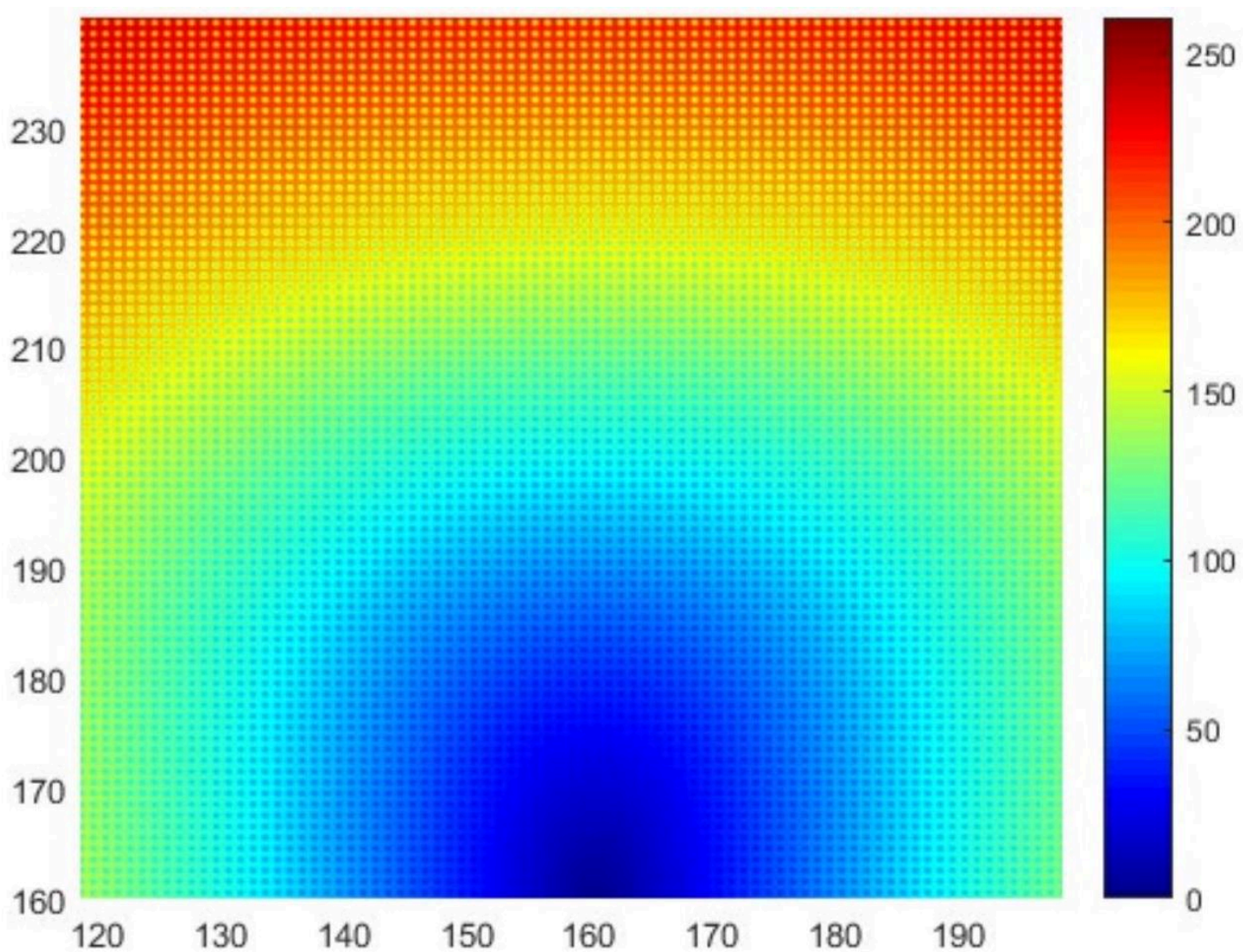
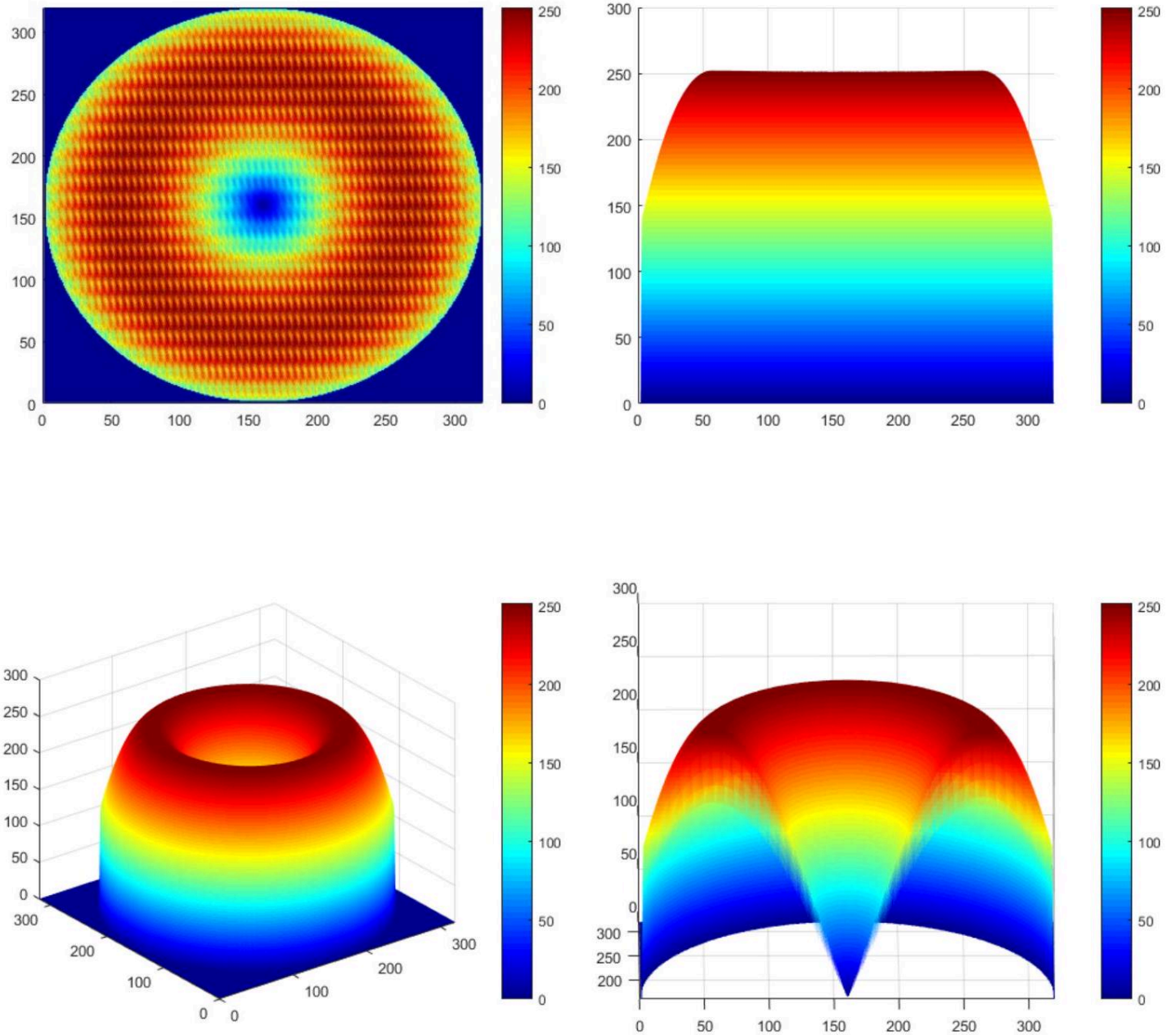




Figure 9: Fig. 8. Fragment of the image presented in Fig. 7, at a scale of 4:1

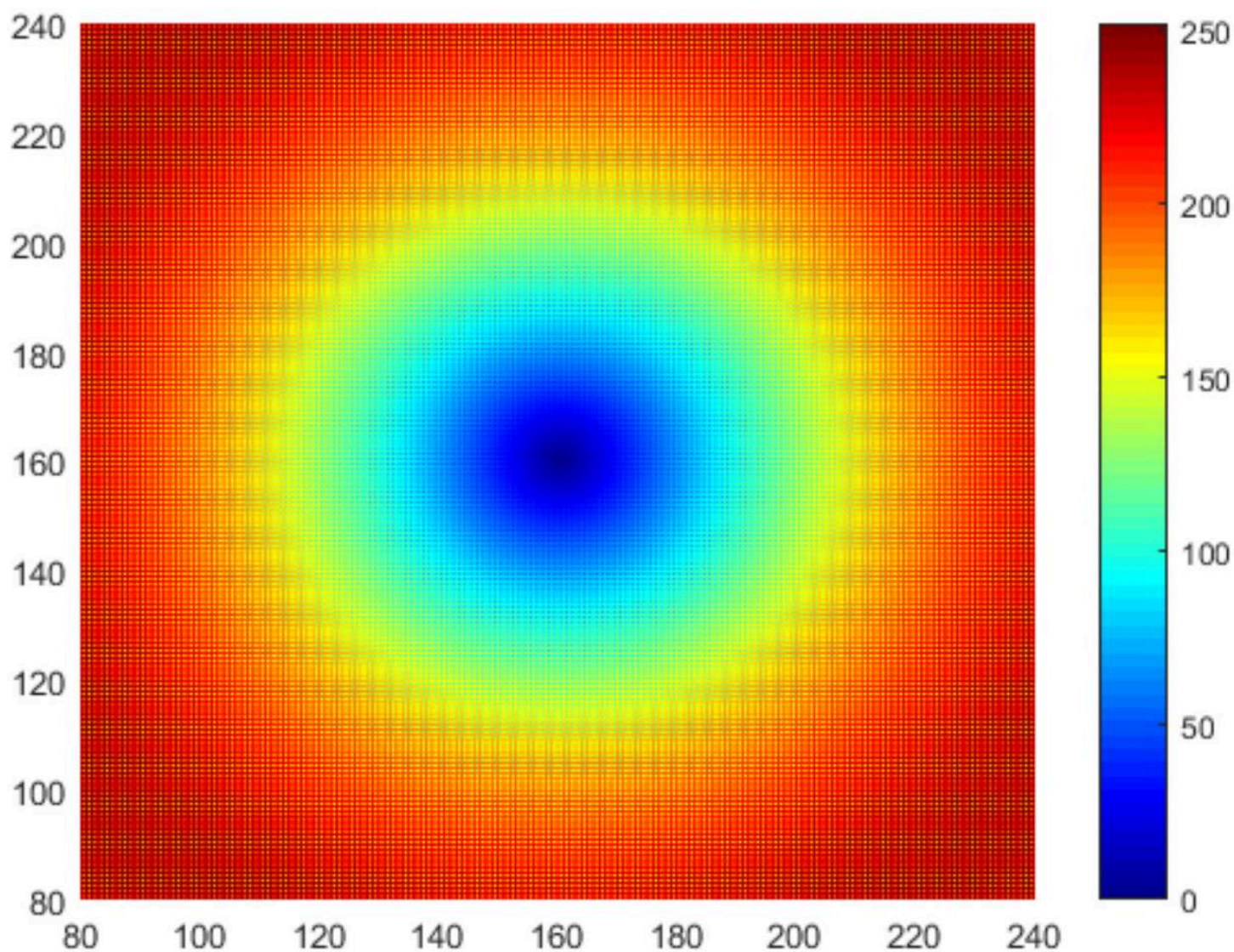


\captionsetup{labelformat=empty}

Figure 10: Fig. 9. The distribution of the field strength  $E$  over the resonator in the 2nd stage of calculations (horizontal section at a height of  $h = 24 * 10^{-6}$  m ), range  $E = 1.37 \div 252.18$  ( V/m )

The appearance of a regular system of strength maxima and minima (Fig. 7-17) reflects the new functional nature of the electromagnetic field's emerging raster lattice over the Aires C20S5G resonator (microprocessor), which begins working as a differentiating system.

For better visualization of the resulting effect, Figures 10-17 show enlarged fragments of the image of the distribution of the strength  $E$  shown in Fig. 9.



\captionsetup{labelformat=empty}  
 Figure 11: Fig. 10. Fragment of the image presented in Fig. 9, at a scale of 2 : 1

圖 11：圖 10。圖 9 中所示影像的片段，比例為 2 : 1



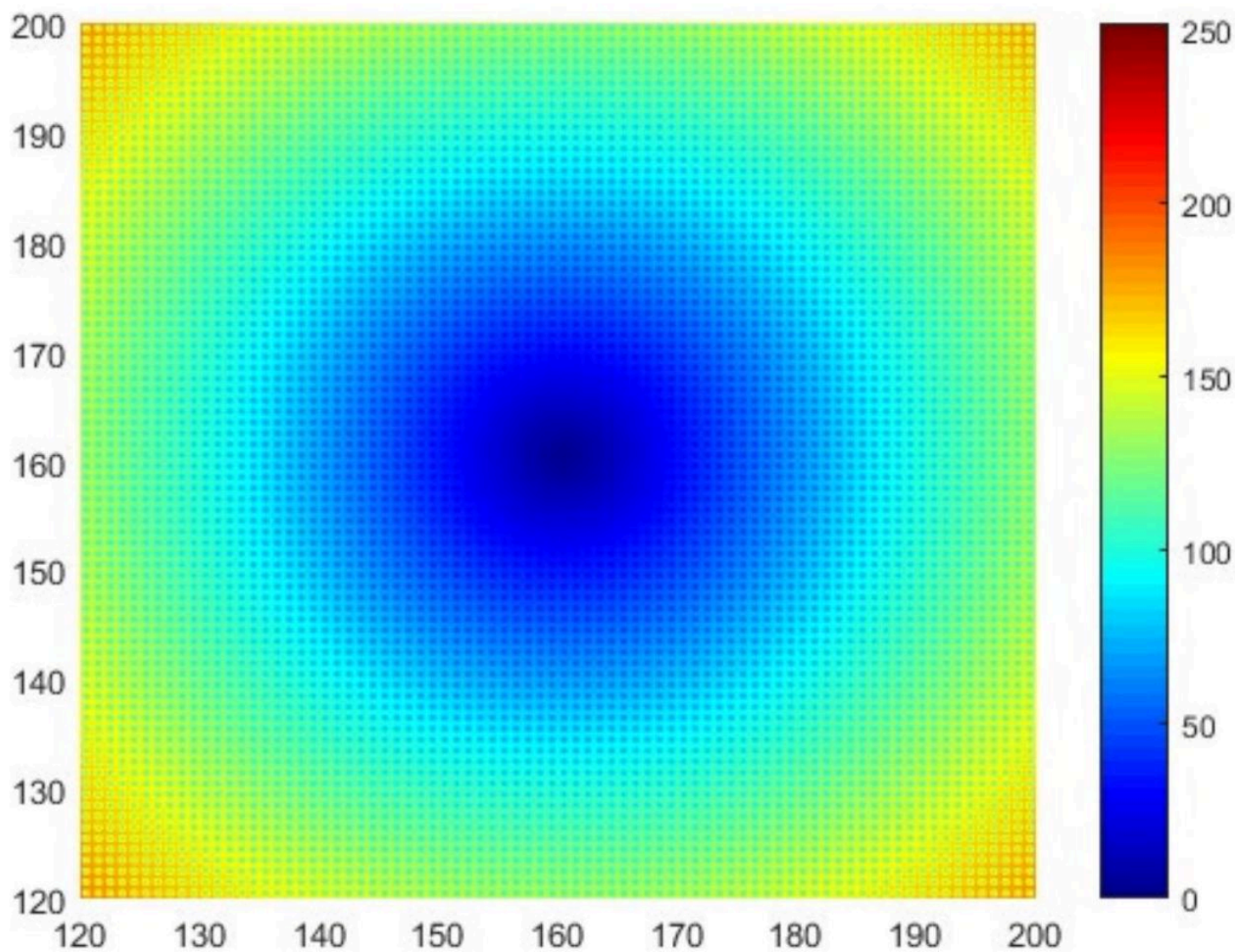


Figure 12: Fig. 11. Fragment of the image presented in Fig. 9, at a scale of 4 : 1

圖 12：圖 11。圖 9 中所示影像的片段，比例為 4 : 1

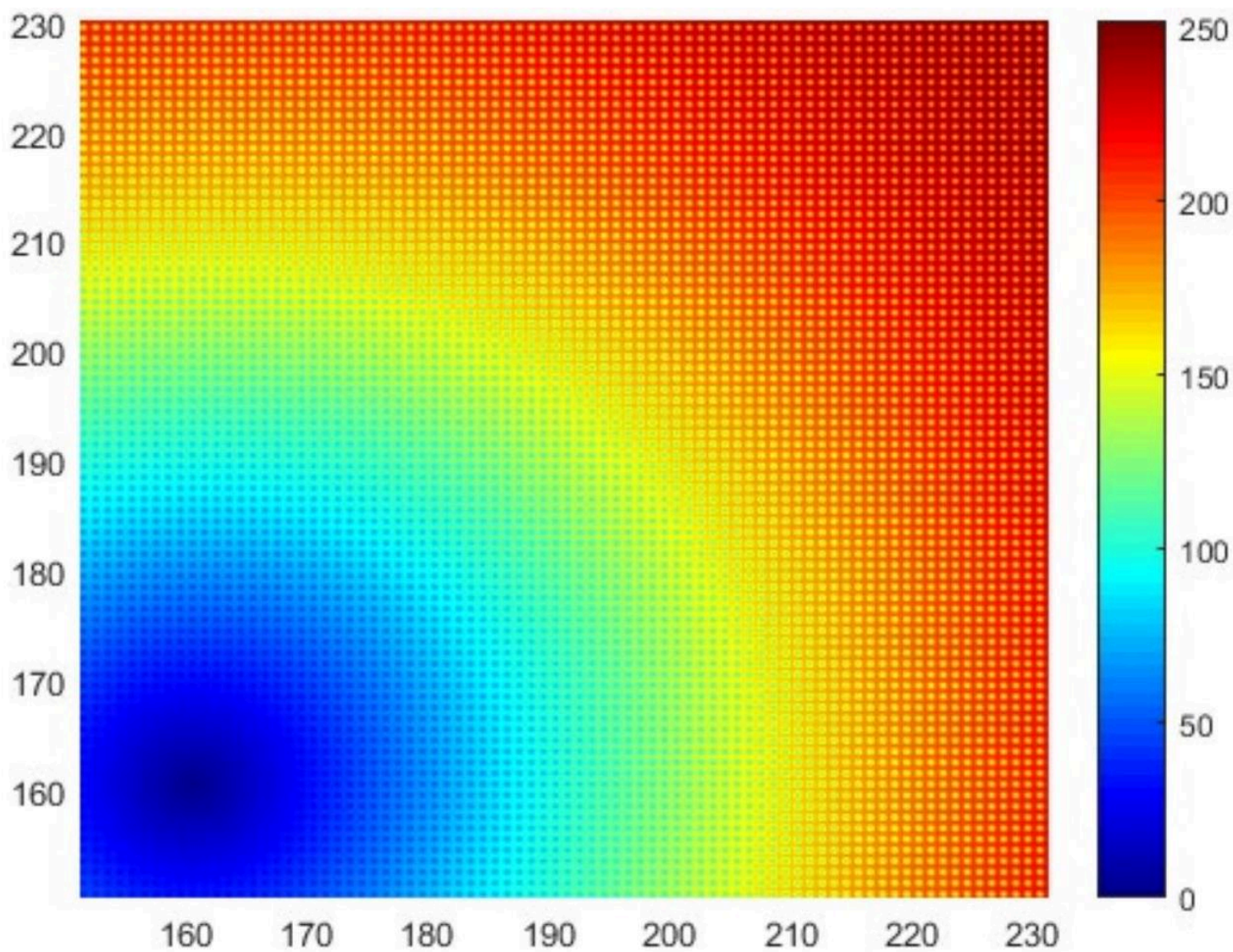


Figure 13: Fig. 12. Fragment of the image presented in Fig. 9, at a scale of 4 : 1

圖 13：圖 12。圖 9 中所示影像的片段，比例為 4 : 1



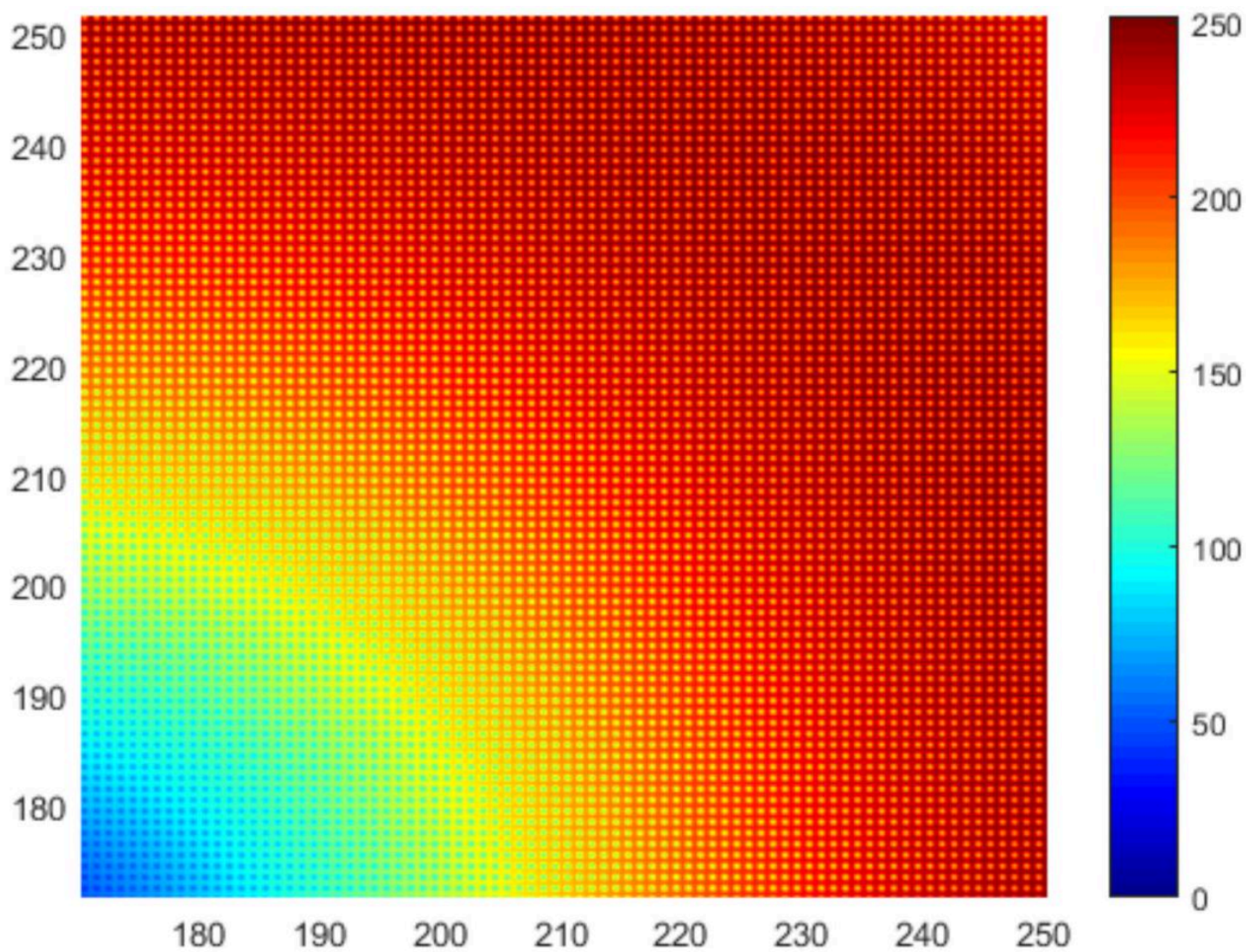


Figure 14: Fig. 13. Fragment of the image presented in Fig. 9, at a scale of 4 : 1

圖 14 : 圖 13 ◦ 圖 9 中所示影像的片段，比例為 4 : 1



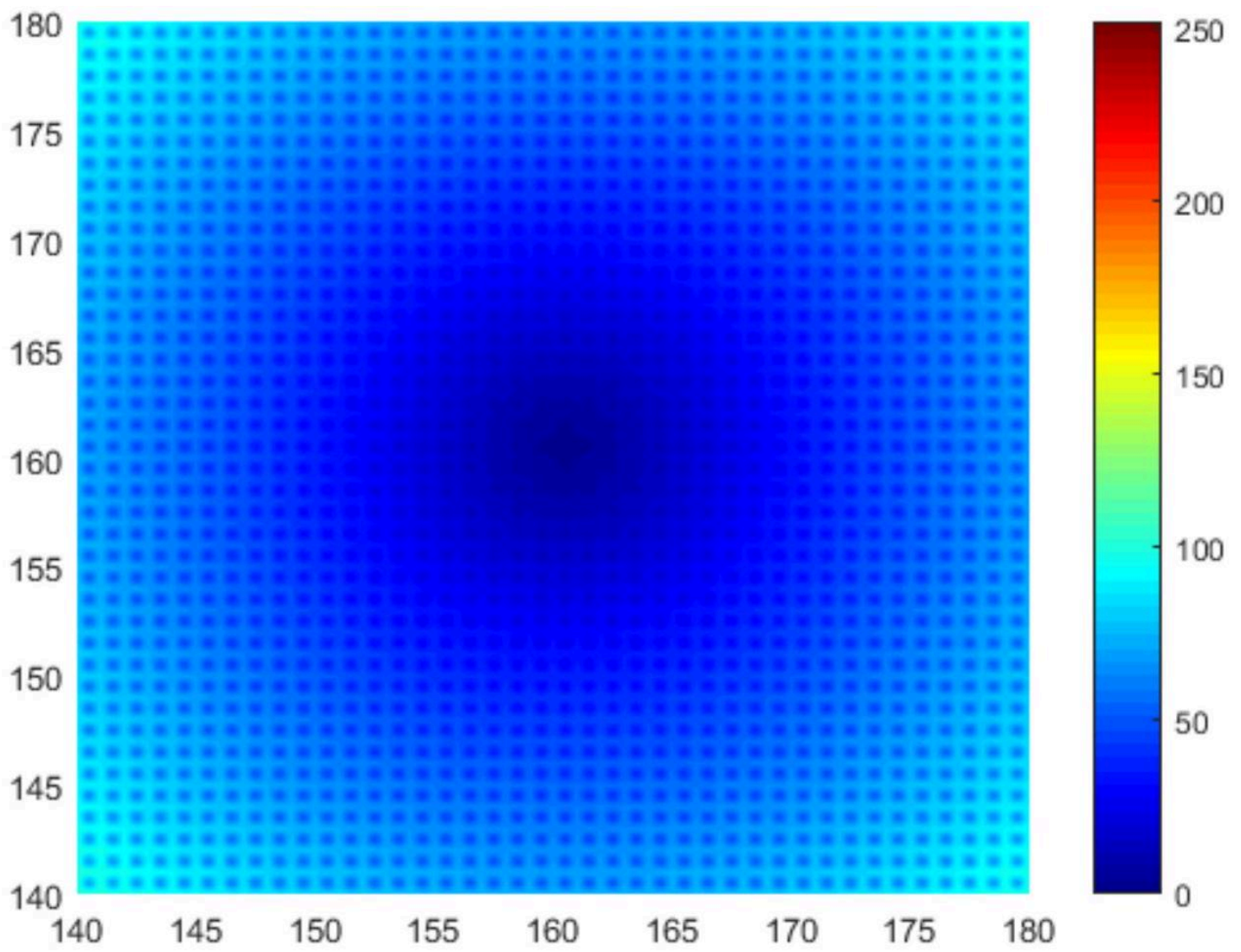
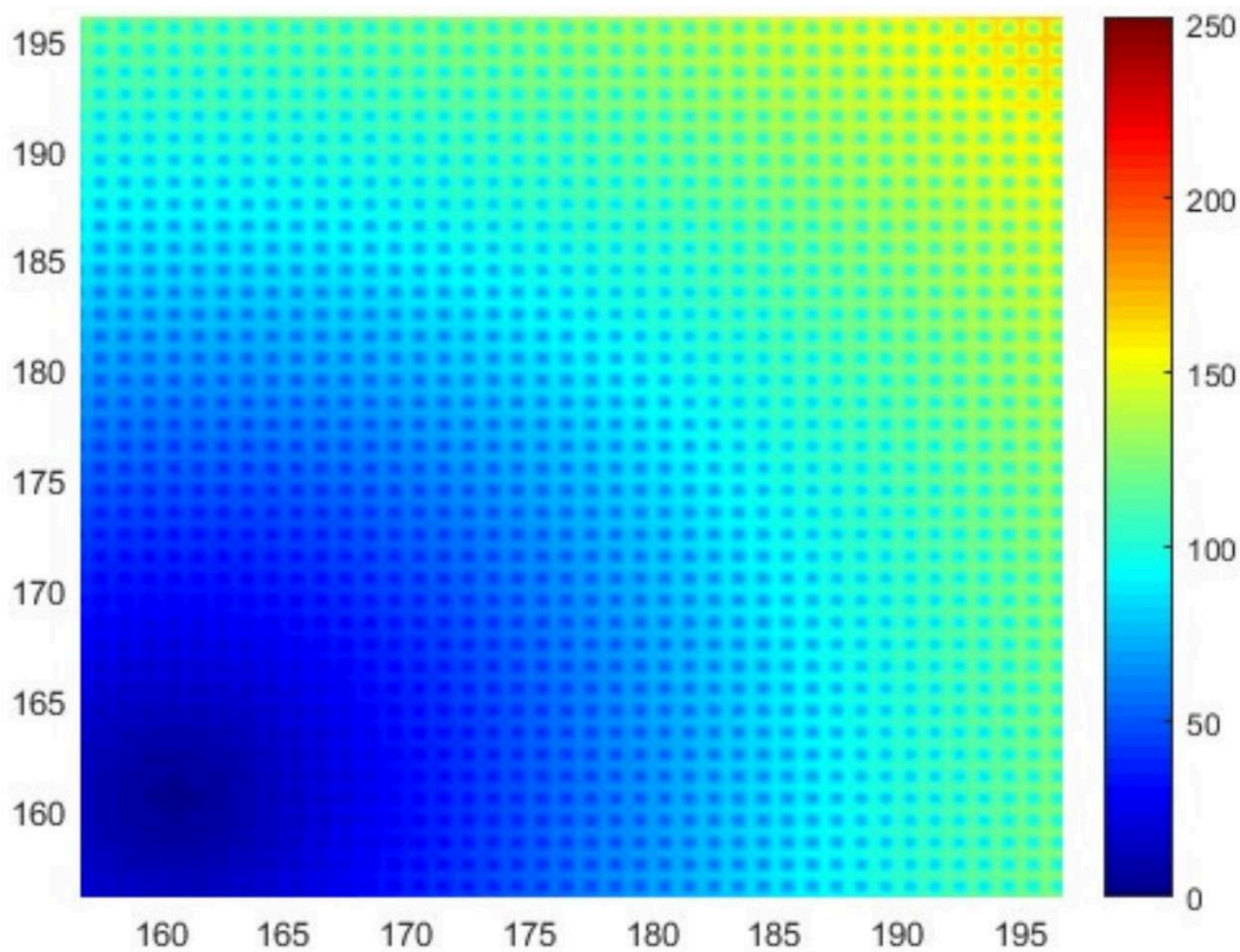


Figure 15: Fig. 14. Fragment of the image presented in Fig. 9, at a scale of 8 : 1

圖 15：圖 14。圖 9 中所示影像的片段，比例為 8 : 1



\captionsetup{labelformat=empty}  
 Figure 16: Fig. 15. Fragment of the image presented in Fig. 9, at a scale of 8 : 1

圖 16 : 圖 15。圖 9 中所示影像的片段，比例為 8 : 1



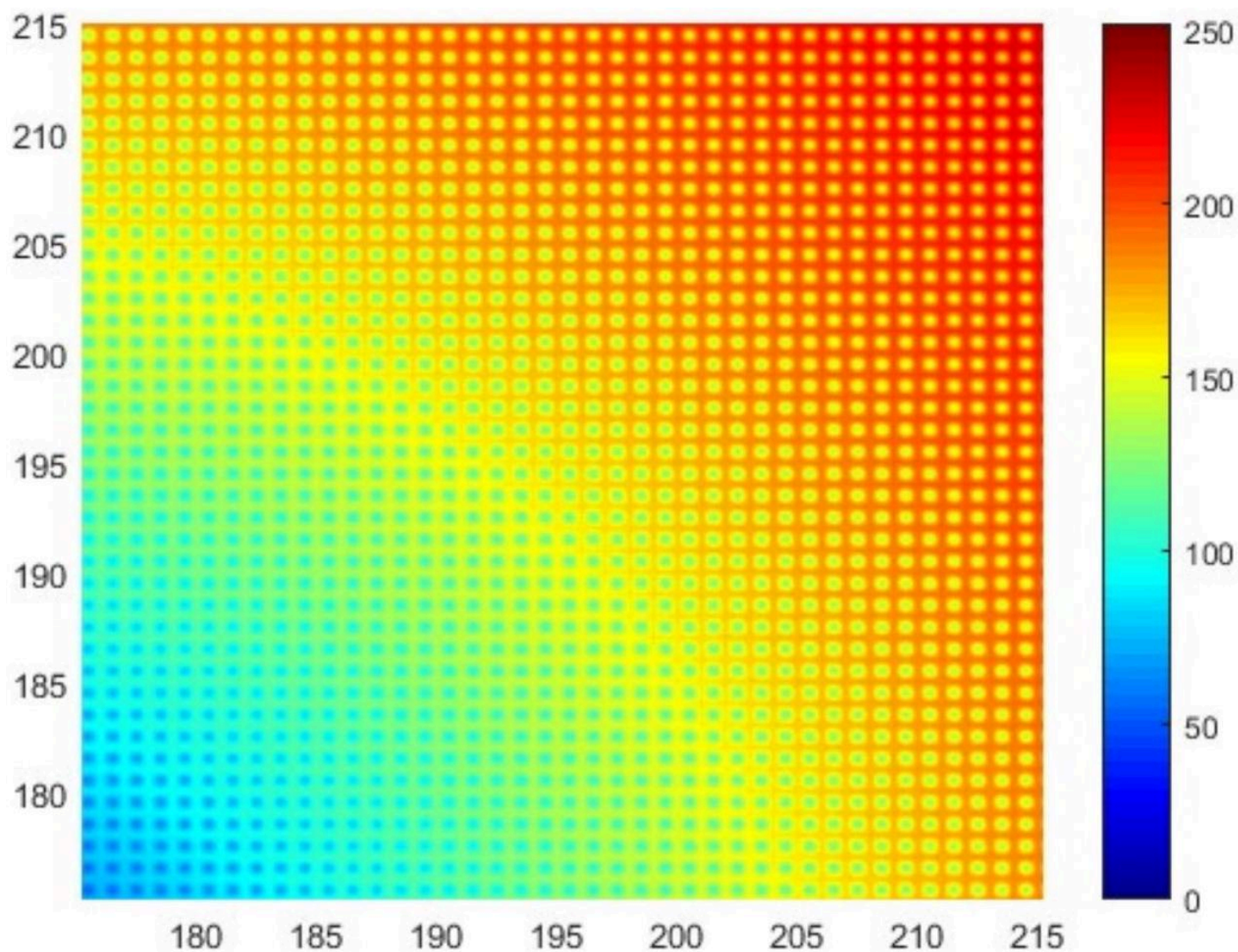


Figure 17: Fig. 16. Fragment of the image presented in Fig. 9, at a scale of 8 : 1

圖 17：圖 16。圖 9 中所示影像的片段，比例為 8 : 1

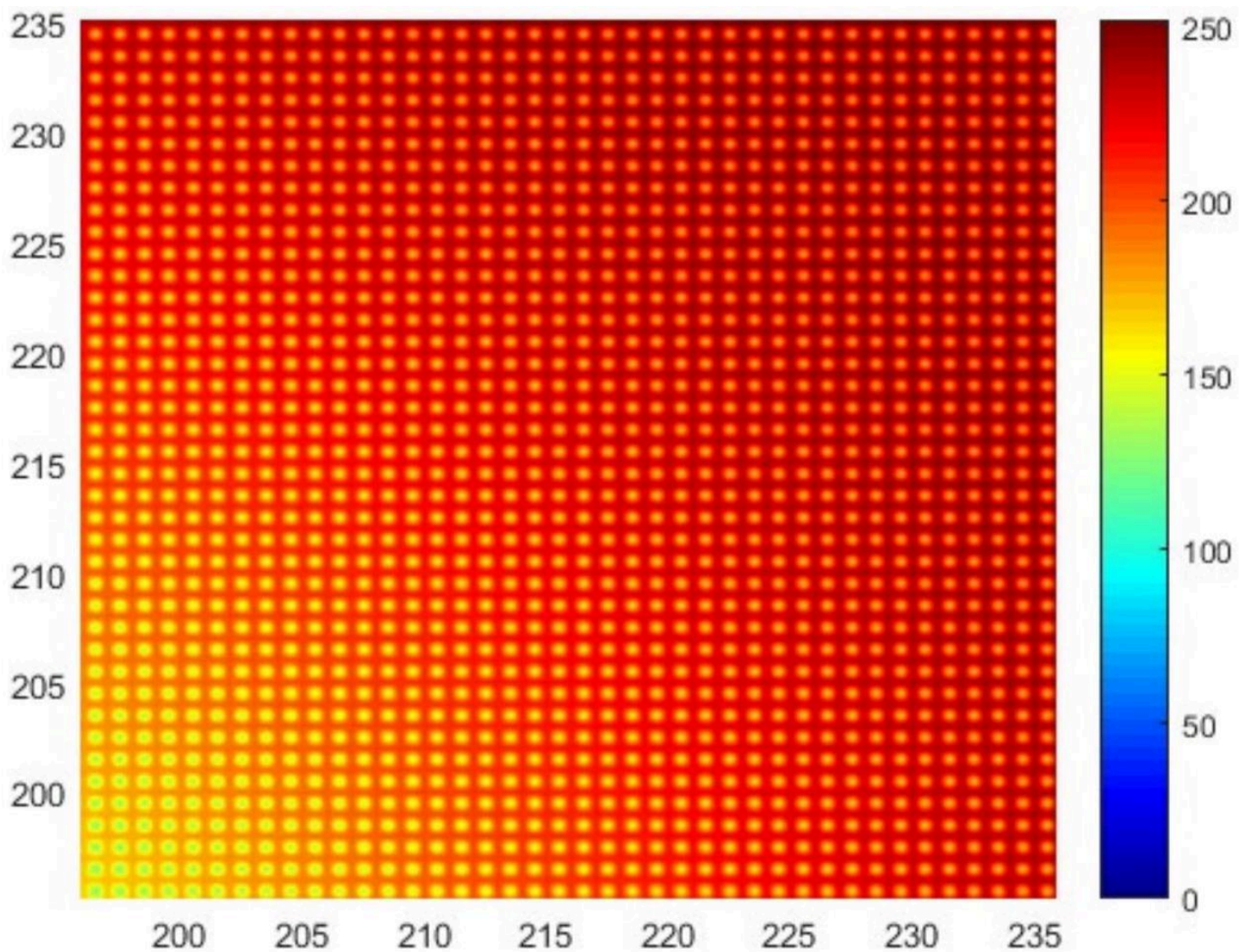


Figure 18: Fig. 17. Fragment of the image presented in Fig. 9, at a scale of 8 : 1

圖 18 : 圖 17 中所示影像的片段，比例為 8 : 1

The 3rd step of the calculation is “Derivative 3”. ➤

After introducing an additional gradation to the existing lattice, a cubic matrix of field strength was obtained with an increase in the maximum strength amplitude to a value of  $E = 355.64$  (V/m) relative to the initial matrix obtained at stage 1 of the calculation (Fig. 18-20). ➤



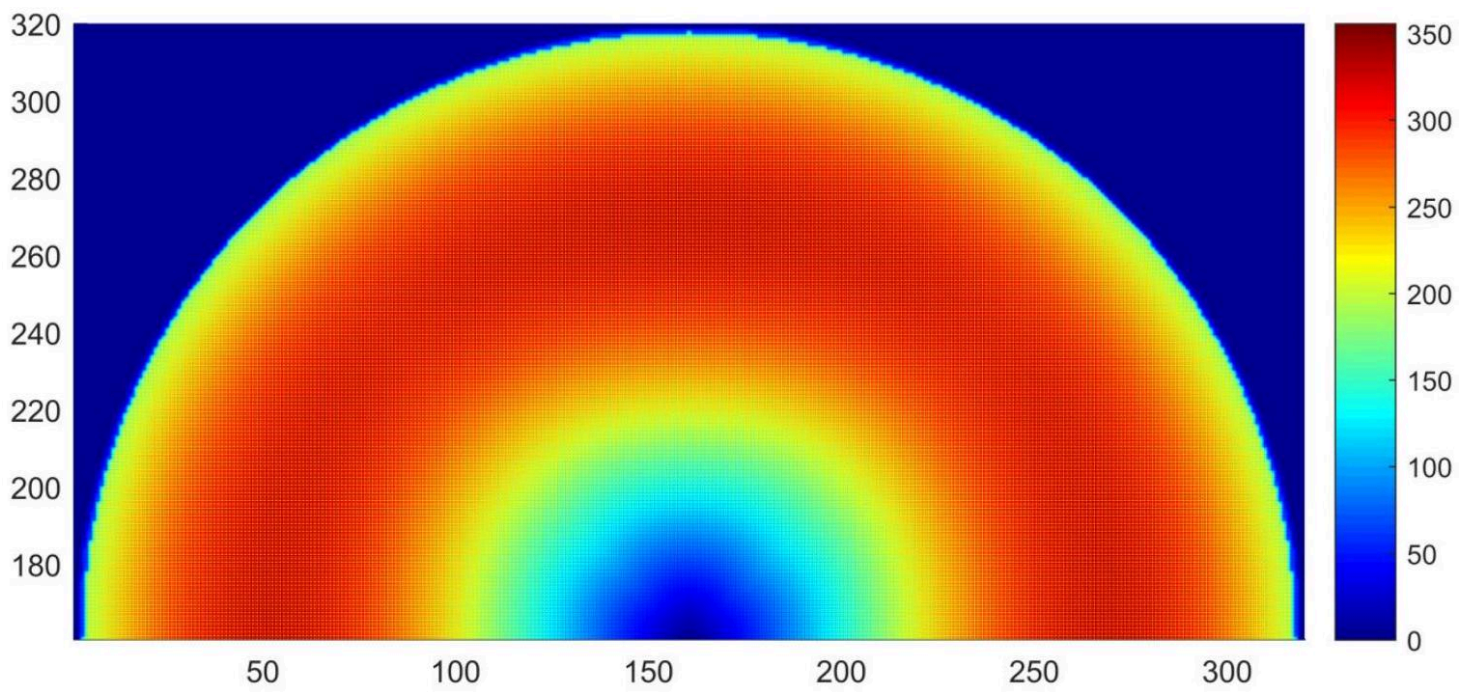



Figure 19: Fig.18. The distribution of the field strength  $E(V/m)$  over the resonator in the 3rd stage of calculations (vertical section through the center) 

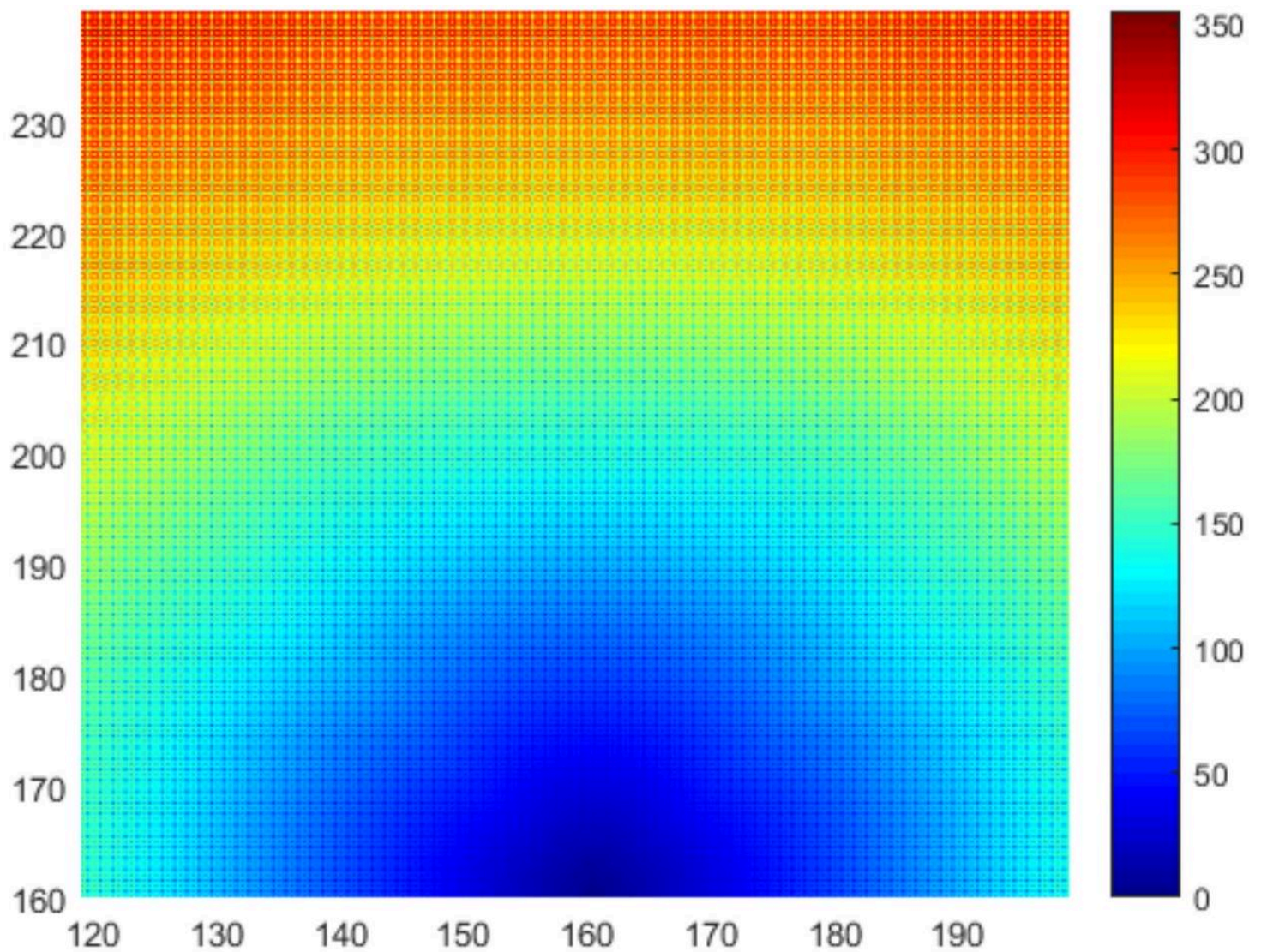

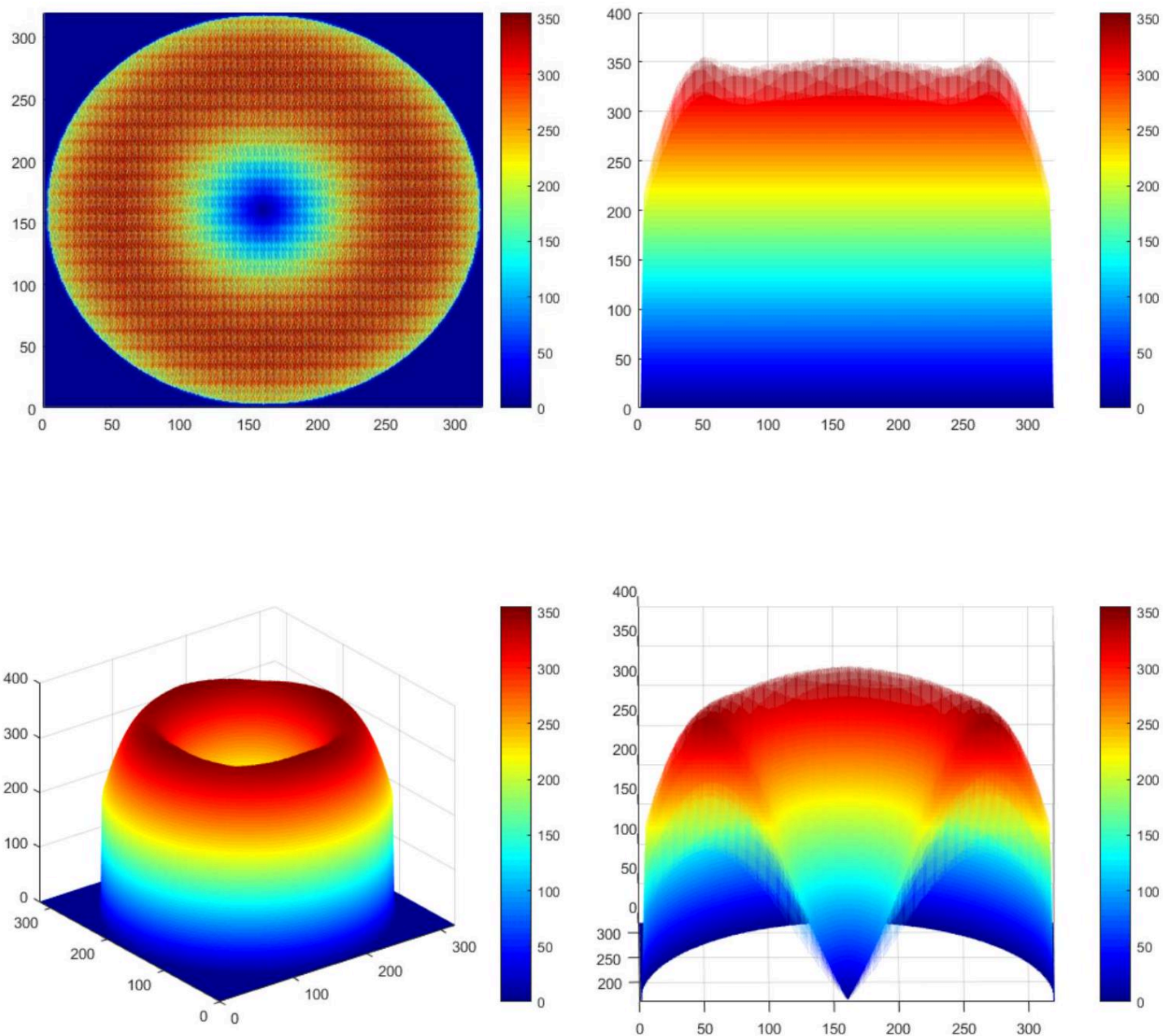


Figure 20: Fig. 19. Fragment of the image presented in Fig. 18, at a scale of 4 : 1 



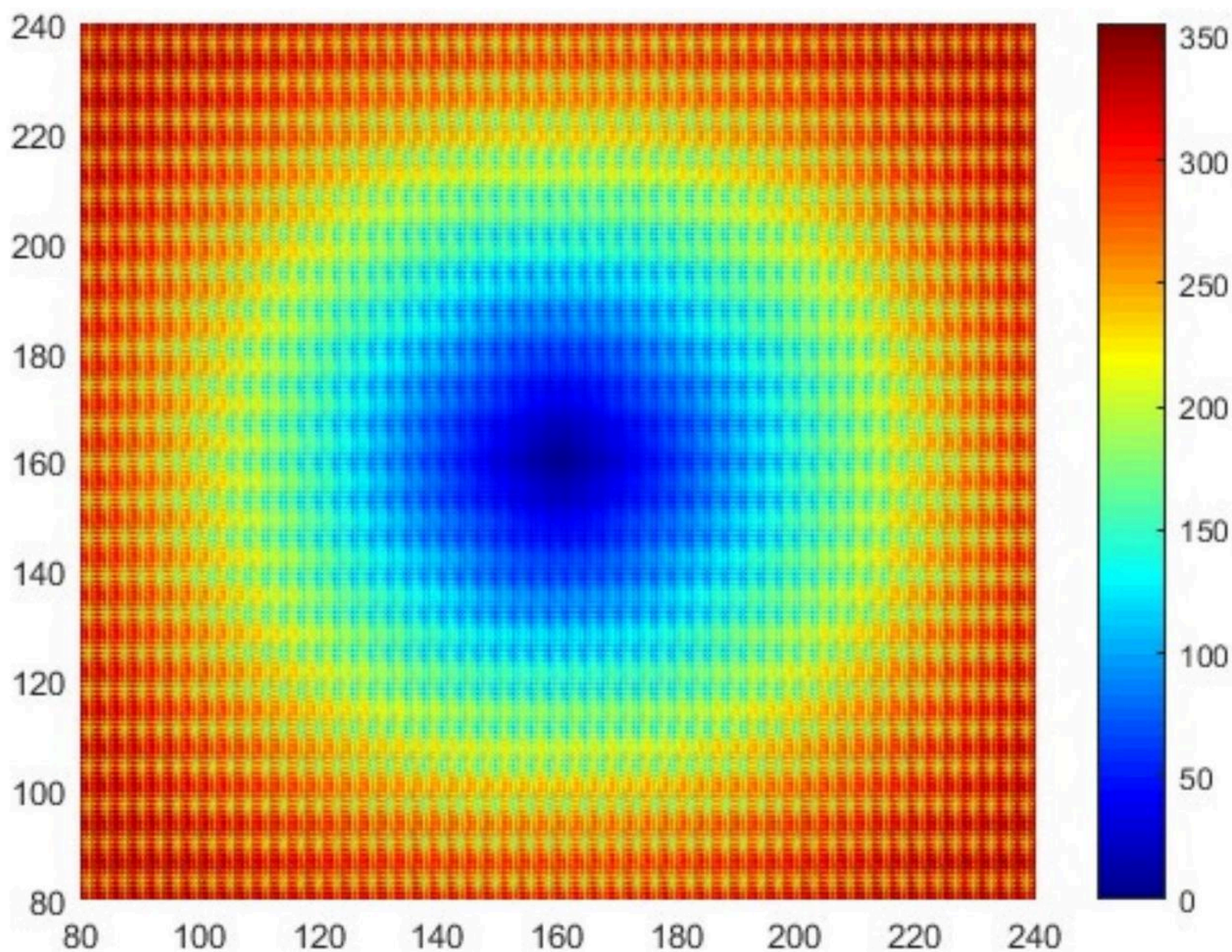


\captionsetup{labelformat=empty}

Figure 21: Fig. 20. The distribution of the field strength  $E$  over the resonator in the 2nd stage of calculations (horizontal section at a height of  $h = 24 * 10^{-6}$  m ), range  $E = 1.37 \div 355.64$ ( V/m) ☺

The appearance of a regular system of strength maxima and minima (Fig. 18-30) reflects the new functional nature of the electromagnetic field's emerging raster lattice over the Aires C20S5G resonator (microprocessor), which begins working as a differentiating system. ☺

For better visualization of the resulting effect, Figures 21-30 show enlarged fragments of the image of the distribution of the strength  $E$  shown in Fig. 20. ☺



\captionsetup{labelformat=empty}  
Figure 22: Fig. 21. Fragment of the image presented in Fig. 20, at a scale of 2 : 1

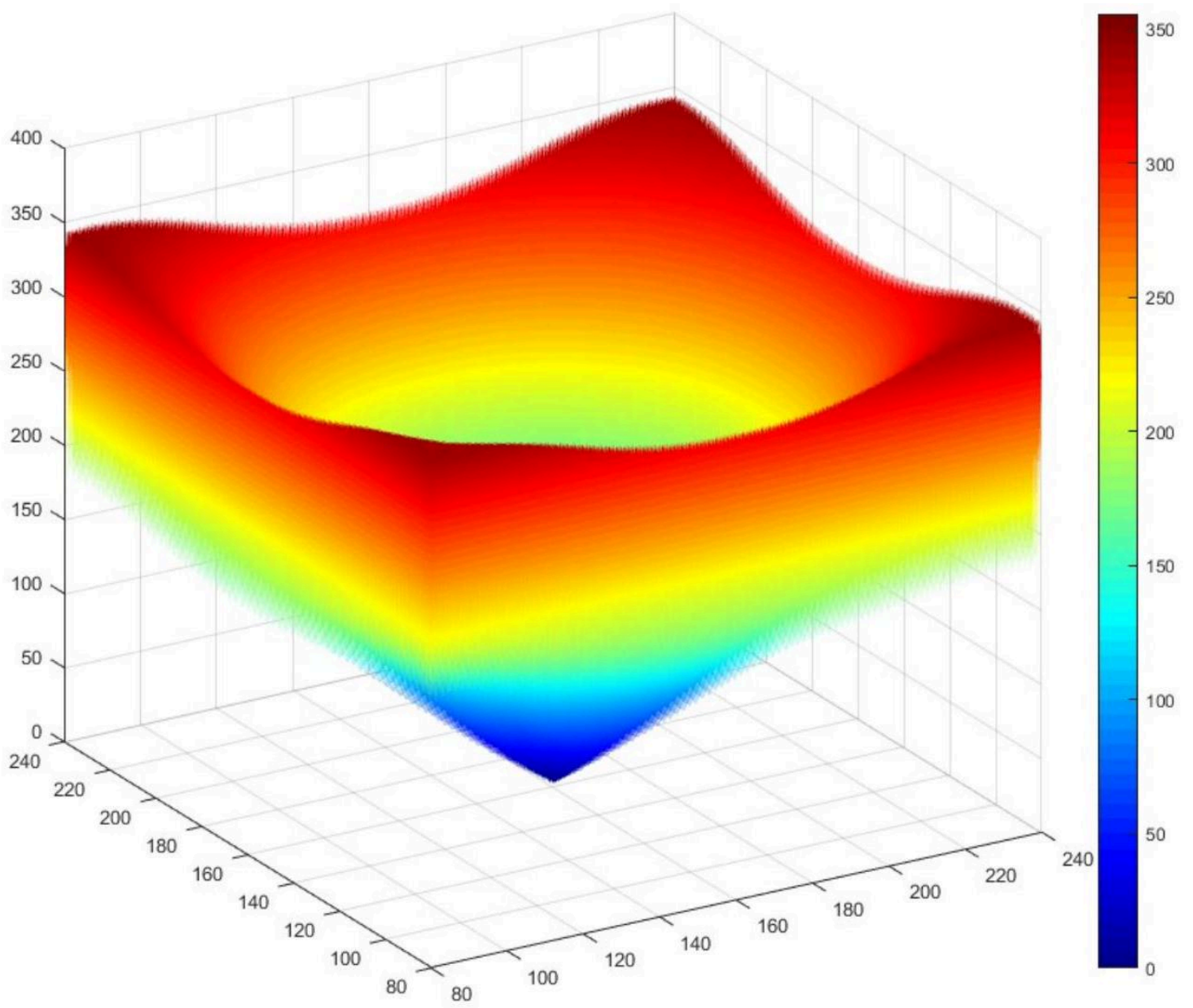


Figure 23: Fig. 22. Fragment of the image presented in Fig. 20, in isometry, at a scale of 2 : 1



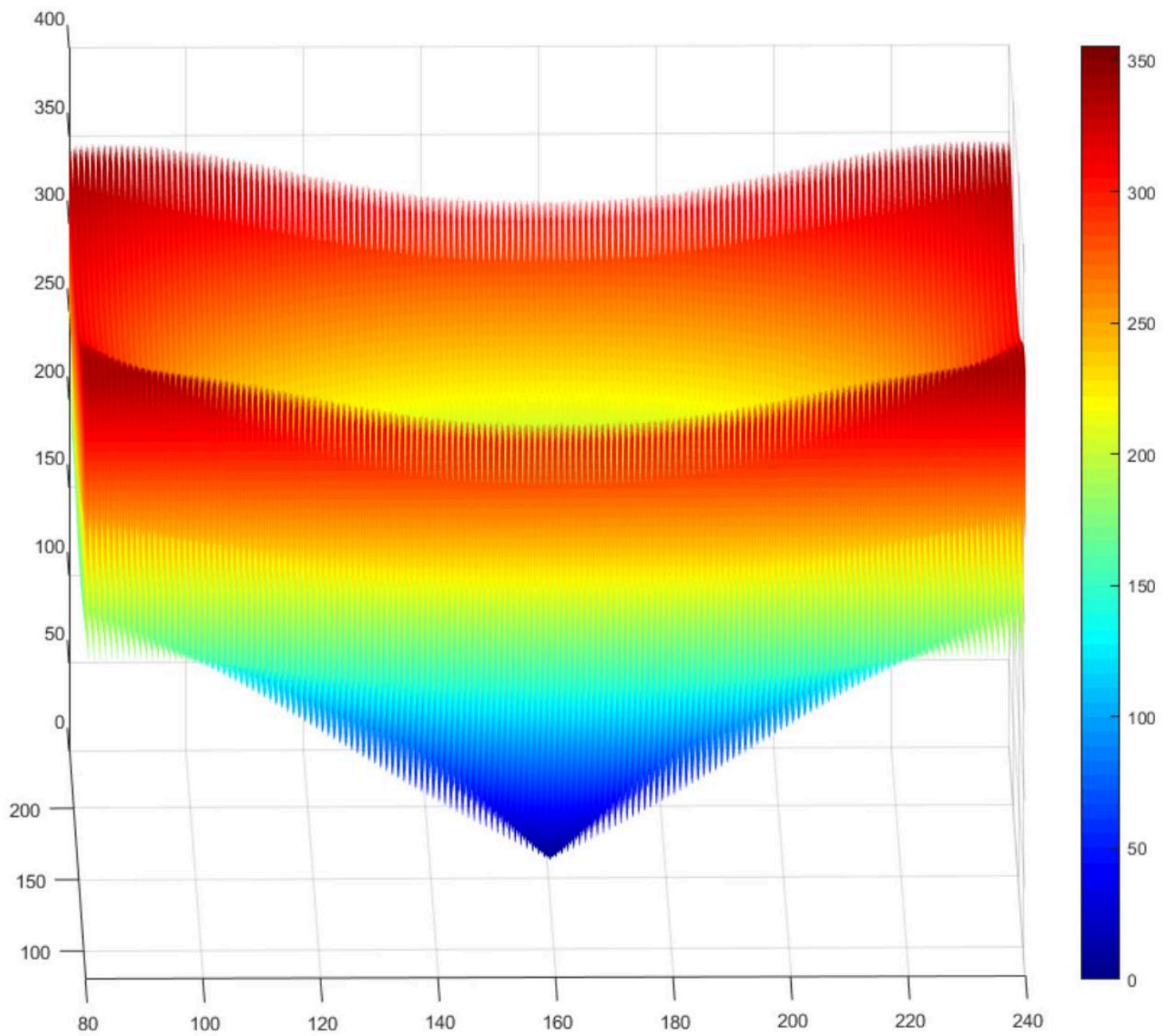


Figure 24: Fig. 23. Fragment of the image presented in Fig. 20, in isometry, at a scale of 2 : 1

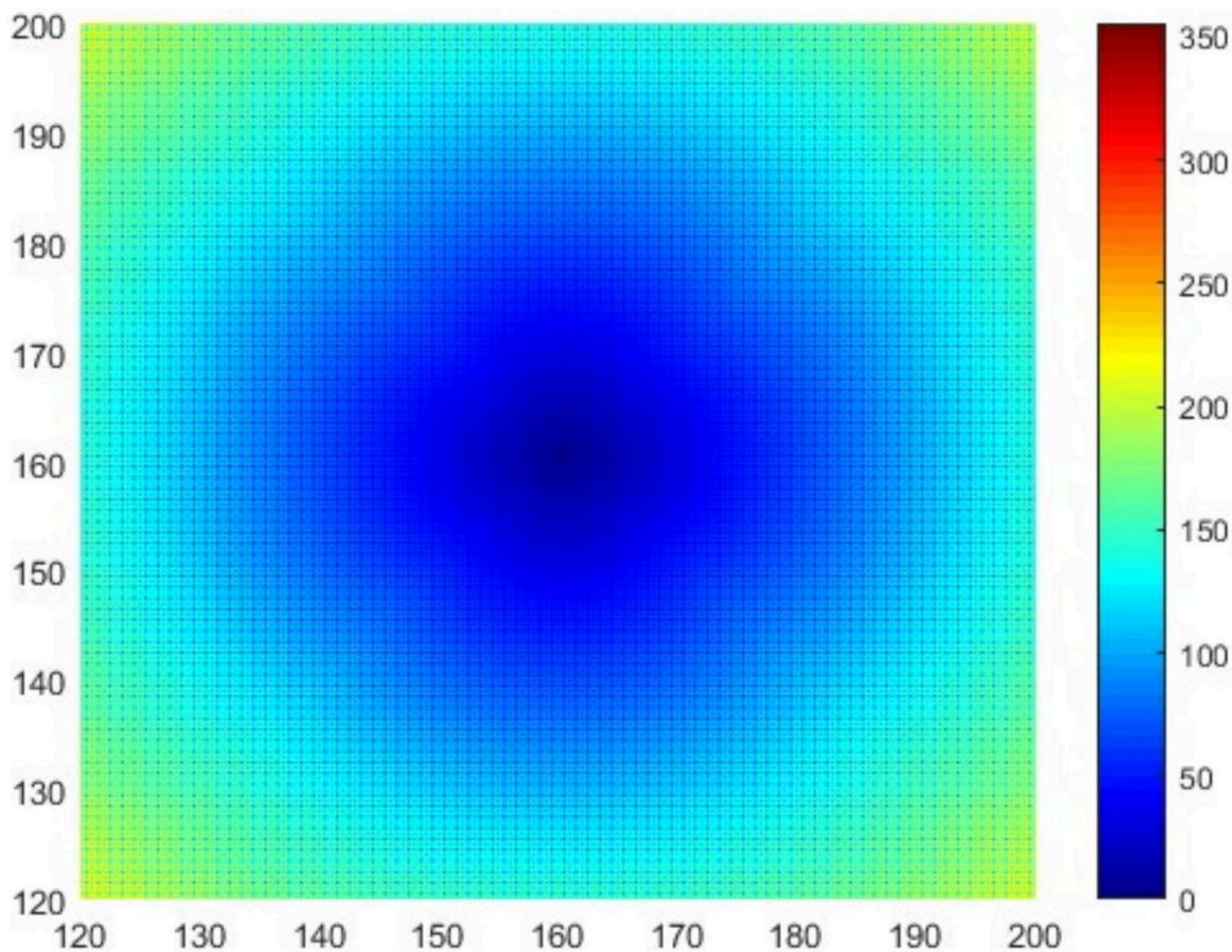
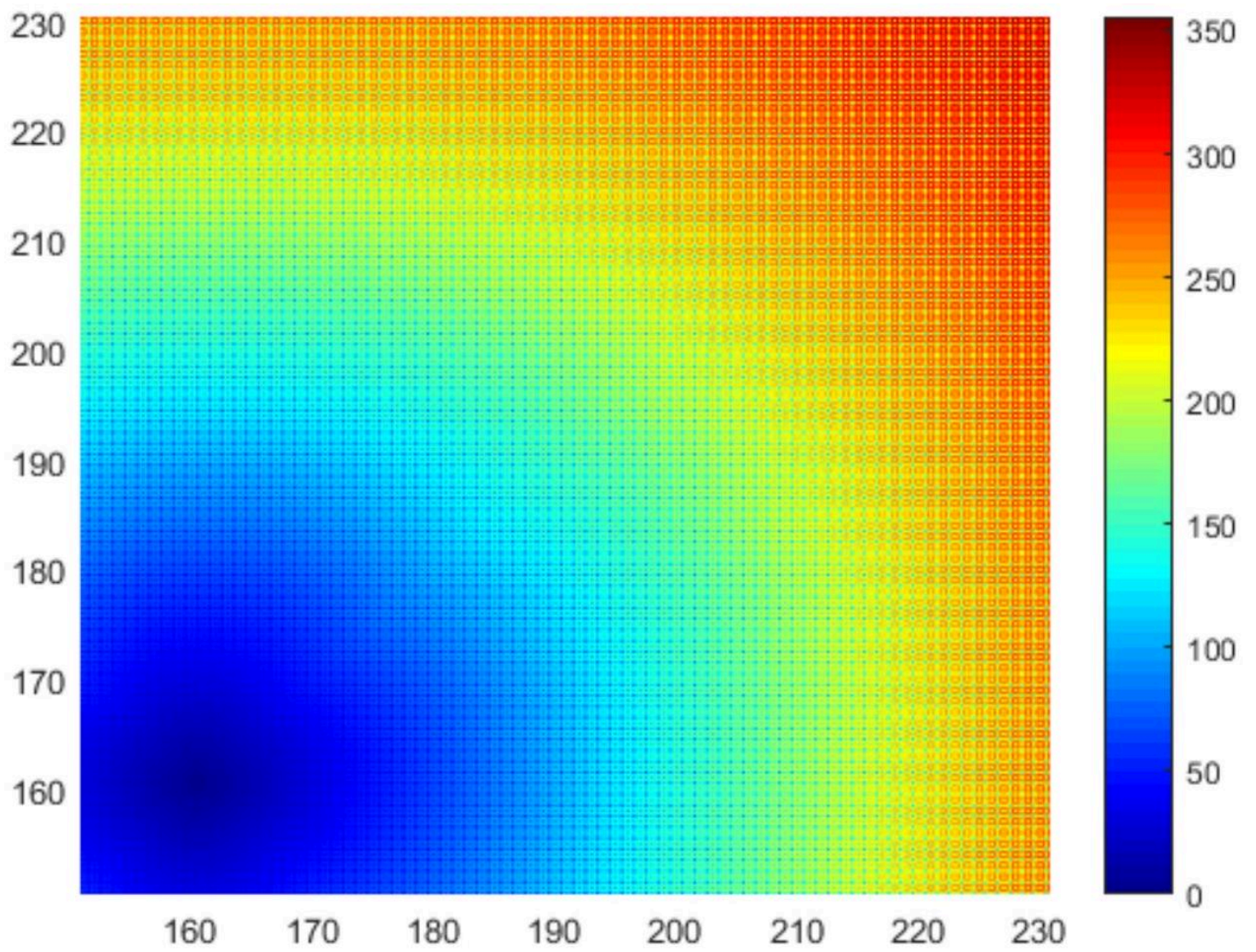


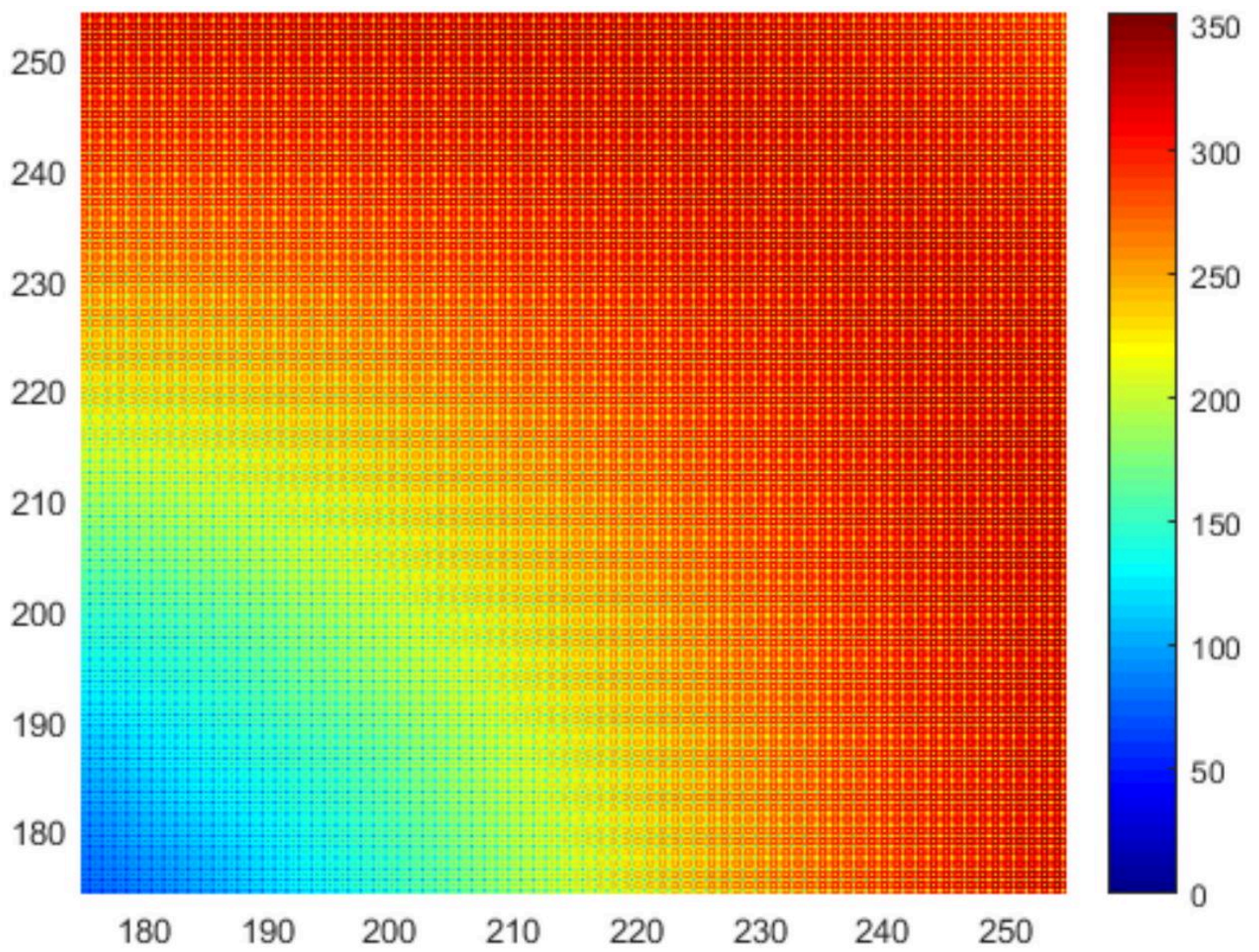
Figure 25: Fig. 24. Fragment of the image presented in Fig. 20, at a scale of 4 : 1



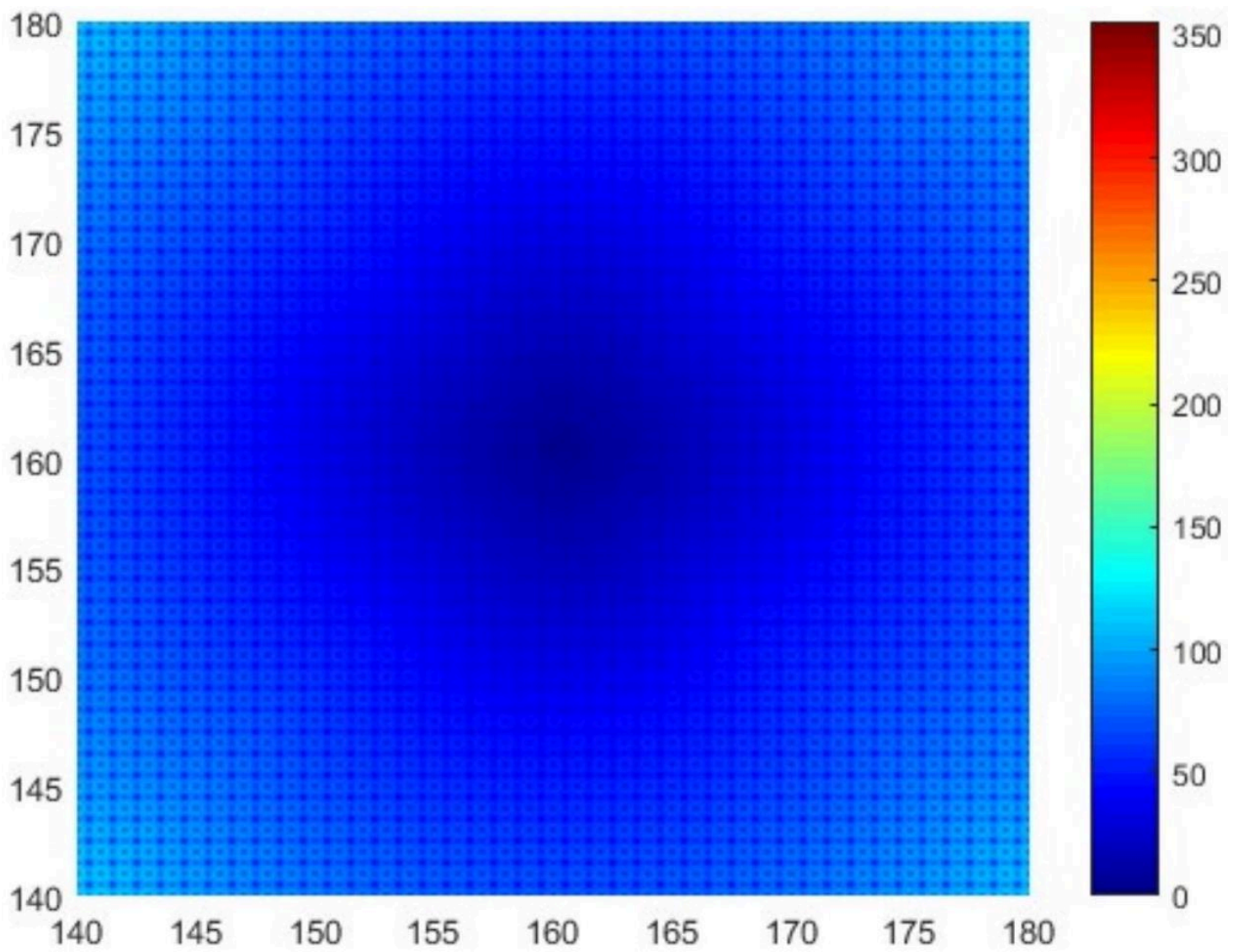


\captionsetup{labelformat=empty}  
Figure 26: Fig. 25. Fragment of the image presented in Fig. 20, at a scale of 4 : 1





\captionsetup{labelformat=empty}  
 Figure 27: Fig. 26. Fragment of the image presented in Fig. 20, at a scale of 4 : 1 ●



\captionsetup{labelformat=empty}  
Figure 28: Fig. 27. Fragment of the image presented in Fig. 20, at a scale of 8 : 1



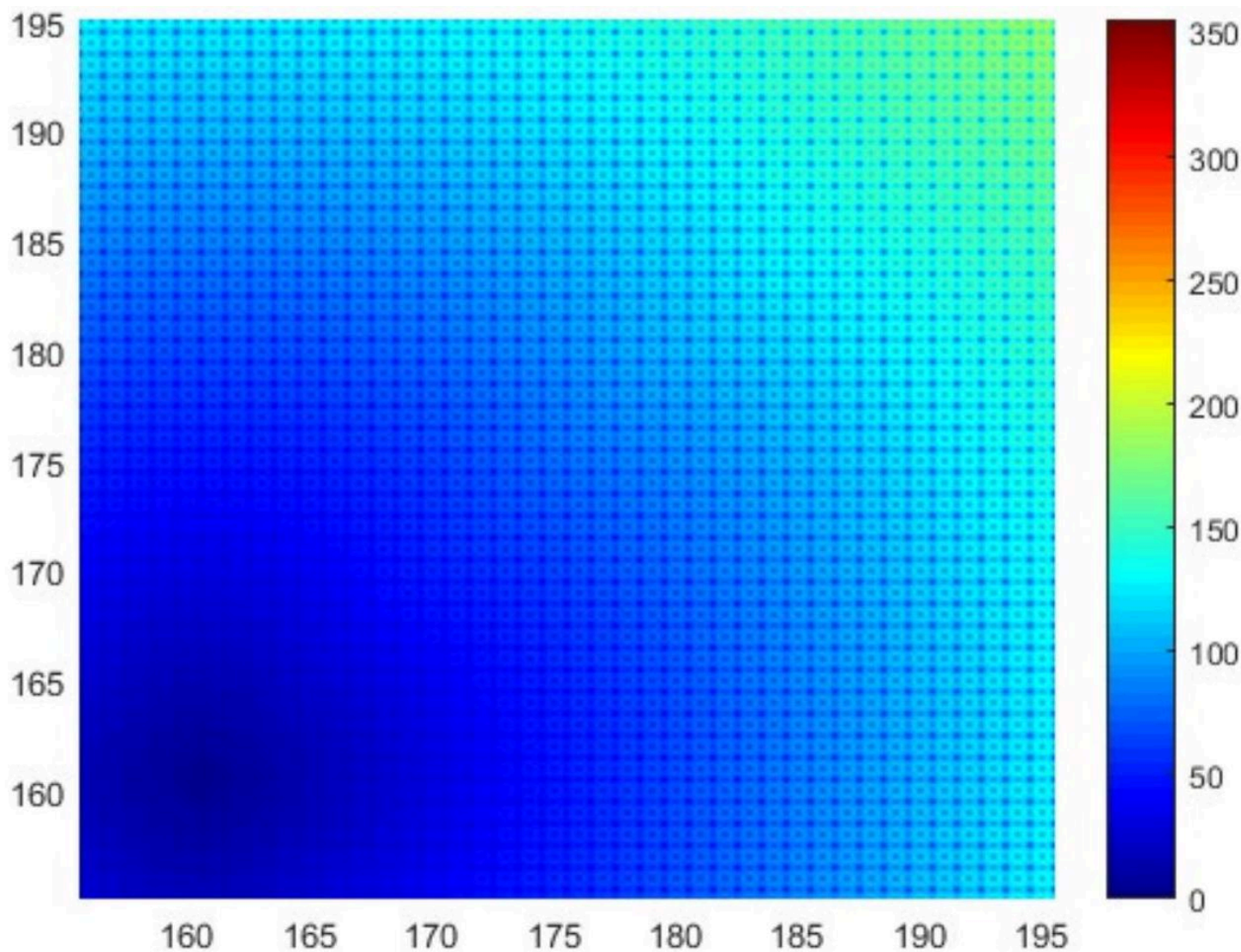


Figure 29: Fig. 28. Fragment of the image presented in Fig. 20, at a scale of 8 : 1

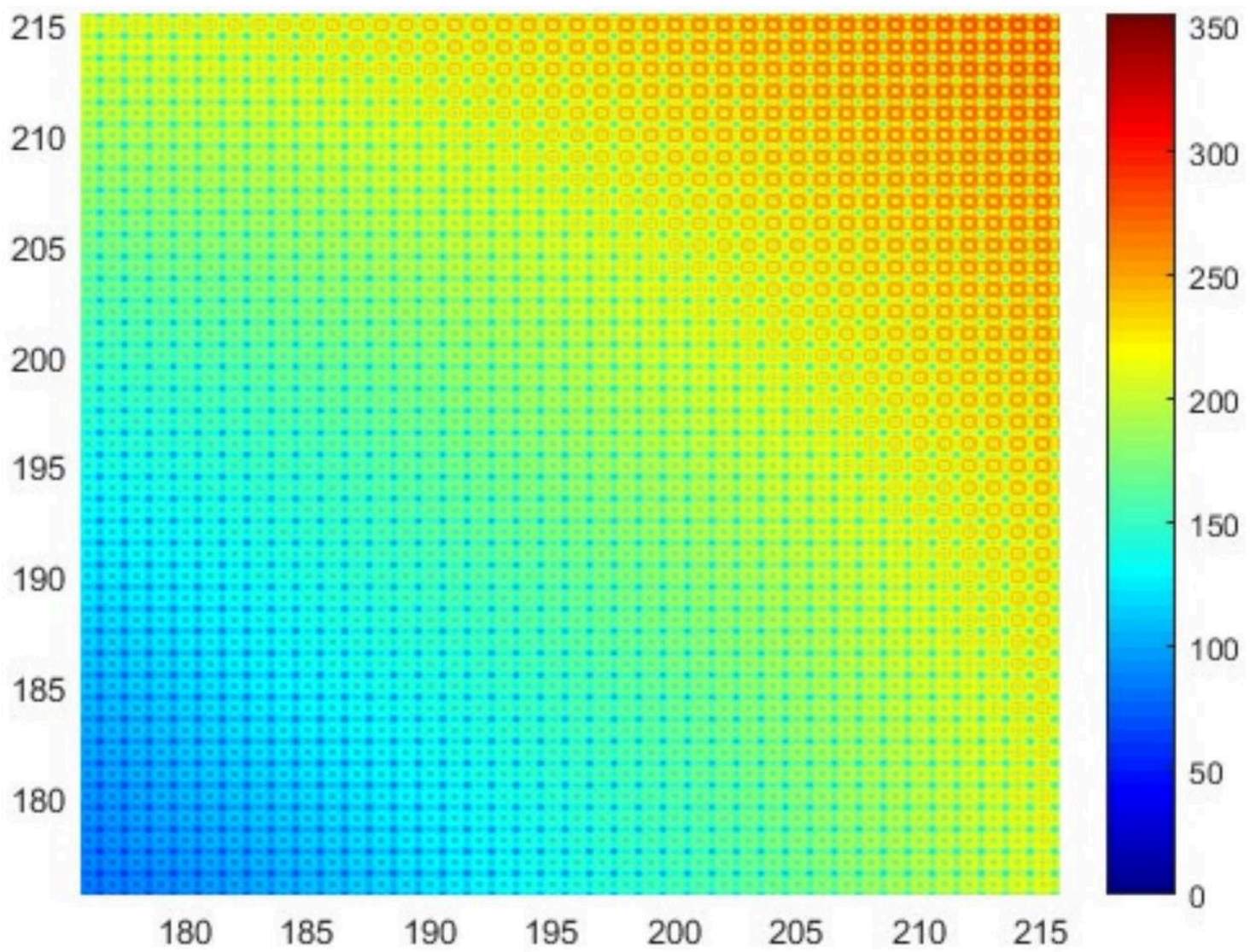


Figure 30: Fig. 29. Fragment of the image presented in Fig. 20, at a scale of 8 : 1



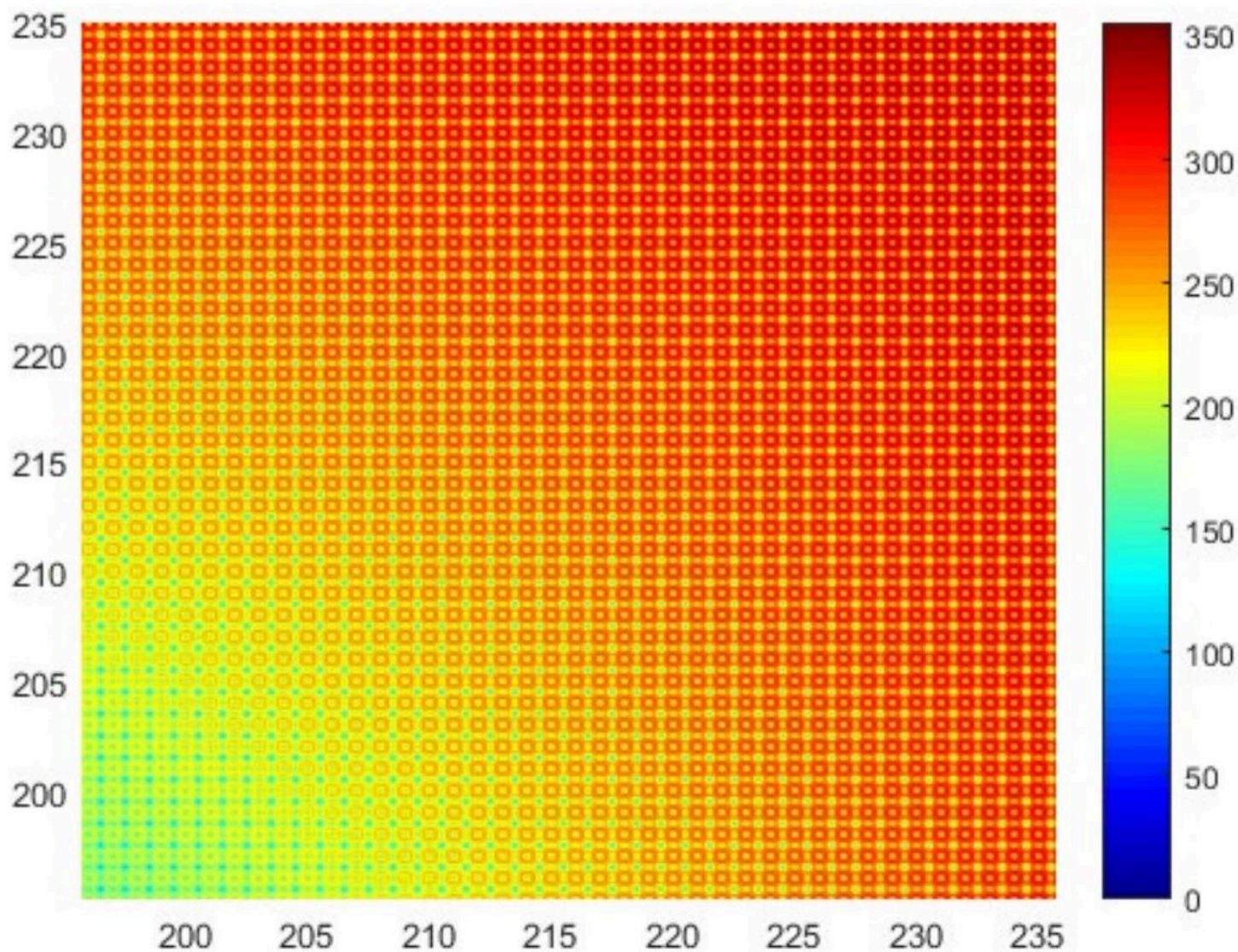


Figure 31: Fig. 30. Fragment of the image presented in Fig. 20, at a scale of 8 : 1

The 4th step of the calculation is “Derivative 4”.

The calculations of the fourth stage obtained a distribution of strength  $E$  and intensity  $I$  of the electromagnetic field in three-dimensional space (Fig. 31-36).



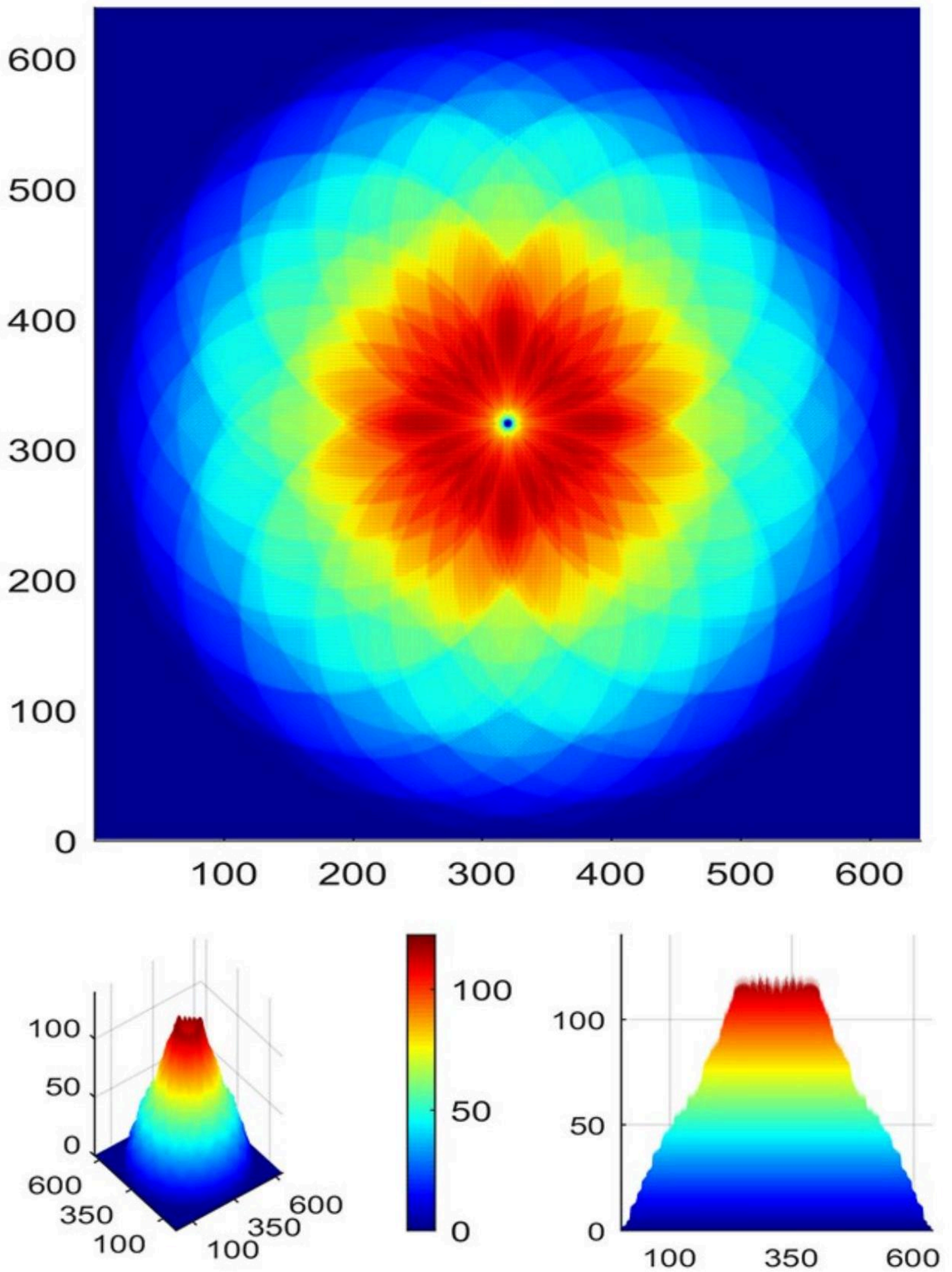

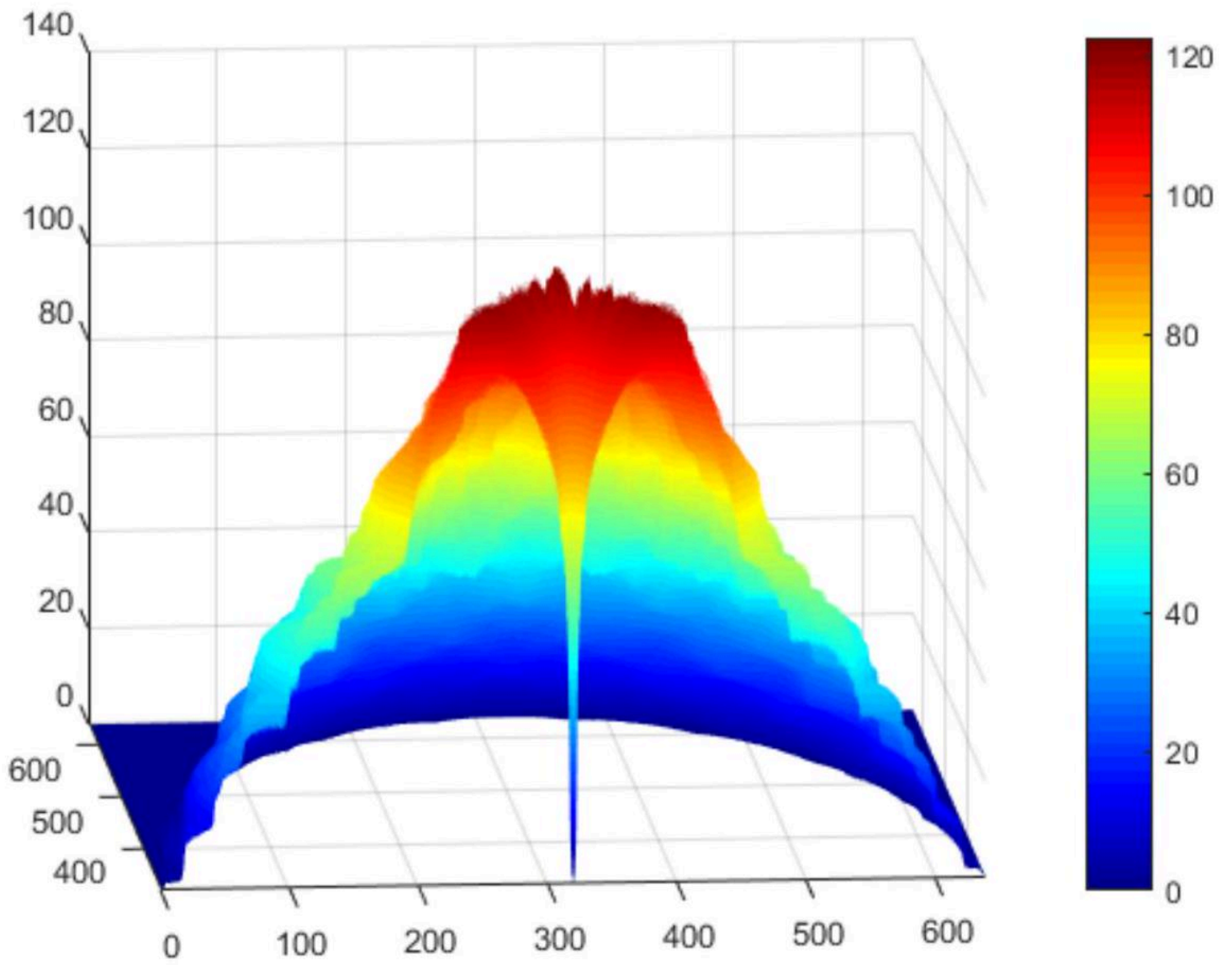

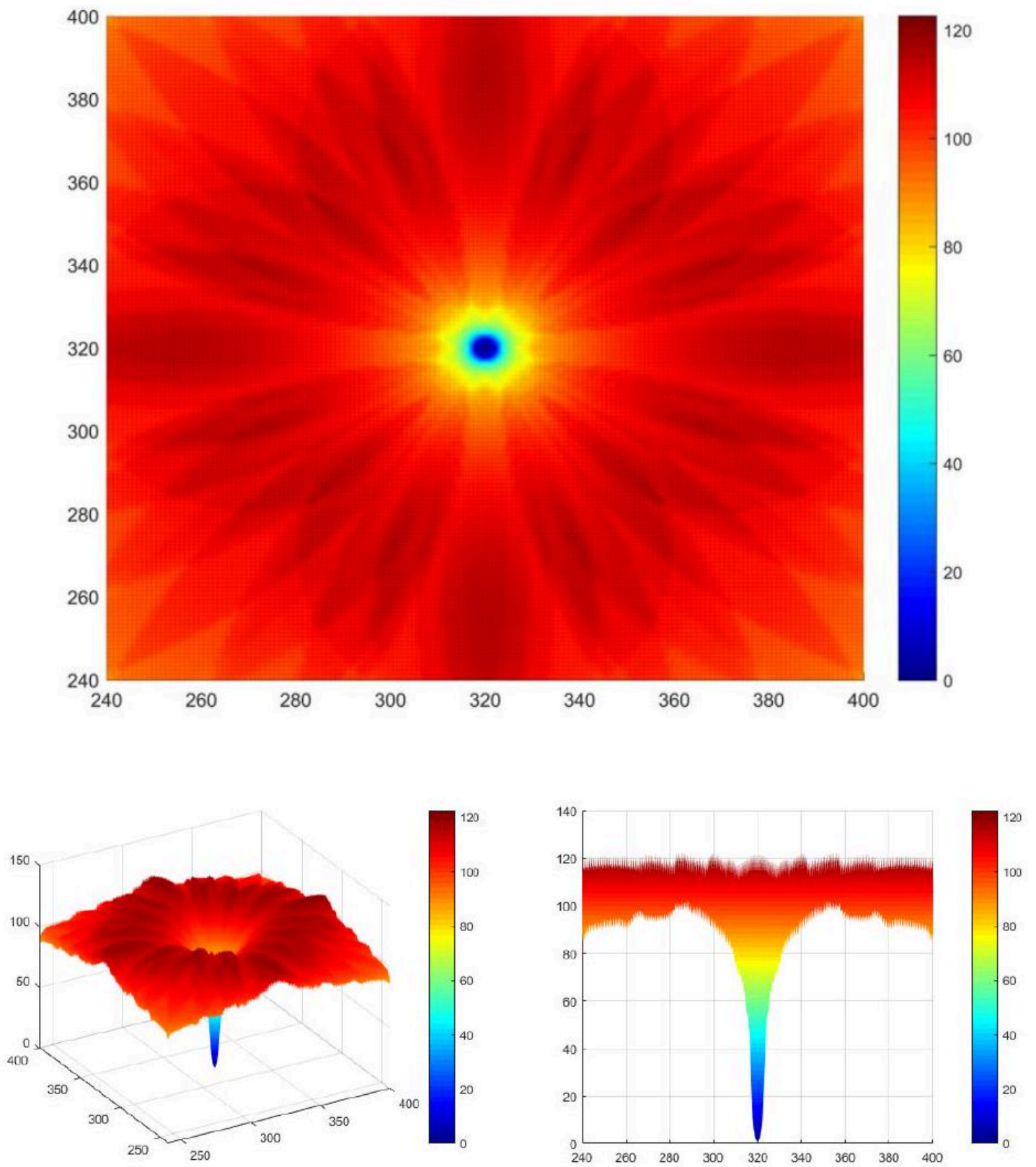


Figure 32: Fig.31. The distribution of the field strength  $E$  over the resonator in the 4 th stage of calculations at a height of  $h = 24 * 10^{-6}$  m in different projections, range  $E = 0.25 \div 122.6$  ( V/m) 



\captionsetup{labelformat=empty}

Figure 33: Fig. 32. The distribution of the field strength  $E$  over the resonator at a height of  $h = 24 * 10^{-6}$  m, Central section. 



\captionsetup{labelformat=empty}

Figure 34: Fig. 33. The distribution of the field strength  $E$  over the resonator at a height of  $h = 24 \times 10^{-6}$  m in different projections, at a scale of 4:1. ☺



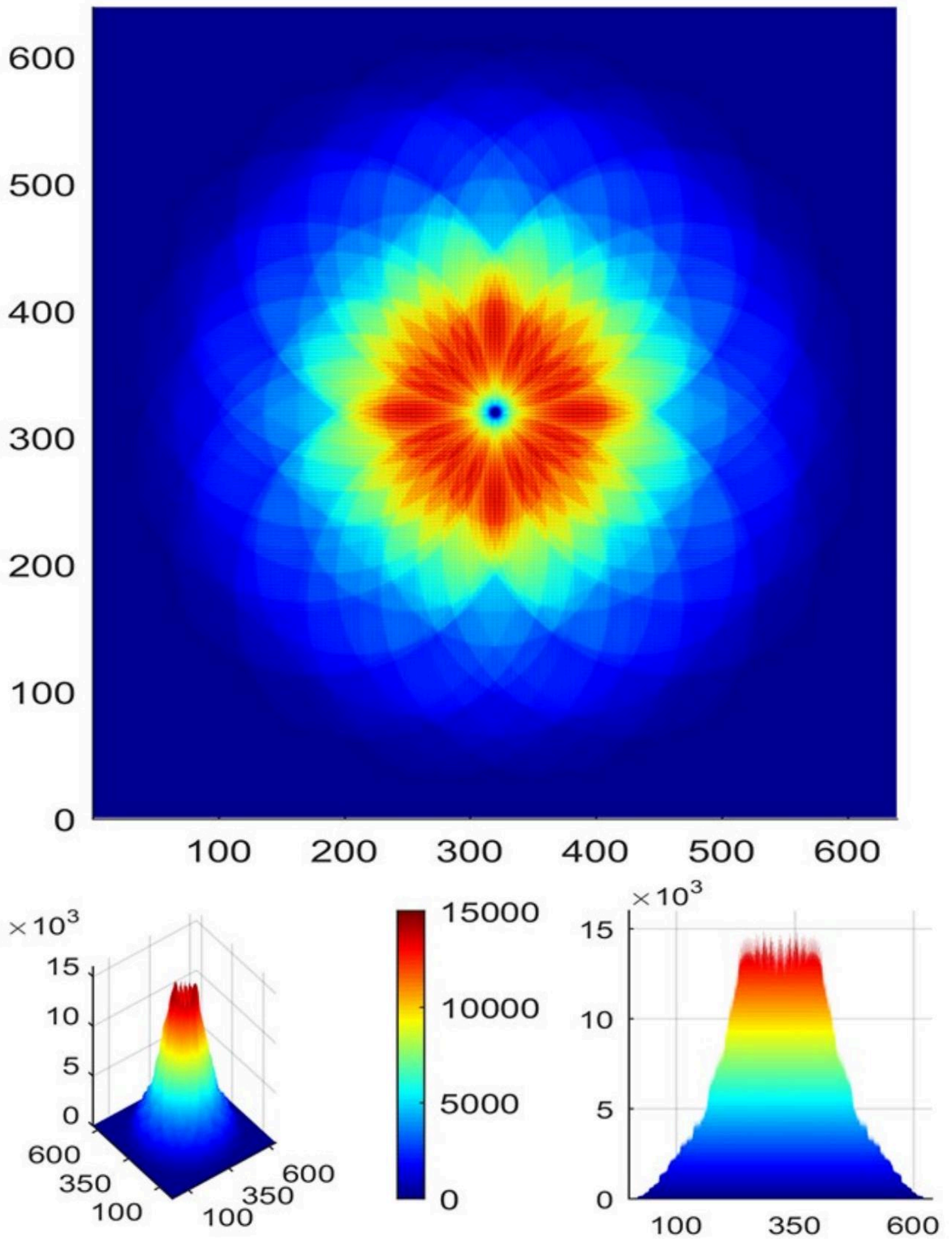
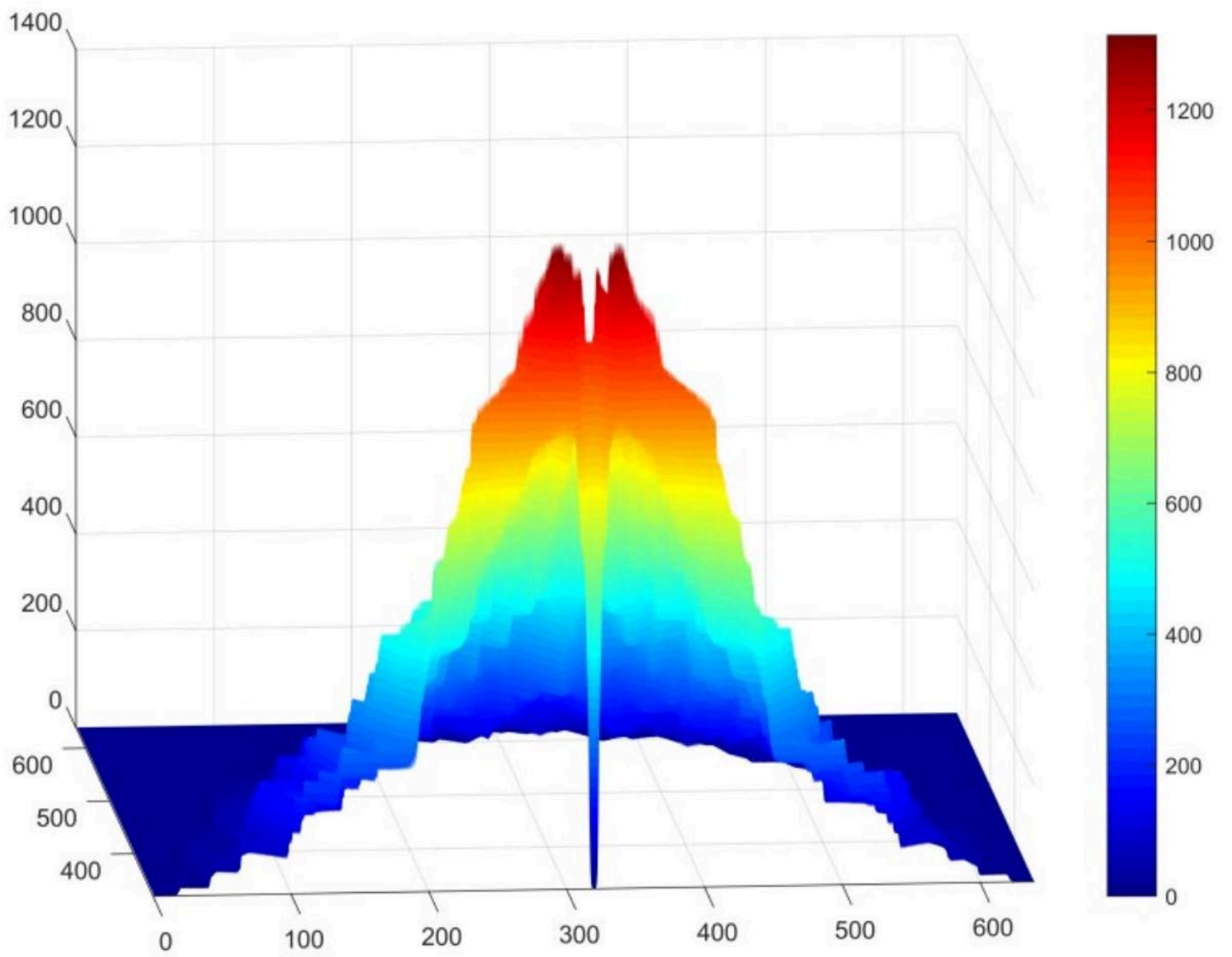

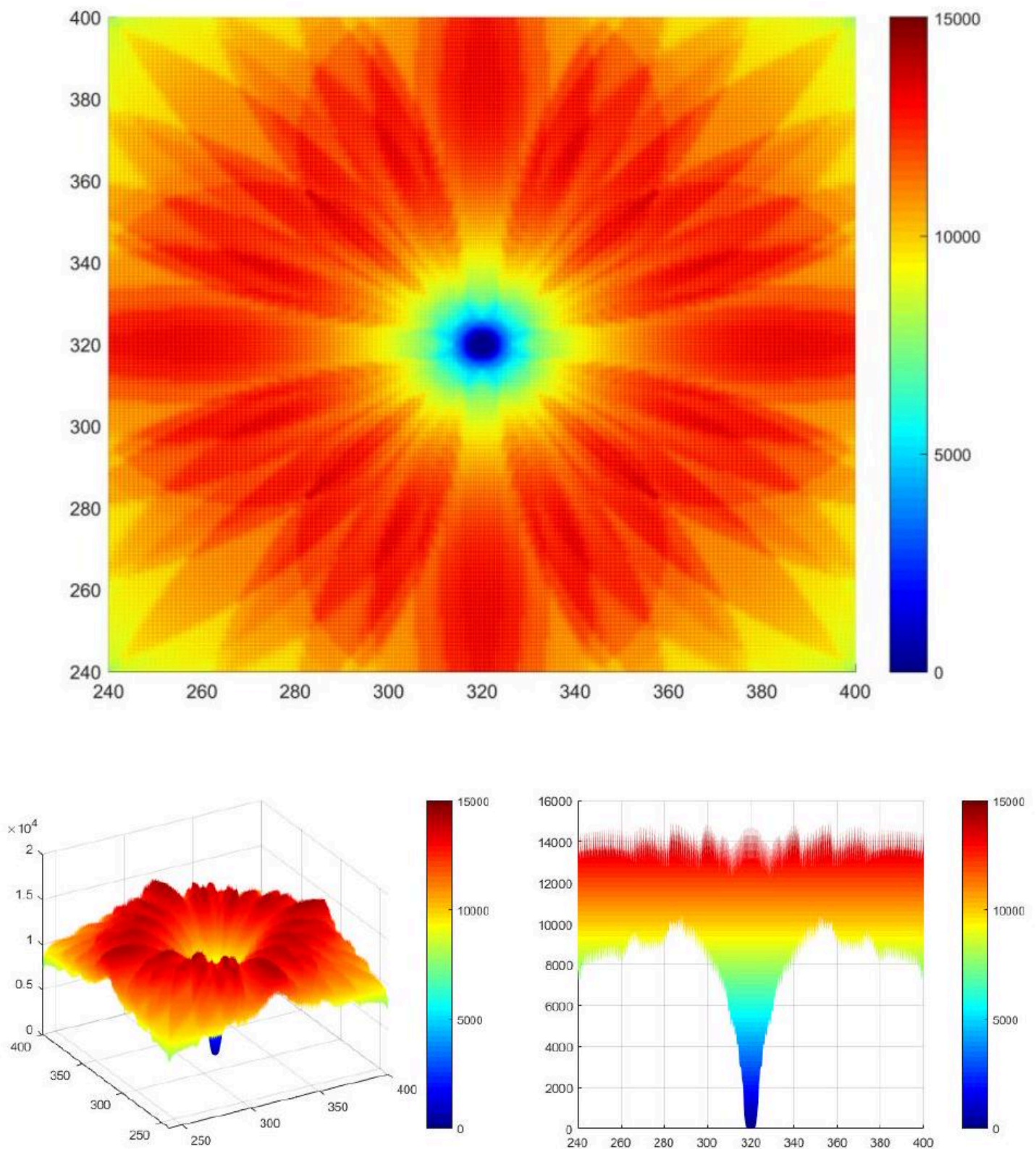


Figure 35: Fig.34. The distribution of the field intensity  $I$  over the resonator in the 4 th stage of calculations at a height of  $h = 24 * 10^{-6}$  m in different projections, range  $I = 0.06 \div 15030.76$  ( W/m<sup>2</sup>)



\captionsetup{labelformat=empty}

Figure 36: Fig. 35. The distribution of the field intensity  $I$  over the resonator at a height of  $h = 24 \times 10^{-6}$  m, Central section. 



\captionsetup{labelformat=empty}

Figure 37: Fig. 36. The distribution of the field intensity  $I$  ( $\text{W}/\text{m}^2$ ) over the resonator at a height of  $h = 24 \times 10^{-6} \text{ m}$  in different projections, at a scale of 4 : 1. ☺

In the central zone of resonant field, we see: ☺

maximum strength followed by a sharp decrease over the circuit's center point:  $E = 122.6 \div 0.25$  ( $\text{V}/\text{m}$ ) (Fig. 31-33); ☺  
 maximum intensity followed by a sharp decrease over the circuit's center point:  $I = 15030.76 \div 0.06$  ( $\text{W}/\text{m}^2$ ) (Fig. 34-36). ☺

Thus, one can clearly see the electromagnetic field's characteristics' pronounced tendency to a minimum amplitude over the center of the circuit.

因此，可清楚地看出電磁場特性在電路中心呈現出明顯趨向最小振幅的現象。



As can be seen from Fig. 31-36, when approaching the center of the circuit, the strength  $E$  increases, reaching its maximum values in the immediate vicinity of the center, as well as the energy flux density  $I$ . And in the very center, as a result of the counteraction of potentials of the ring of strength, when their values are multiplied, there is a sharp change in the characteristics of the electromagnetic field: the strength tends to a maximum, and the amplitude approaches zero. Thus, the circuit's central zone is analogous to the point of singularity in quantum physics, i.e. the energy density there is as high as possible, and the amplitude tends to zero, which corresponds to the previously presented the matching principle expressed by the formula (1), ☺

$$\sum_{k=1}^n X^k + \sum_{k=1}^n Y^k + \sum_{k=1}^n Z^k + \dots + \sum_{k=1}^n N^k \rightarrow 0$$

which also implies the formation of a resonant field analogous to the intrinsic topology of the resonator. ☺

The consequence of this response is the redistribution of the field's energy flux density  $I$  with its nonlinear growth from the edges to the center of the resonator with a difference of  $\sim 250512.67$  times: from  $0.06(\text{ W/m}^2)$  to  $15030.76(\text{ W/m}^2)$ . Further, within the ring of maximum response intensity, a counter resonance forms along its diameters, causing the values of the potentials participating in this process to be multiplied. As a result of counterharmonization with respect to amplitudes, frequencies, phases, and the radiation pattern, there is a maximally neutral zone in the center and, since an active potential always redistributes from zones of maximum amplitude activity to a neutral zone, the potential density at the central point increases sharply and is constantly maintained, forming a stationary field, and the amplitude tends to zero, which initiates the singularity phenomenon. As a result, the focal point of the vector interaction of all processes with a common potential ☺

$(I_{\max})^2 = (15030.76)^2 = 225923746.18(\text{ W/m}^2)$  emerges at the center. ☺

Since the energy flux density of the field is proportional to the fourth power of the frequency:  $I \sim \omega^4$ , then the response frequency will also change:  $\Delta\omega \sim \sqrt[4]{\Delta I} = \sqrt[4]{250512.67} = 22.37$ , i.e. in 22.37 times will increase with respect to the original 28 GHz parameter and will be 626.36 GHz . ☺

Thus, the directional harmonization of the wave processes with respect to amplitudes, phases, frequency, and the interaction diagram of the resonator's annular fractal topology initiates a stationary, maximally coherent point structure of high density with a minimum electric field intensity, which indicates the high neutrality of this zone.

因此，就振幅、相位、頻率以及諧振器環形分形拓撲的相互作用圖而言，波動過程的定向協調會啟動一個穩定、極度相干且高密度的點狀結構，其電場強度達到最小值，這顯示該區域具有高度中性化。

In this case, the redistribution is not smooth and monotonic, but occurs in accordance with the profile features of the resonator's topological structure. Due to these features, the shape of the emerging field (electromagnetic superposition) over the resonator takes the form of a complex spatial hologram, tending toward multilevel symmetry and consisting of a large number of regular interpenetrating spherical surfaces of sizes that are multiples of one another and determined by the fractal structure and the dimensions of the annular grooves on the surface of the resonator. ☺

Figures 37-52 show the distribution of strength  $E$  and intensity  $I$  arising from the resonator of the field reflex with a height of  $7.632 \times 10^{-3} \text{ m}$  in various horizontal sections with a step of  $20h (0.48 \times 10^{-3} \text{ m})$  from the surface of the resonator. ☺

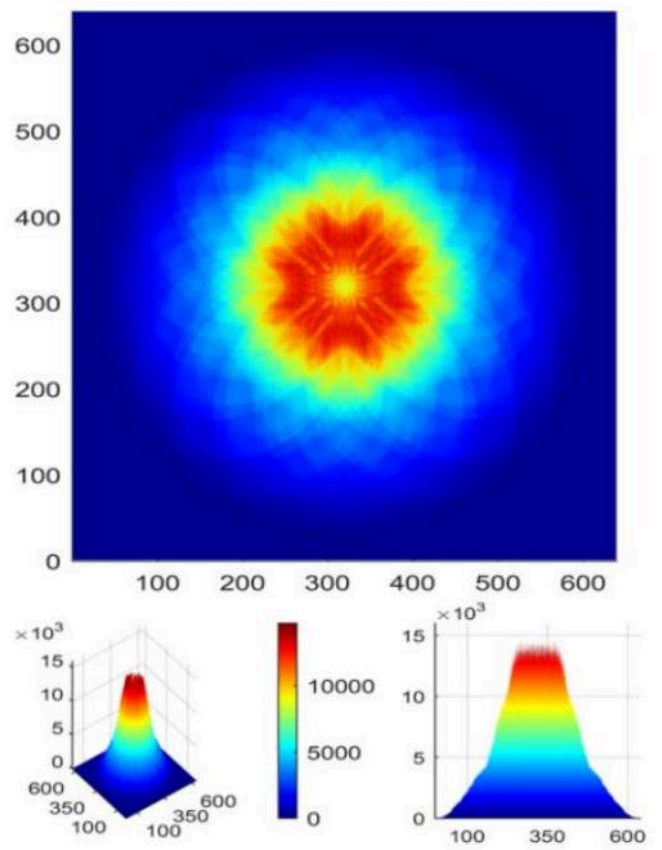
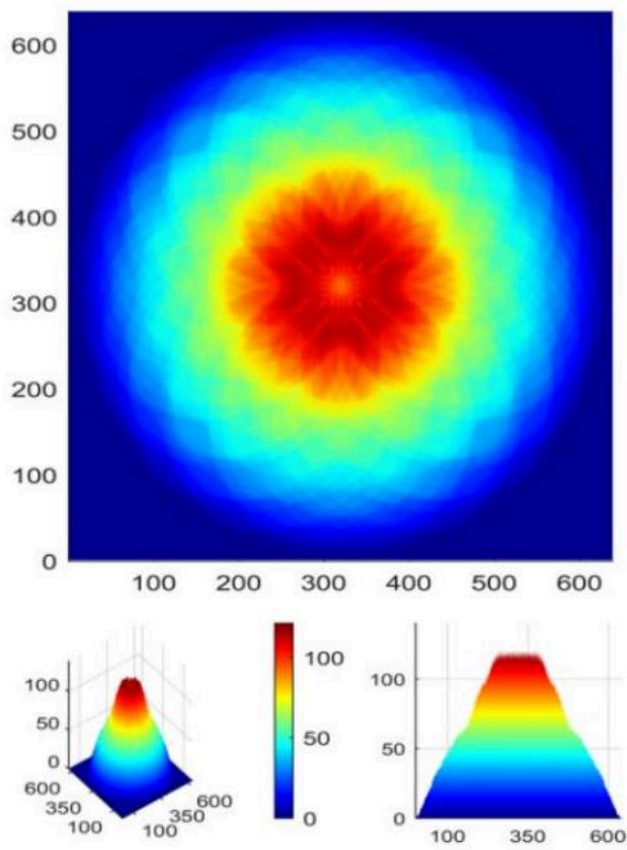


Figure 38: Fig.37. Strength  $E$  (on the left) and intensity  $I$  (on the right) at level  $20h$  ( $0.48 \times 10^{-3}$  m)

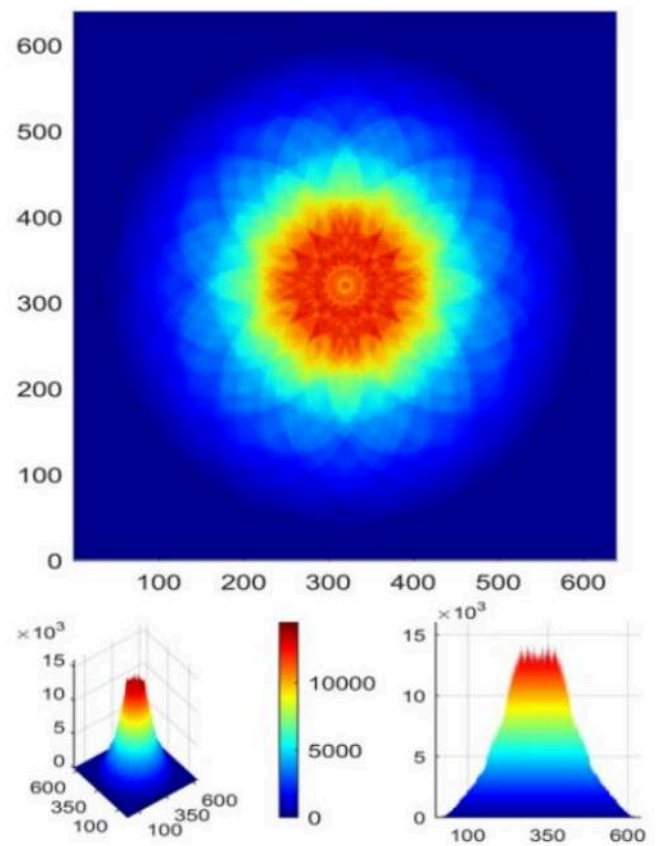
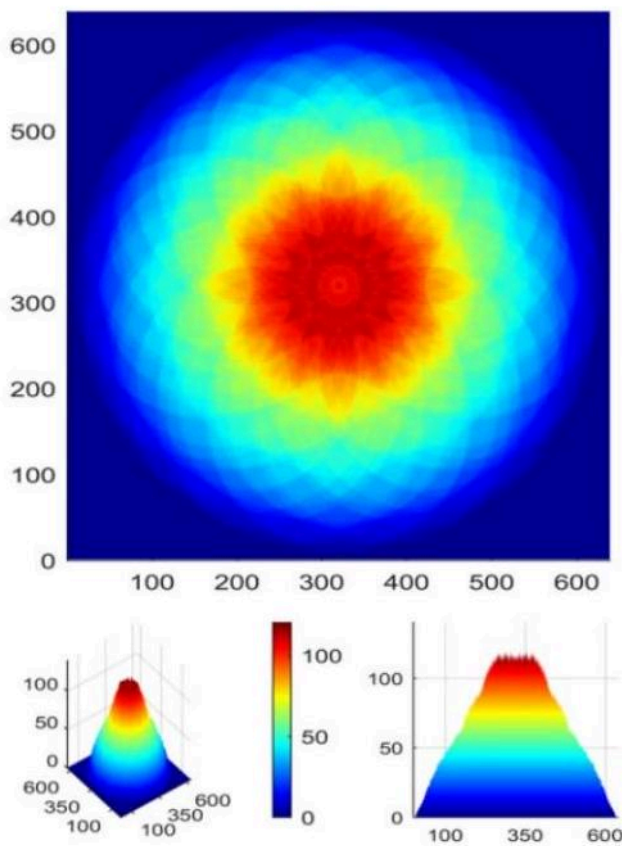
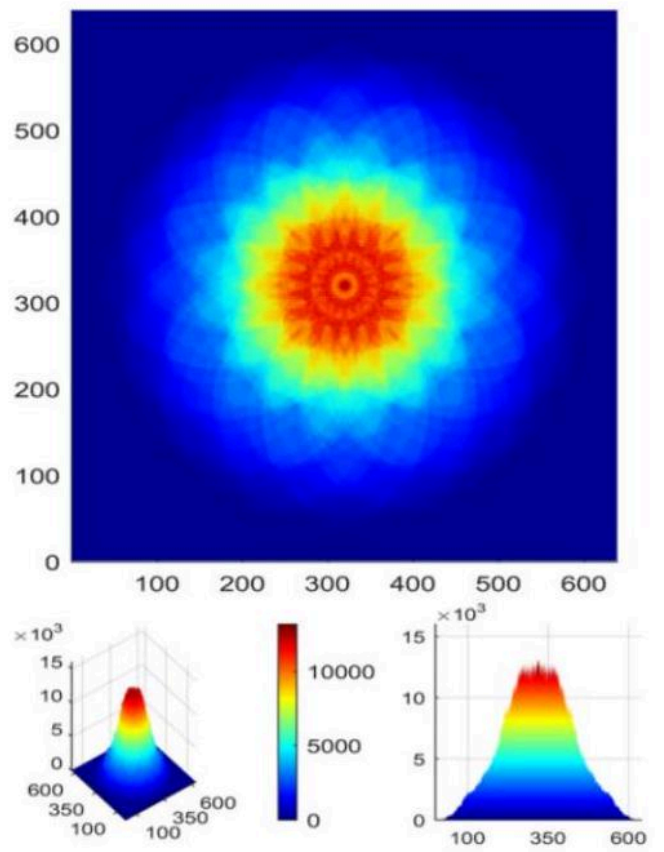
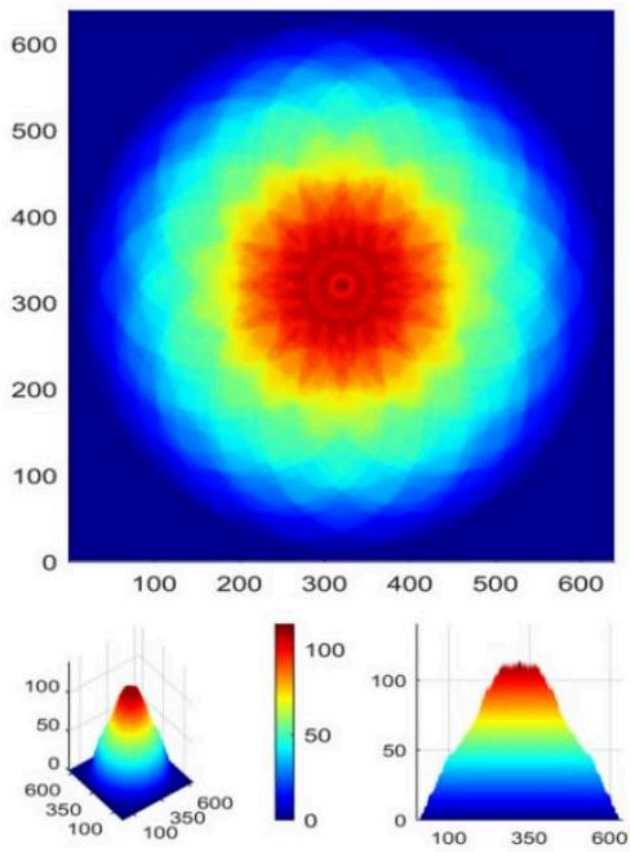
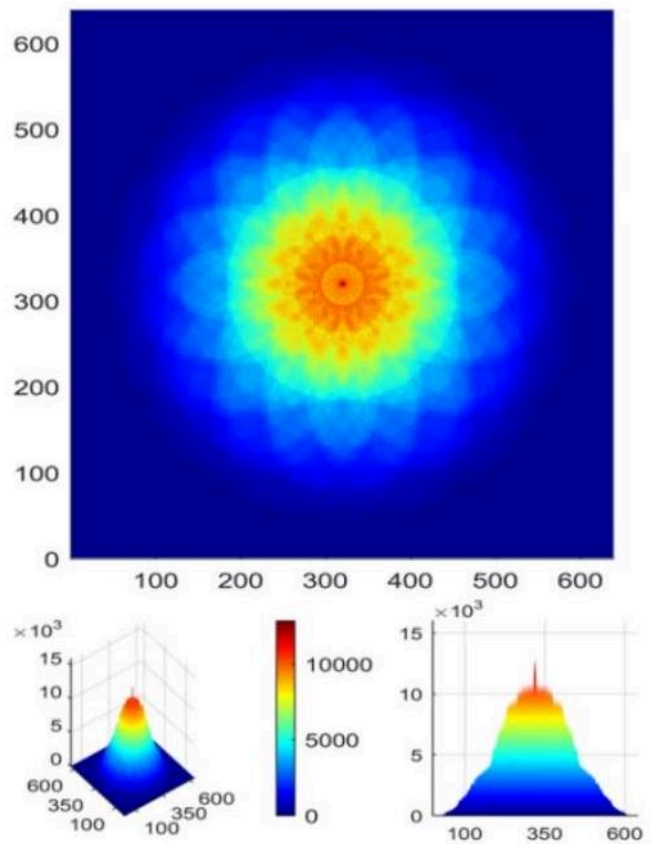
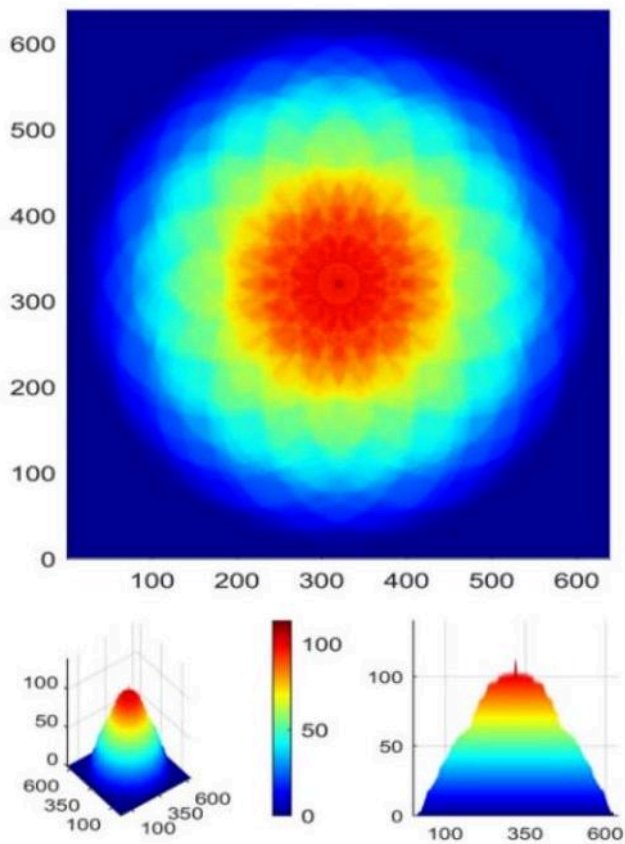


Figure 39: Fig.38. Strength  $E$  (on the left) and intensity  $I$  (on the right) at level  $40h$  ( $0.96 \times 10^{-3}$  m)



\captionsetup{labelformat=empty}

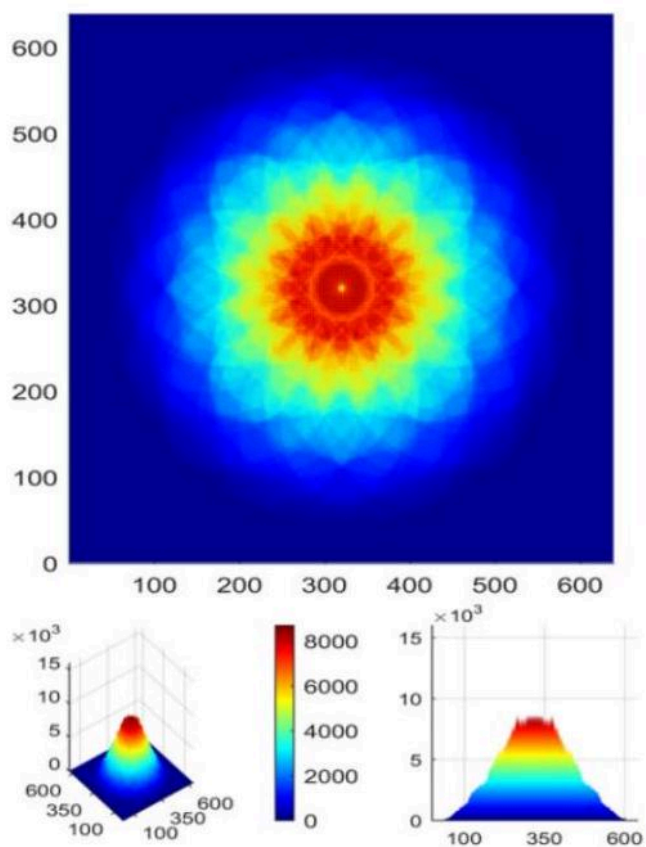
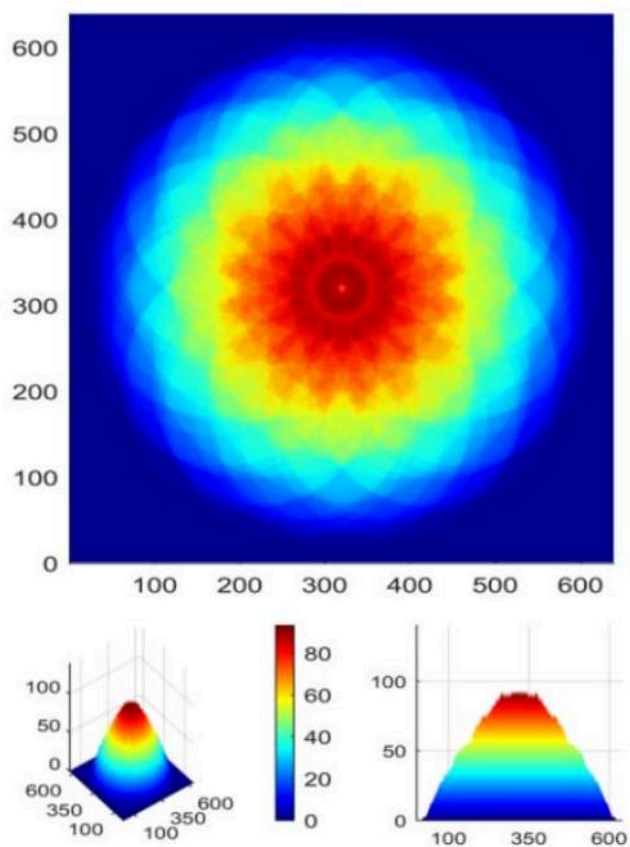
Figure 40: Fig.39. Strength  $E$  (on the left) and intensity  $I$  (on the right) at level 60 h ( $1.44 \times 10^{-3}$  m)



\captionsetup{labelformat=empty}

Figure 41: Fig.40. Strength  $E$  (on the left) and intensity  $I$  (on the right) at level 80h ( $1.92 \times 10^{-3}$  m)

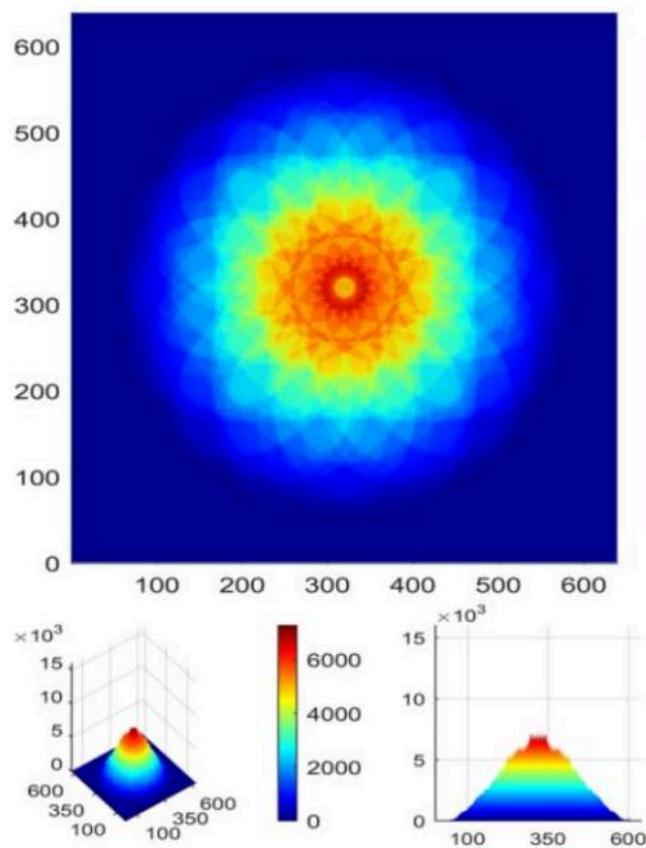
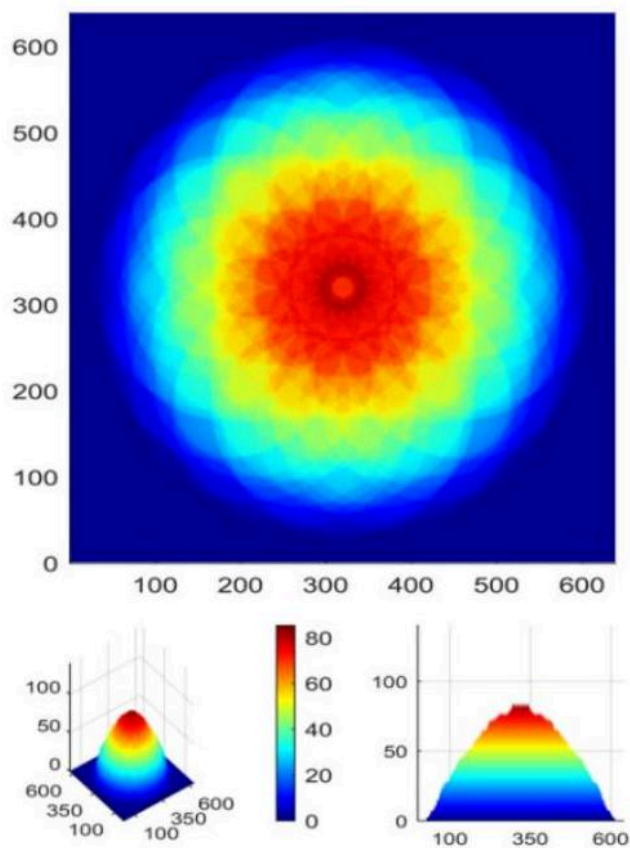




\captionsetup{labelformat=empty}

Figure 42: Fig.41. Strength  $E$  (on the left) and intensity  $I$  (on the right) at level  $100\text{ h}$  ( $2.4 \times 10^{-3}\text{ m}$ )

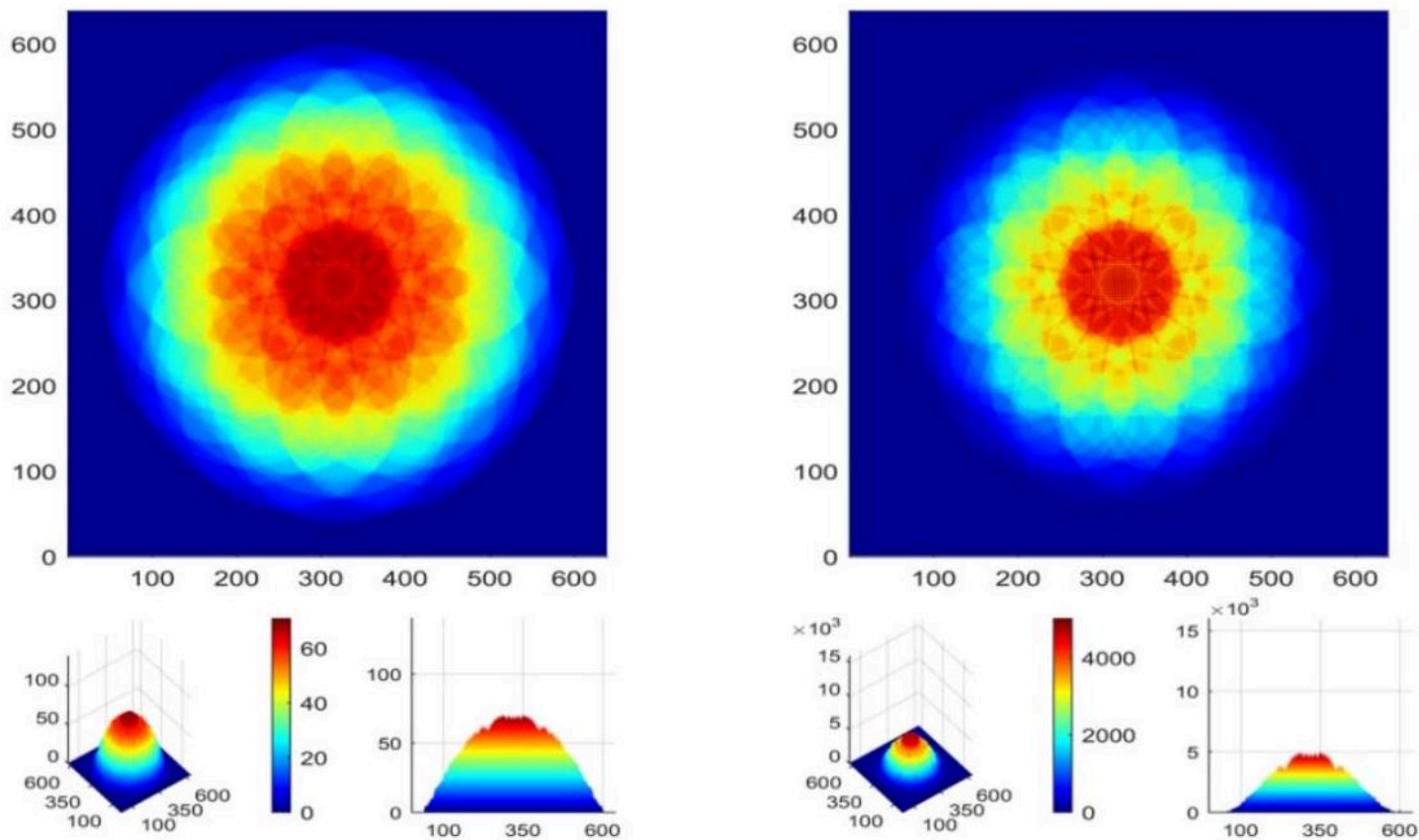
圖 42：圖 41。強度  $E$ （左側）與強度  $I$ （右側）在等級  $100\text{ h}$  ( $2.4 \times 10^{-3}\text{ m}$ )



\captionsetup{labelformat=empty}

Figure 43: Fig.42. Strength  $E$  (on the left) and intensity  $I$  (on the right) at level 120 h ( $2.88 * 10^{-3}$  m)

圖 43：圖 42。強度  $E$ （左側）與強度  $I$ （右側）在等級 120 h ( $2.88 * 10^{-3}$  m)



\captionsetup{labelformat=empty}

Figure 44: Fig.43. Strength  $E$  (on the left) and intensity  $I$  (on the right) at level 140 h ( $3.36 * 10^{-3}$  m)

圖 44：圖 43。強度  $E$ （左側）與強度  $I$ （右側）在等級 140 h ( $3.36 * 10^{-3}$  m)

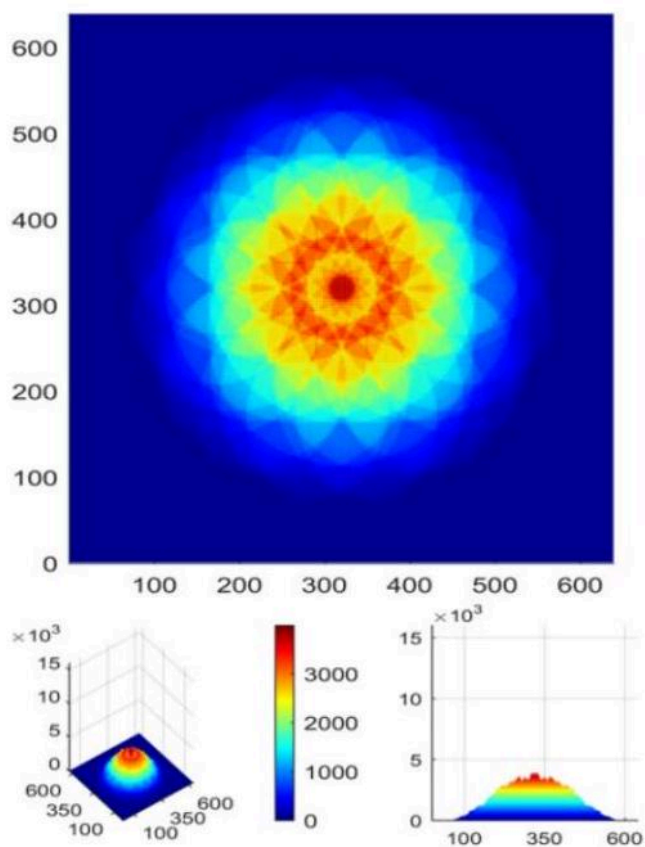
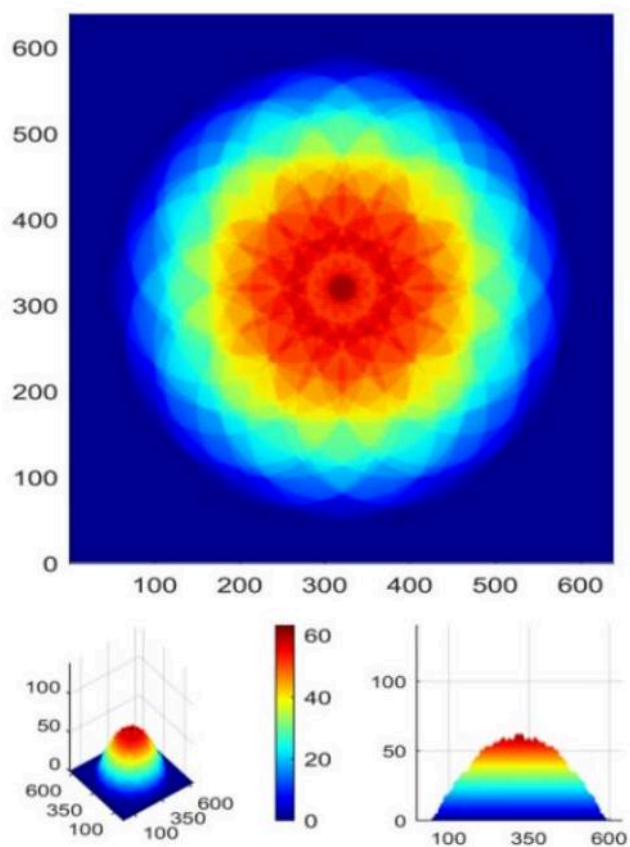


Figure 45: Fig.44. Strength  $E$  (on the left) and intensity  $I$  (on the right) at level 160 h ( $3.84 \times 10^{-3}$  m)

圖 45：圖 44。強度  $E$ （左）與強度  $I$ （右），在等級 160 h ( $3.84 \times 10^{-3}$  m)

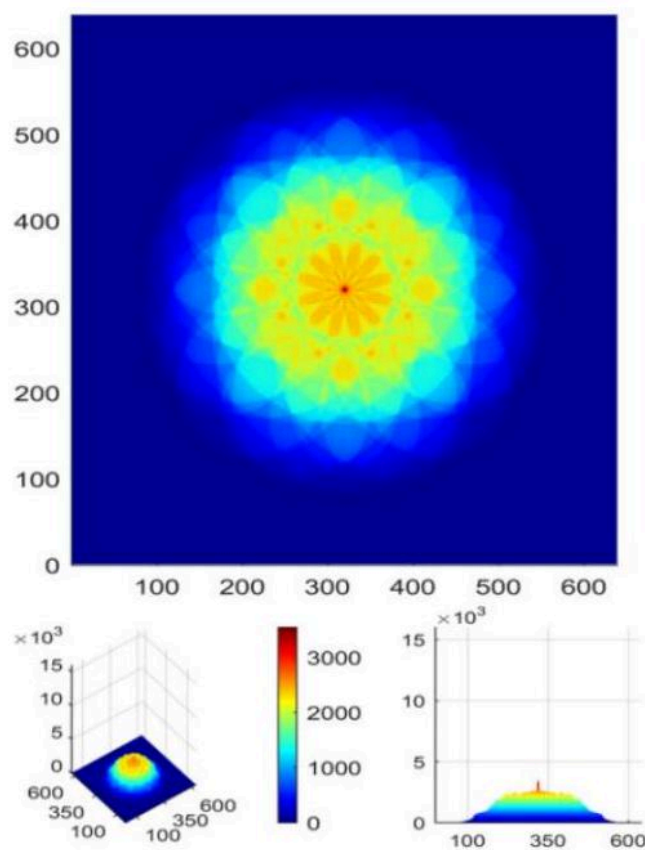
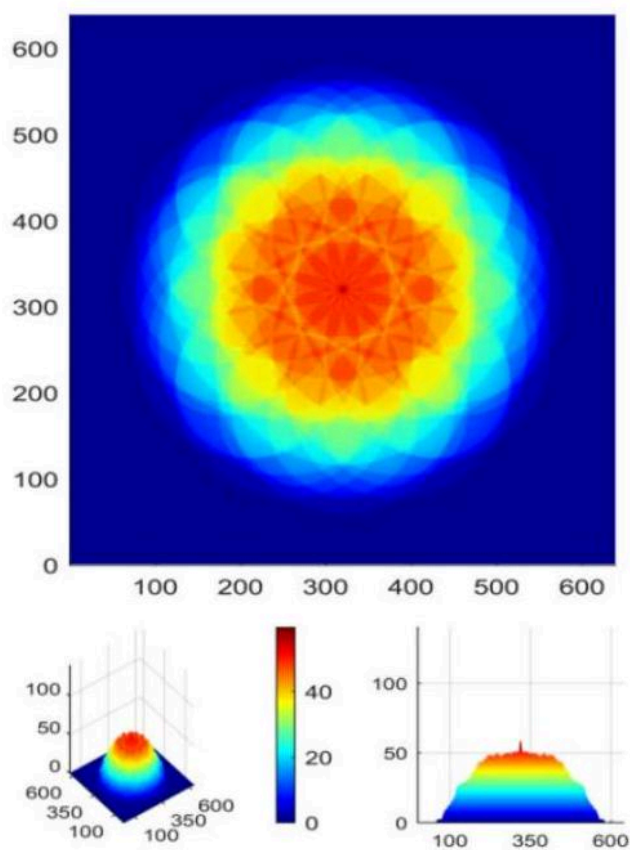
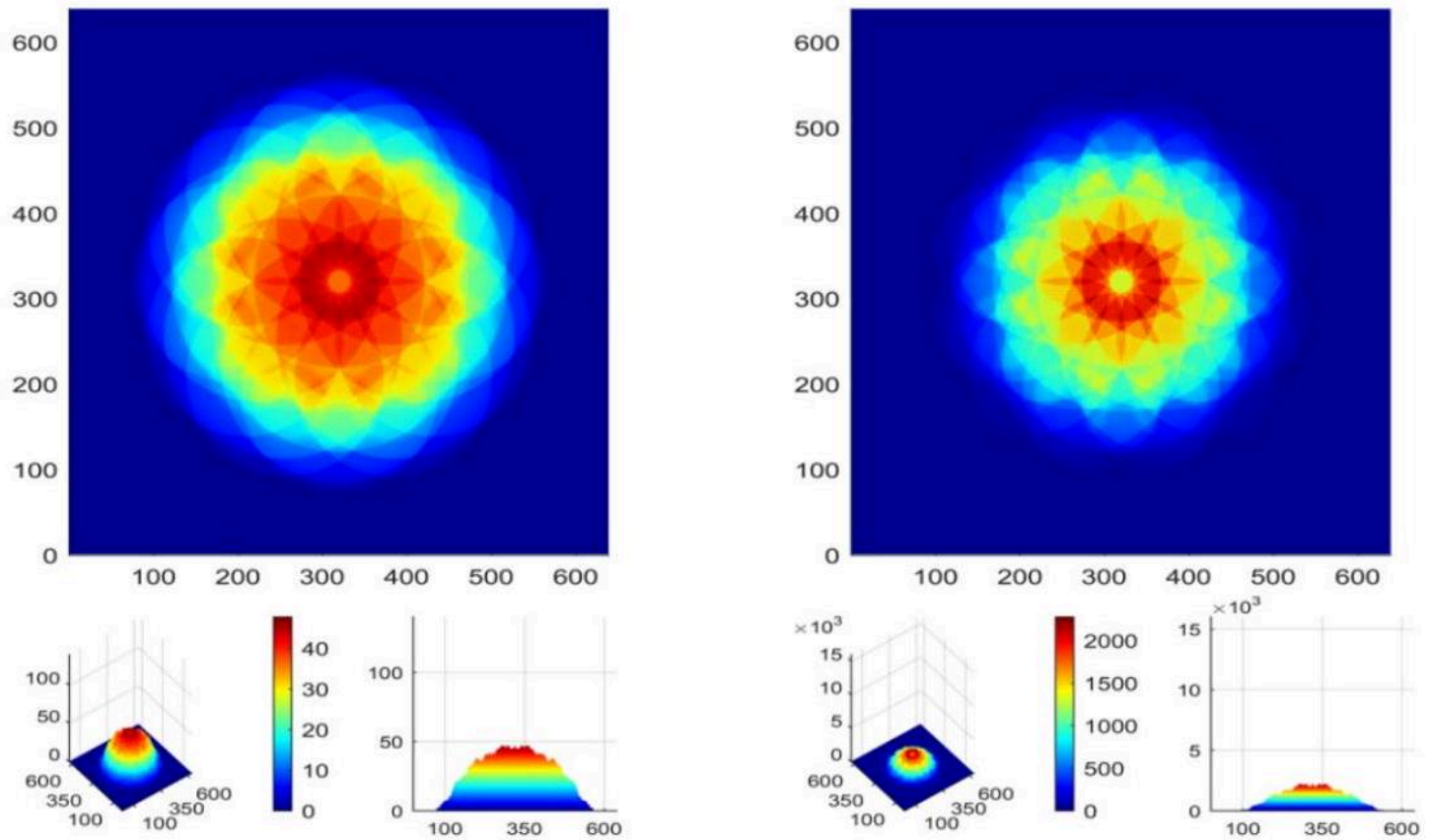




Figure 46: Fig.45. Strength  $E$  (on the left) and intensity  $I$  (on the right) at level  $180\text{ h}$  ( $4.32 \times 10^{-3}\text{ m}$ )

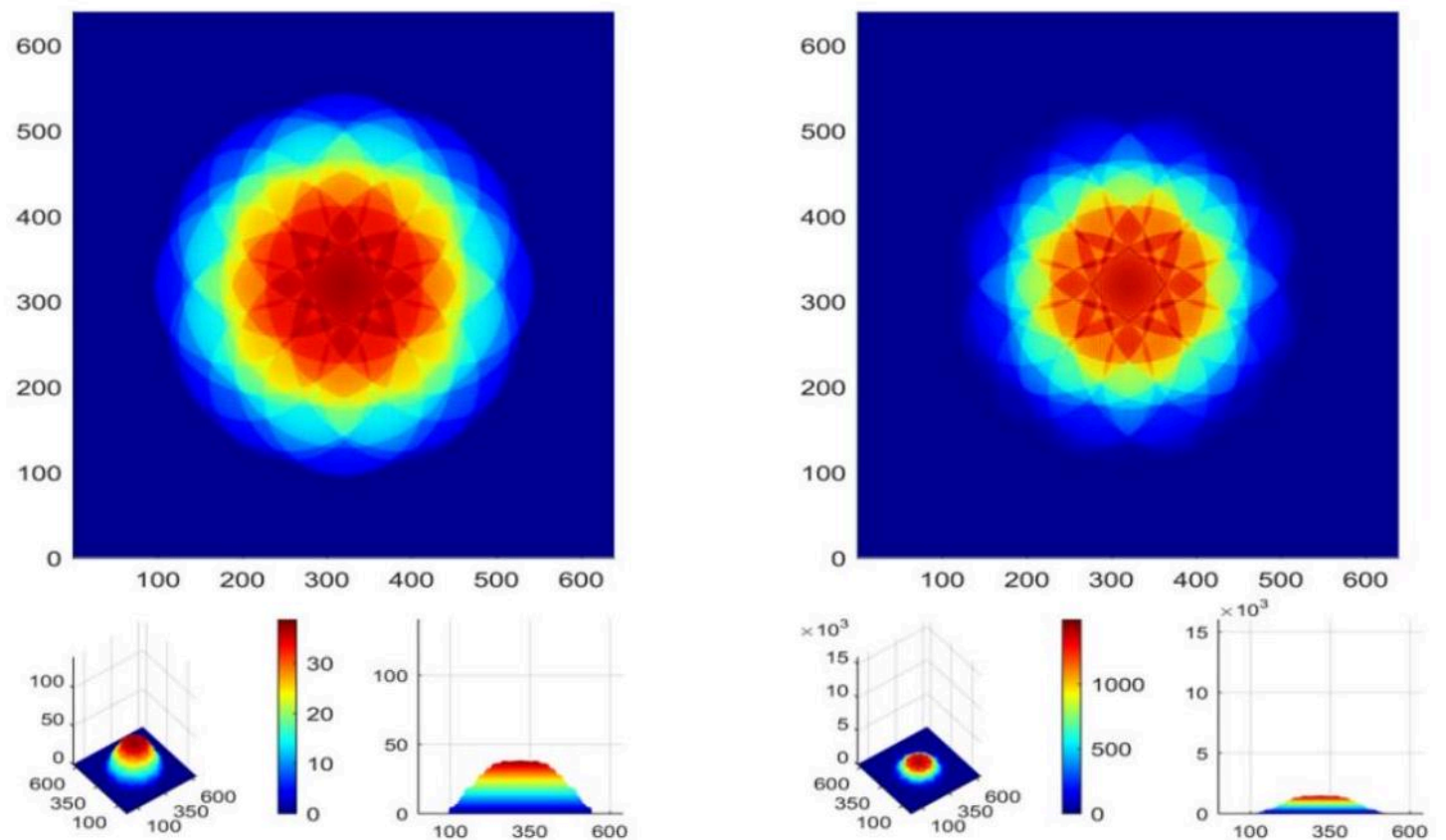
圖 46：圖 45。強度  $E$ （左側）與強度  $I$ （右側）在等級  $180\text{ h}$  ( $4.32 \times 10^{-3}\text{ m}$ )



\captionsetup{labelformat=empty}

Figure 47: Fig.46. Strength  $E$  (on the left) and intensity  $I$  (on the right) at level  $200\text{ h}$  ( $4.8 \times 10^{-3}\text{ m}$ )

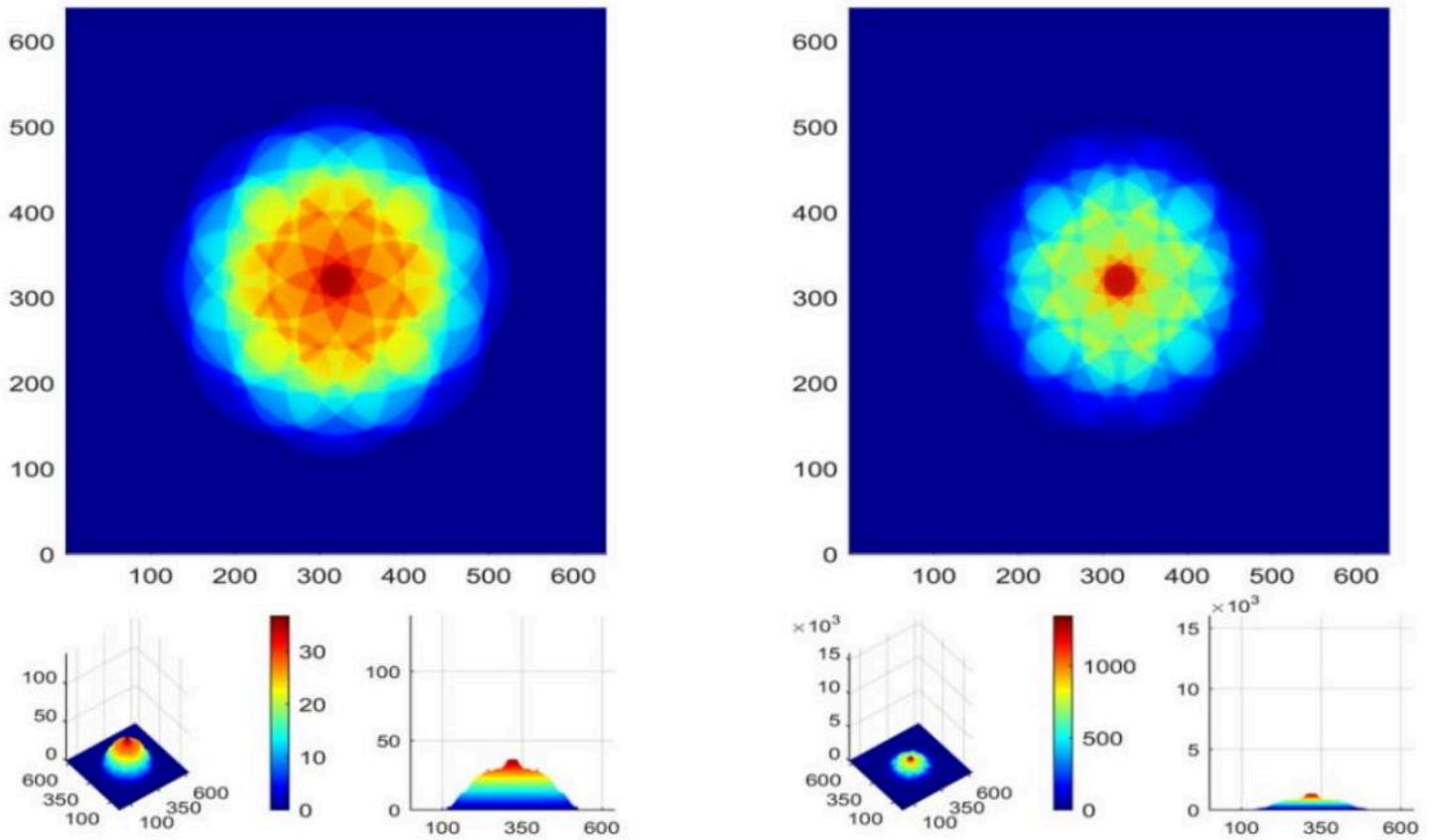
圖 47：圖 46。強度  $E$ （左側）與強度  $I$ （右側）在等級  $200\text{ h}$  ( $4.8 \times 10^{-3}\text{ m}$ )



\captionsetup{labelformat=empty}

Figure 48: Fig.47. Strength  $E$  (on the left) and intensity  $I$  (on the right) at level 220 h ( $5.28 \times 10^{-3}$  m)

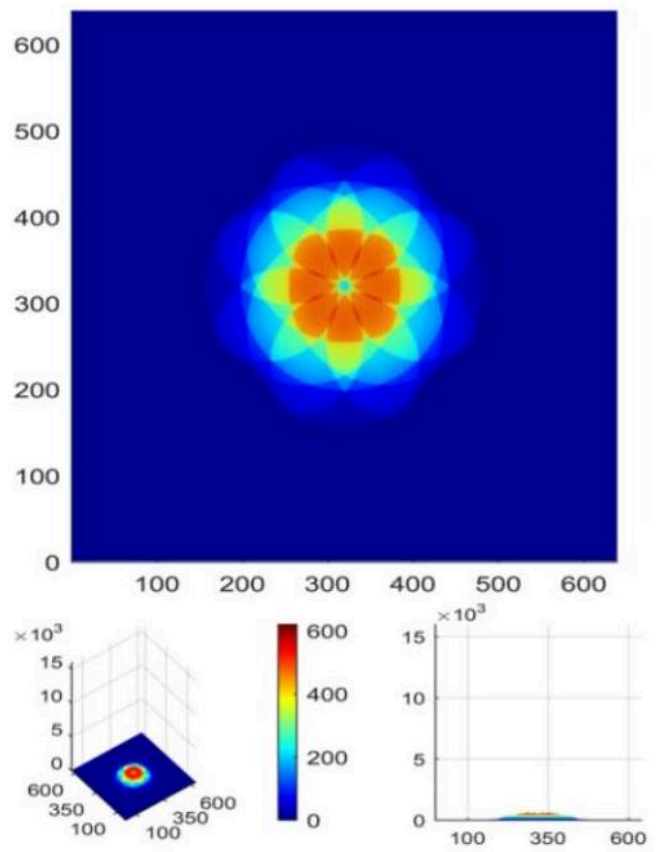
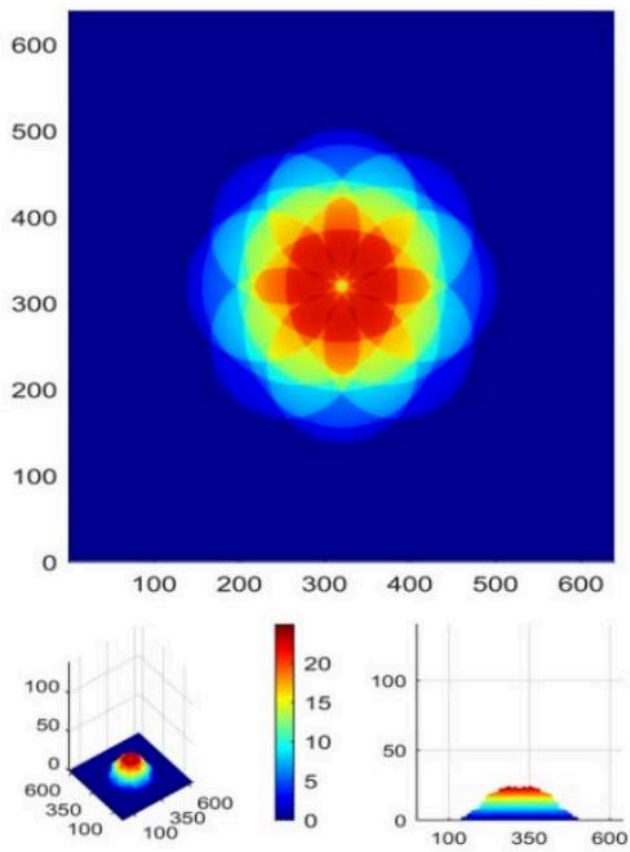
圖 48：圖 47。強度  $E$ （左側）與強度  $I$ （右側）在等級 220 h ( $5.28 \times 10^{-3}$  m)



\captionsetup{labelformat=empty}

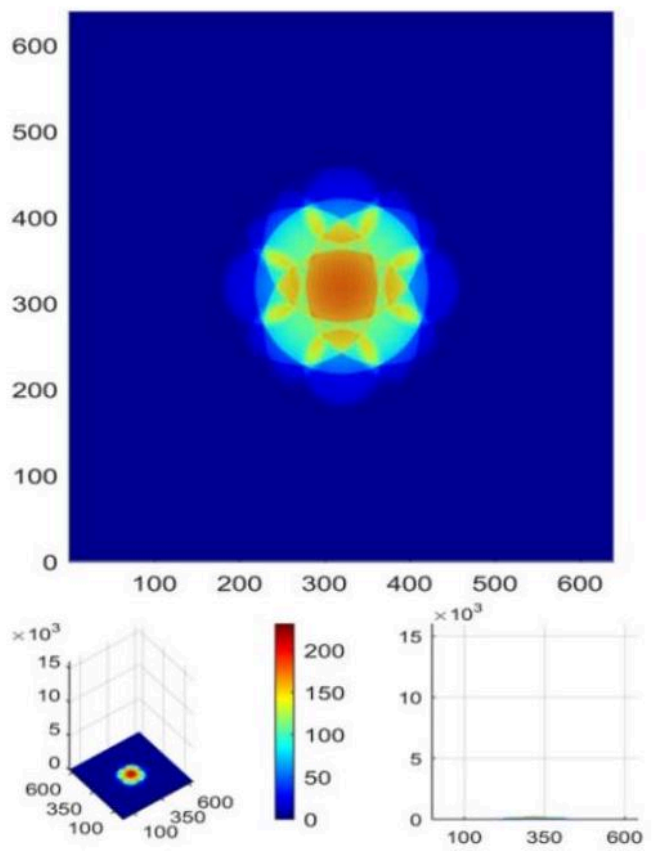
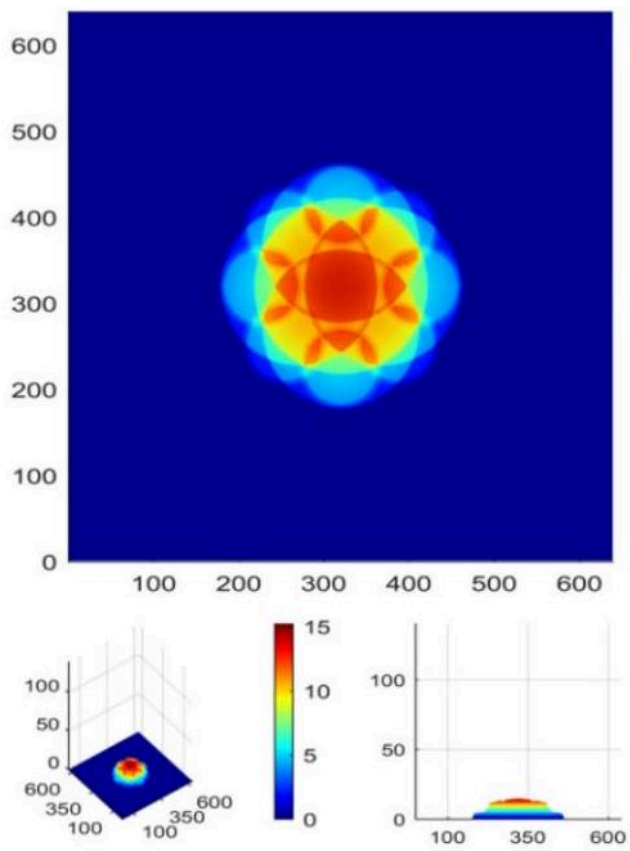
Figure 49: Fig.48. Strength  $E$  (on the left) and intensity  $I$  (on the right) at level 240 h ( $5.76 \times 10^{-3}$  m)

圖 49：圖 48。強度  $E$ （左側）與強度  $I$ （右側）在等級 240 h ( $5.76 \times 10^{-3}$  m)



\captionsetup{labelformat=empty}

Figure 50: Fig.49. Strength  $E$  (on the left) and intensity  $I$  (on the right) at level 260 h ( $6.24 \times 10^{-3}$  m)



\captionsetup{labelformat=empty}

Figure 51: Fig.50. Strength  $E$  (on the left) and intensity  $I$  (on the right) at level 280 h ( $6.72 \times 10^{-3}$  m)

圖 51：圖 50。強度  $E$ （左）與強度  $I$ （右）在等級 280 h ( $6.72 \times 10^{-3}$  m)



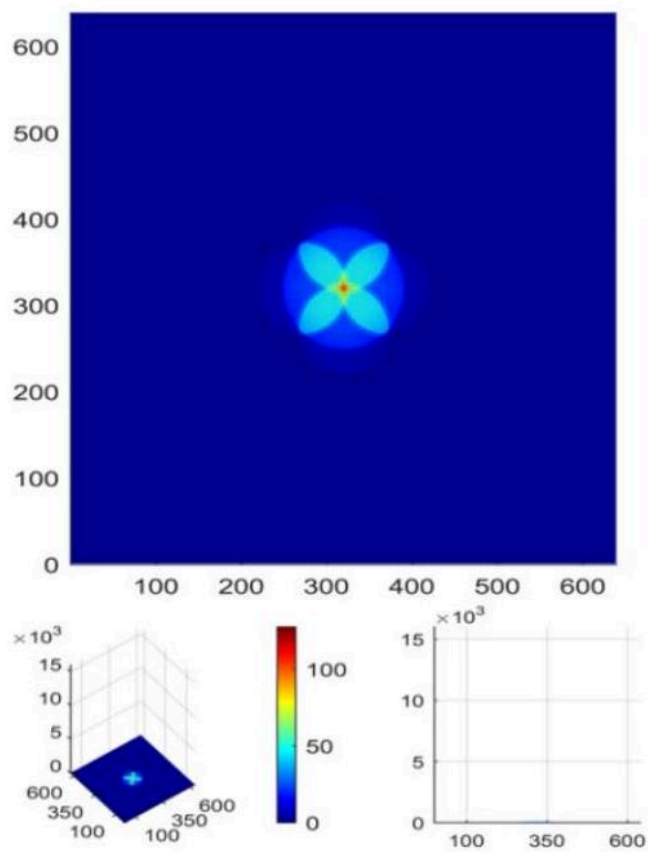
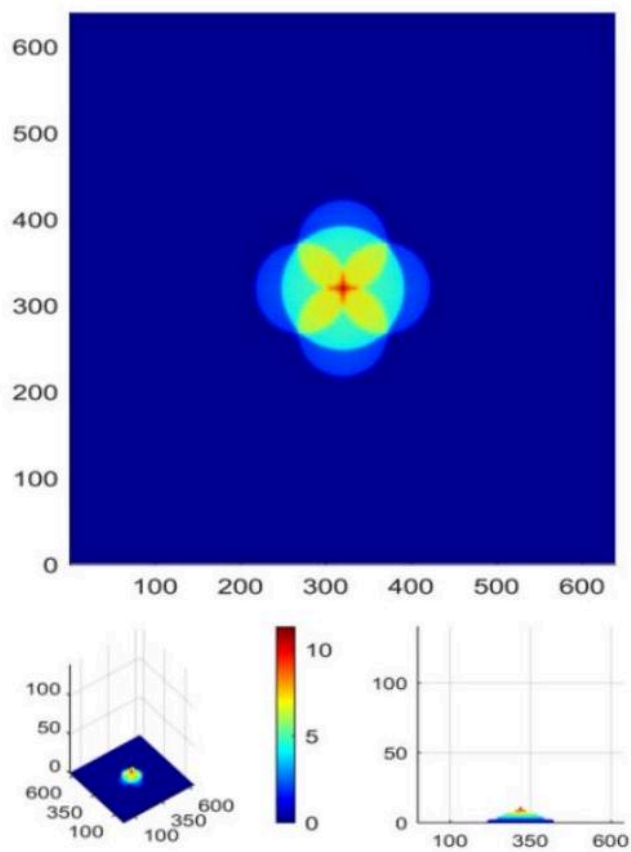


Figure 52: Fig.51. Strength  $E$  (on the left) and intensity  $I$  (on the right) at level 300 h ( $7.2 \times 10^{-3}$  m)

圖 52：圖 51。強度  $E$ （左）與強度  $I$ （右）在等級 300 h ( $7.2 \times 10^{-3}$  m)

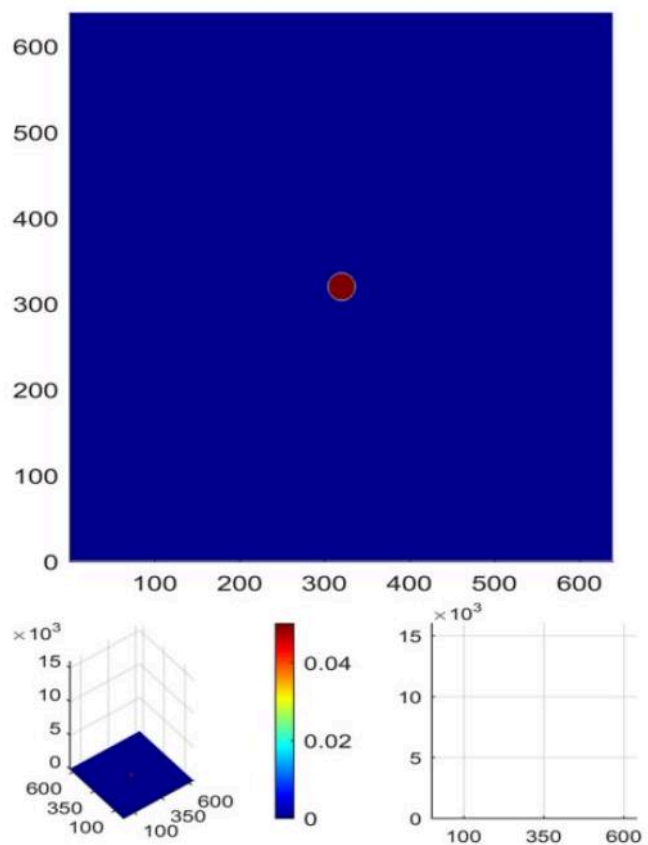
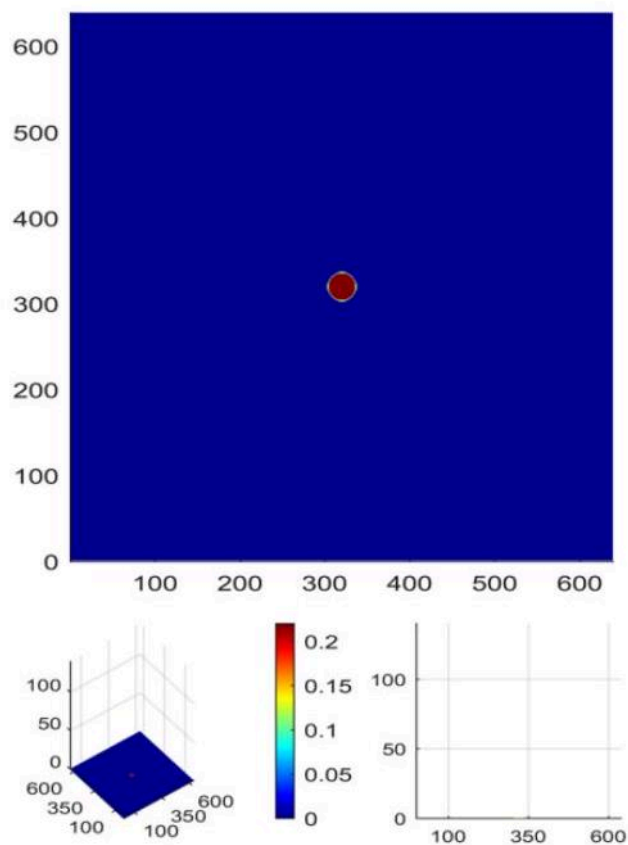


Figure 53: Fig.52. Strength  $E$  (on the left) and intensity  $I$  (on the right) at level  $318h$  ( $7.632 * 10^{-3}$  m)

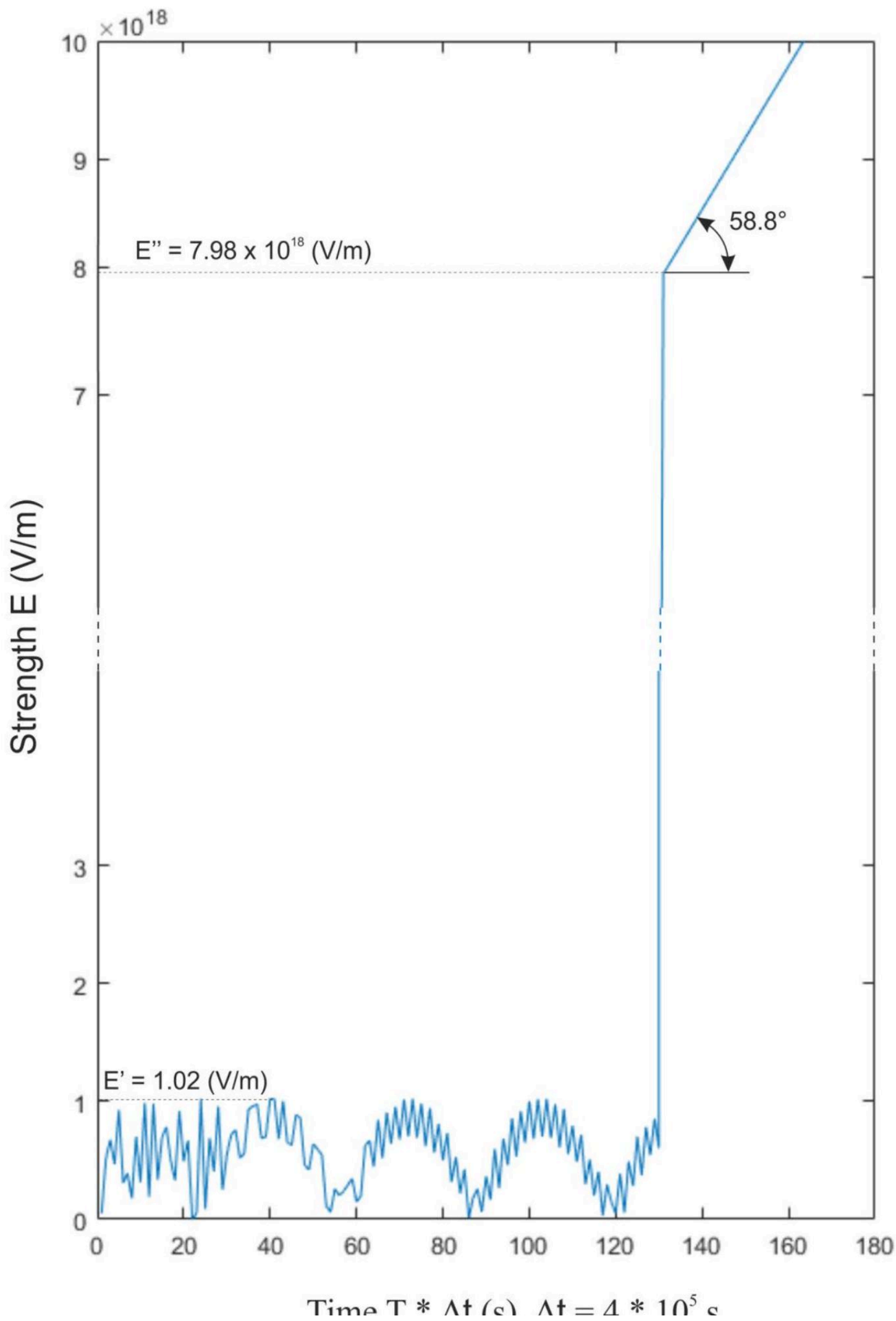
圖 53：圖 52。強度  $E$ （左）與強度  $I$ （右）在等級  $318h$  ( $7.632 * 10^{-3}$  m)

The presented images (Figures 37-52) objectively reflect the resulting wave superposition and confirm the nature of the dynamics of strength  $E$  and intensity  $I$  of the electromagnetic field described earlier.

所呈現的影像（圖 37–52）客觀地反映了最終波的疊加，並證實先前所描述的電磁場強度  $E$  與強度  $I$  動態的性質。

When calculating the C20S5G resonator's interaction with incident radiation at a frequency of 28 GHz, analysis of the electric field strength  $E$  above the central point of the circuit at a height  $h = 24 * 10^{-6}$  mm was performed over time with various intervals  $\Delta t$  (Figures 53-78) with initial time  $t = 0$  s.

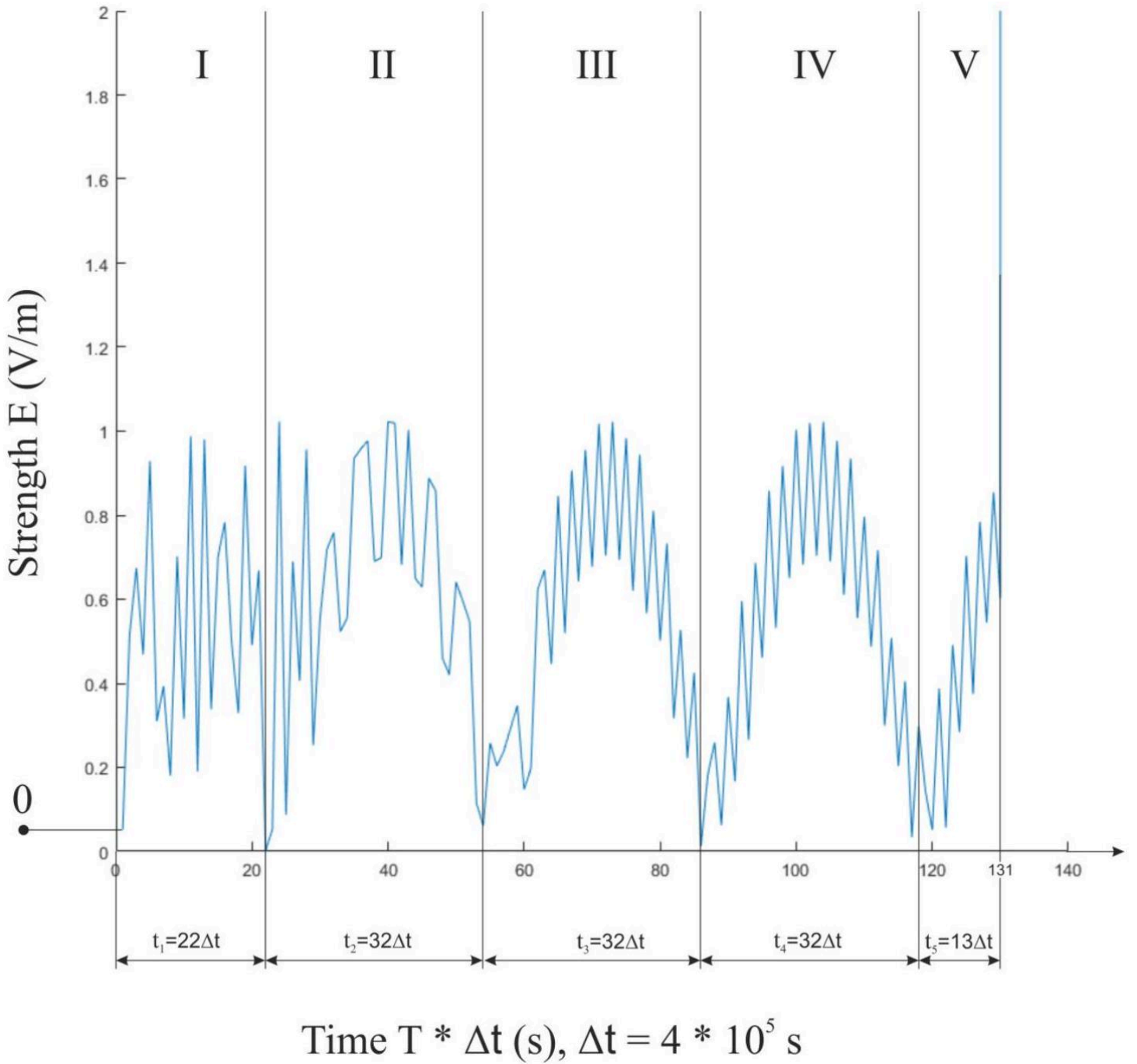
Fig. 53 presents a general graph of the dynamics of the electromagnetic field over time  $E(T)$ , which has a series of successive stages that have characteristic differences from each other, thus making it possible to describe the process in general.





\captionsetup{labelformat=empty}

Figure 54: Fig. 53. General graph of field strength as a function of time:  $E(T)$ , limit when  $t = 131\Delta t$ .




\captionsetup{labelformat=empty}

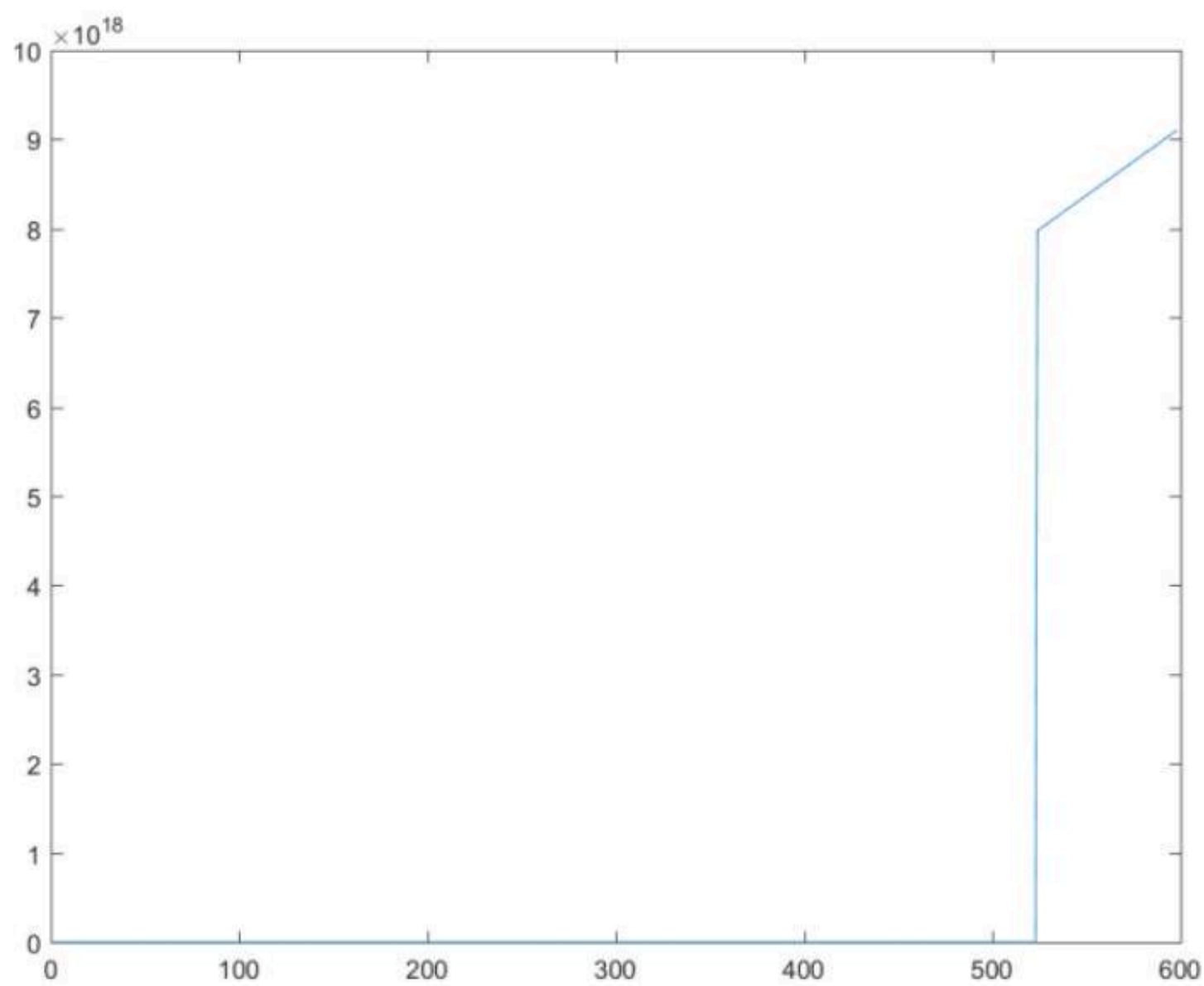
Figure 55: Fig. 54. Fragment of the General graph  $E(T)$  presented on Fig. 53, limit at a  $t = 131\Delta t$ .


Analyzing the graph of field strength  $E$  as a function of time  $T$  over the center point of the Aires C20S5G resonator circuit (Fig. 54) showed that at the first stage (I) of the process, the total modulation of the field strength is rather unstable, while the amplitude dynamics are concentrated relative to the horizontal. The time period of this stage is  $t_1 = 22\Delta t$ . It should also be noted that a regular internal rhythm of subwave categories is present throughout the process.

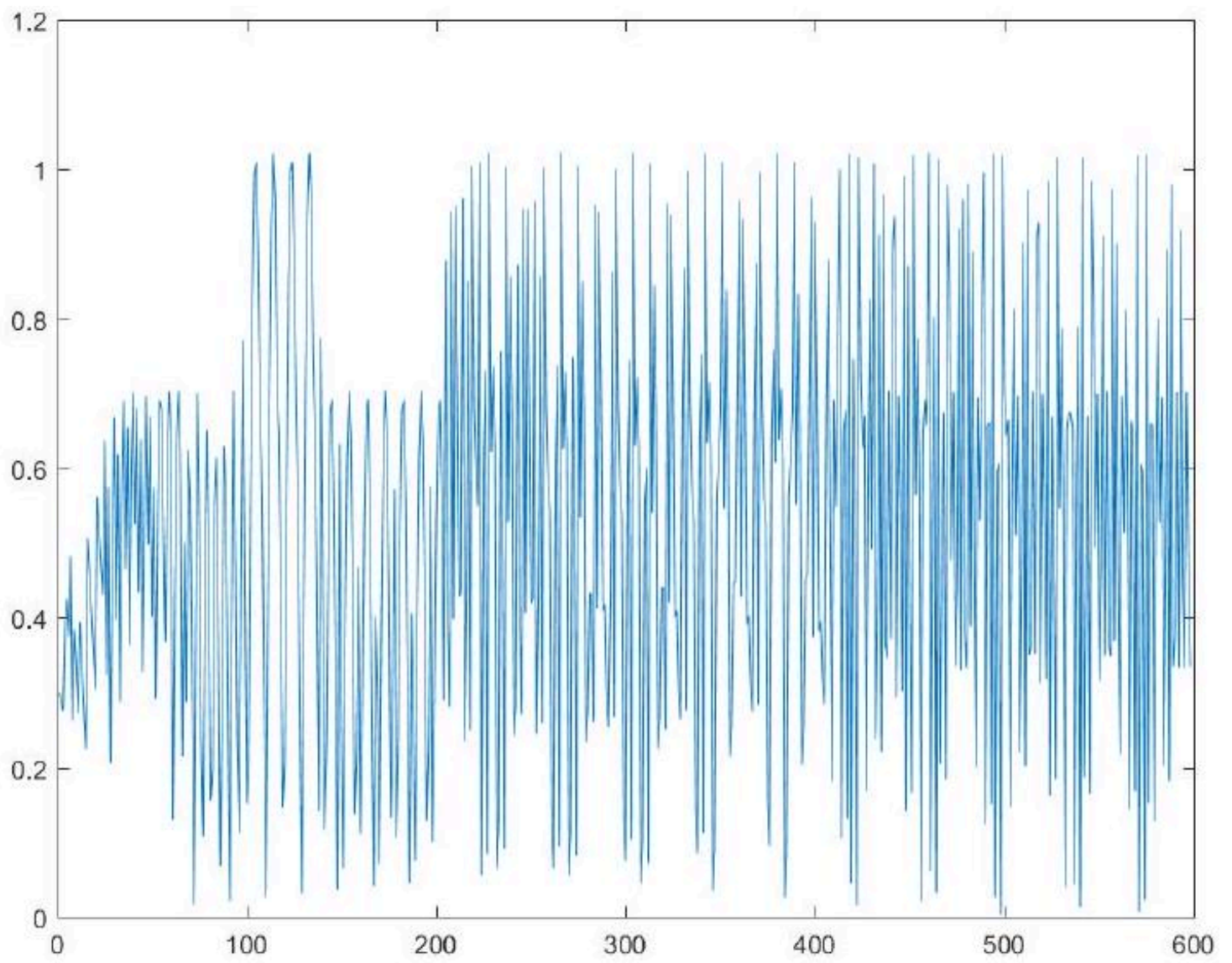
Starting from the second stage (II-IV), the system enters a stable cycle ( $t_2 = 32\Delta t, t_3 = 32\Delta t, t_4 = 32\Delta t$ ), that is characterized by a half-wave sinusoid, i.e. the circuit works as a diode bridge, transforming the variable nature of the cyclic process into a constant form, which also leads to an increase in frequency. Moreover, the total energy of the field does not increase, since otherwise the system will not be able to hold it, but an additional buildup of potential occurs with intrastructural compaction, ordering, and optimization of the structural interrelations of the potential, i.e. the existing structure is taken to the maximum possible level.


At the last stage (V), as seen in Fig. 54, after 13 periods of  $\Delta t$ , the system enters the zone where there is a sharp, instantaneous jump in potential to  $7.98 \cdot 10^{18}$  (V/m). After that, the collection of potential begins to move continuously in

a straight line at an angle of  $\sim 58.8^\circ$  (Fig. 53). This corresponds to the transformation of the entire system to a quantum form. 

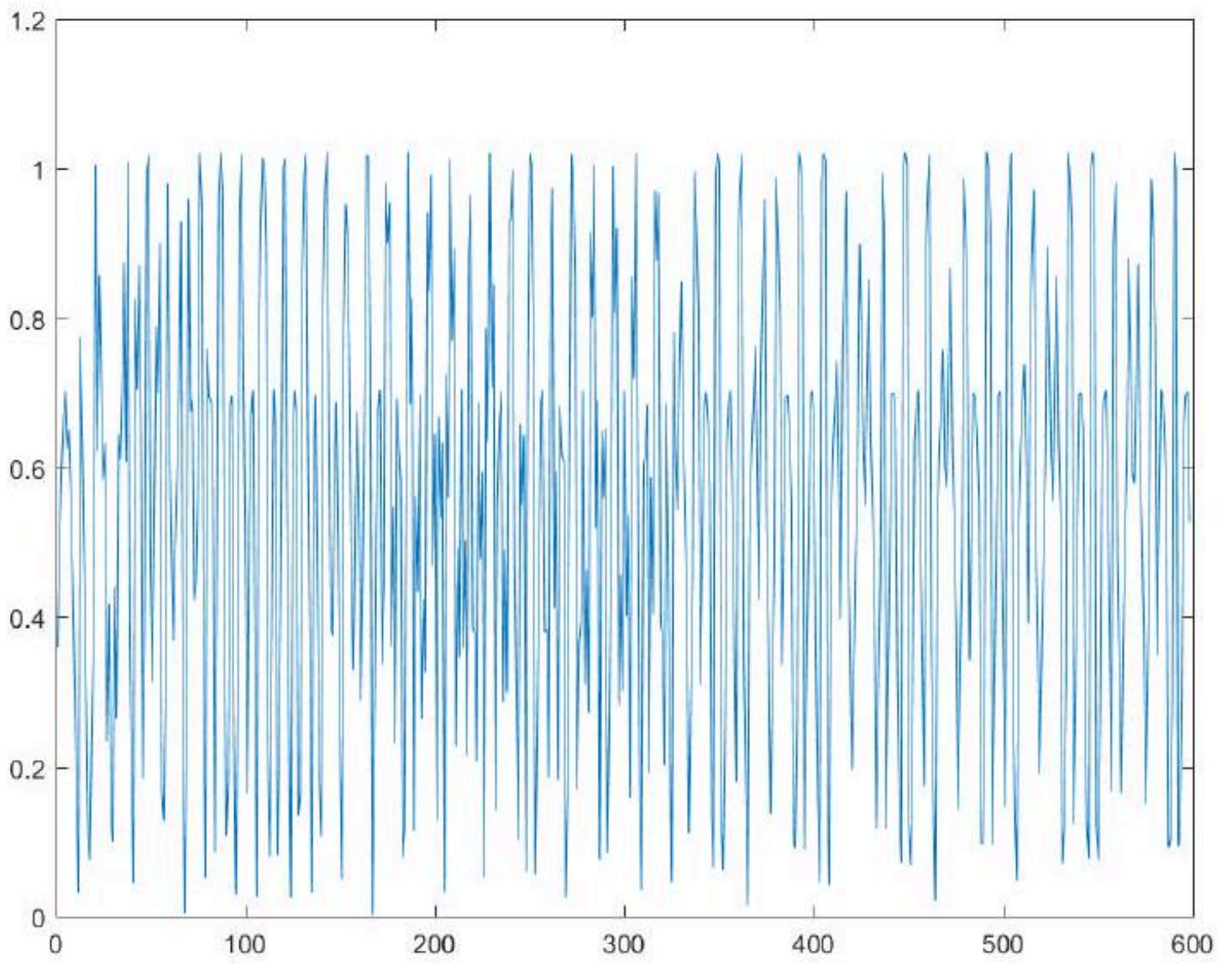


$\captionsetup{labelformat=empty}$   
Figure 56: Fig. 55. Graph of field strength over time  $E(T), \Delta t = 10^5 s$  



\captionsetup{labelformat=empty}  
Figure 57: Fig. 57. Graph of field strength over time  $E(T), \Delta t = 10^3 s$  





\captionsetup{labelformat=empty}  
Figure 58: Fig. 56. Graph of field strength over time  $E(T)$ ,  $\Delta t = 10^4 s$  C

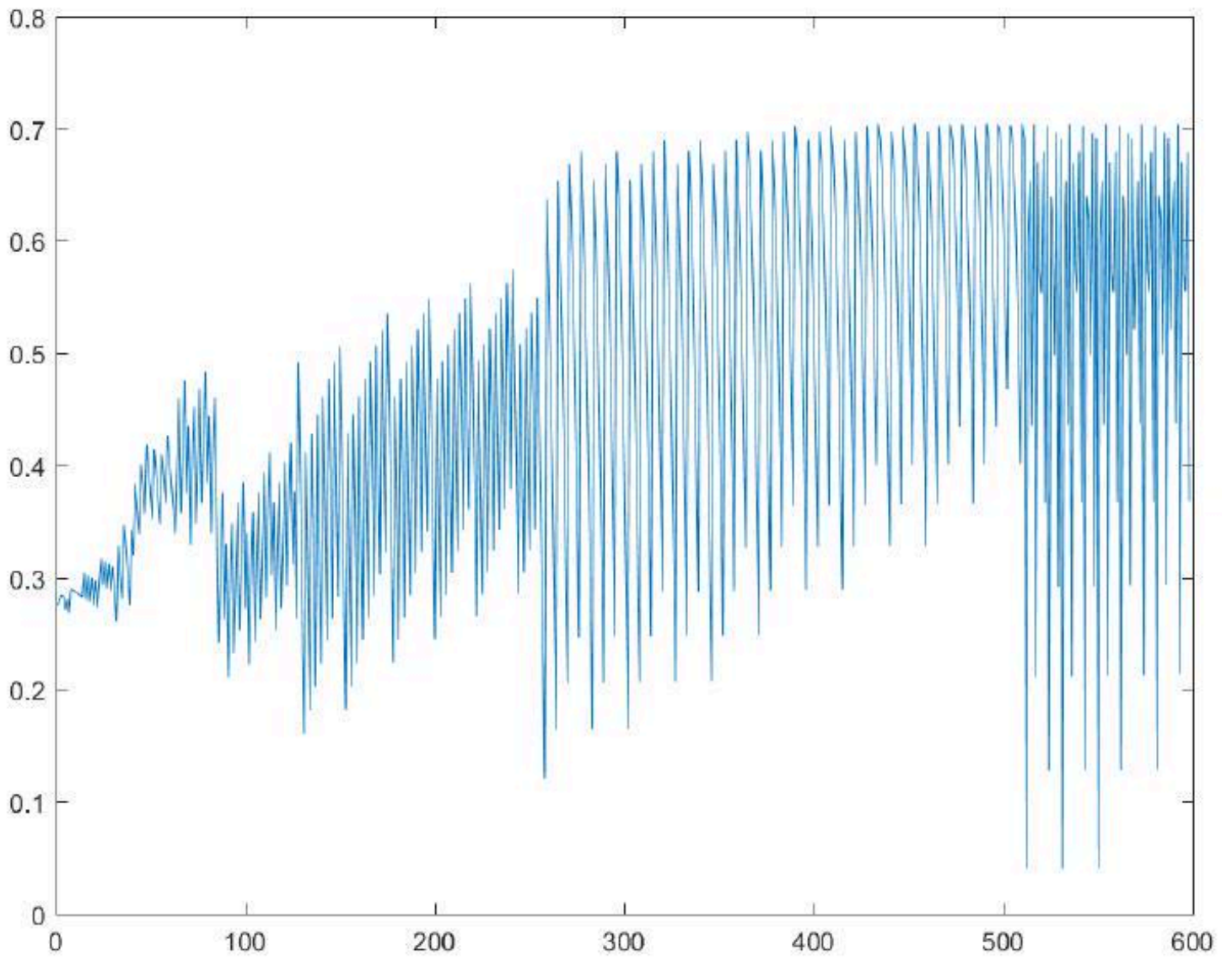


Figure 59: Fig. 58. Graph of field strength over time  $E(T)$ ,  $\Delta t = 10^2 s$

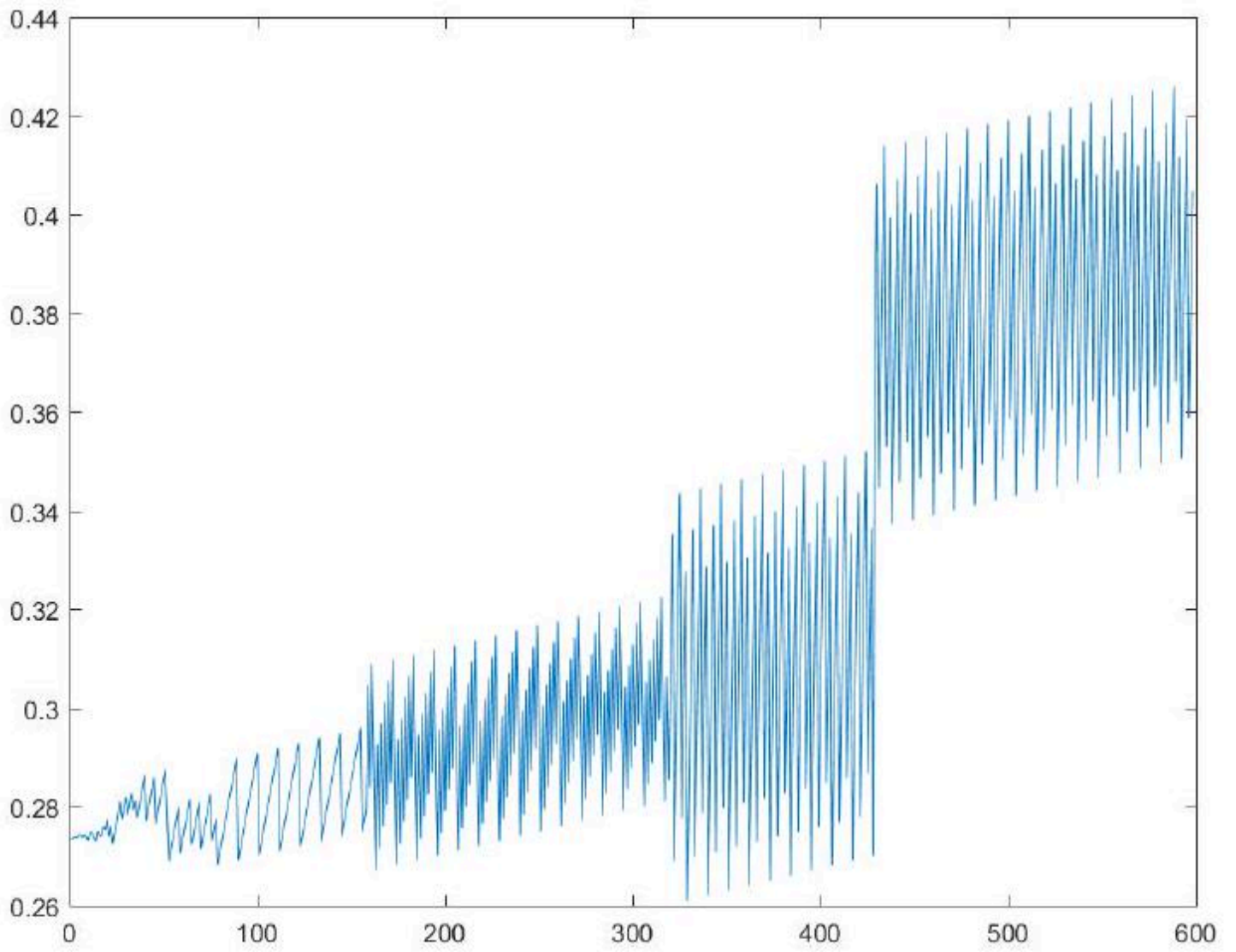
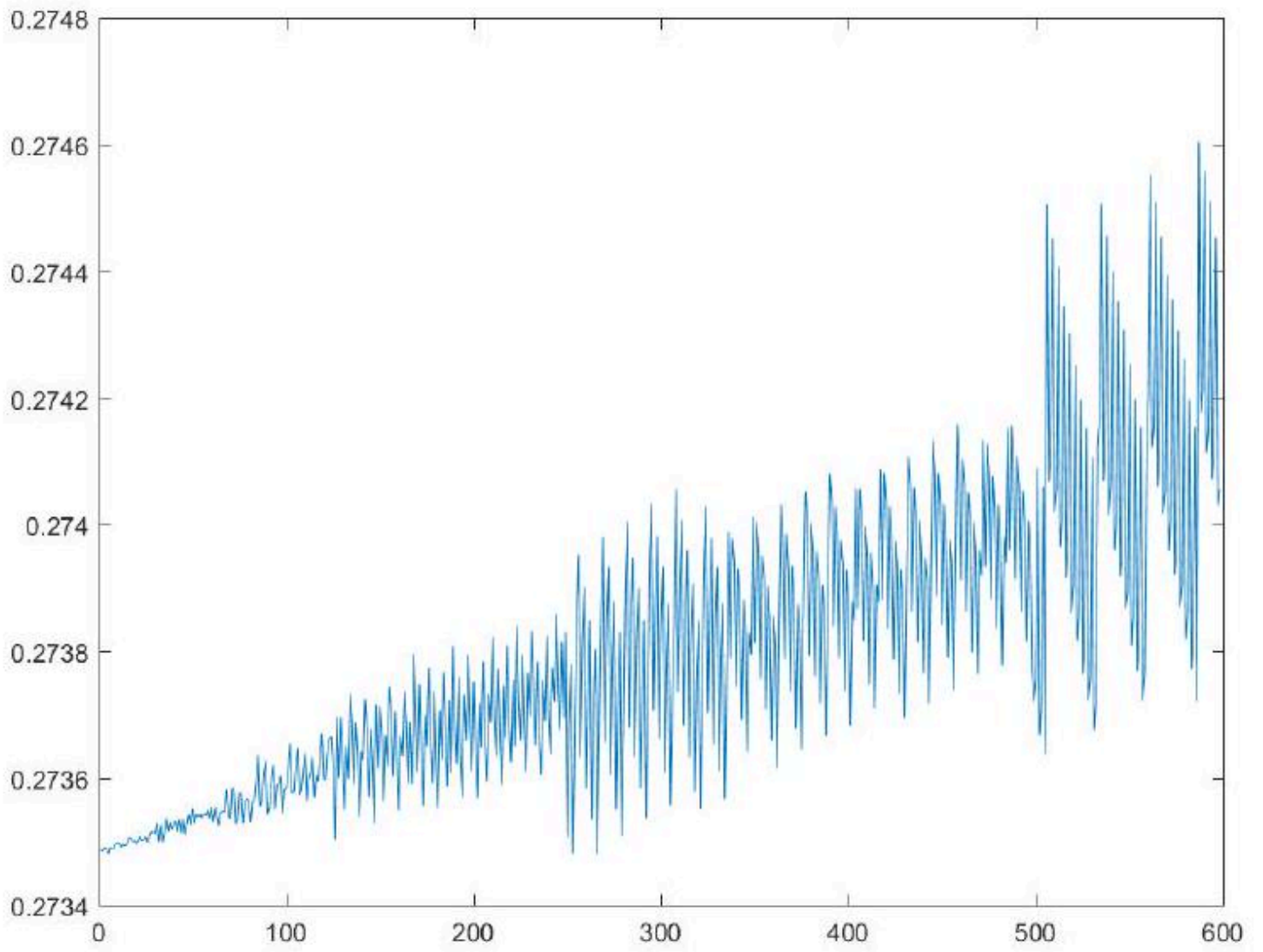

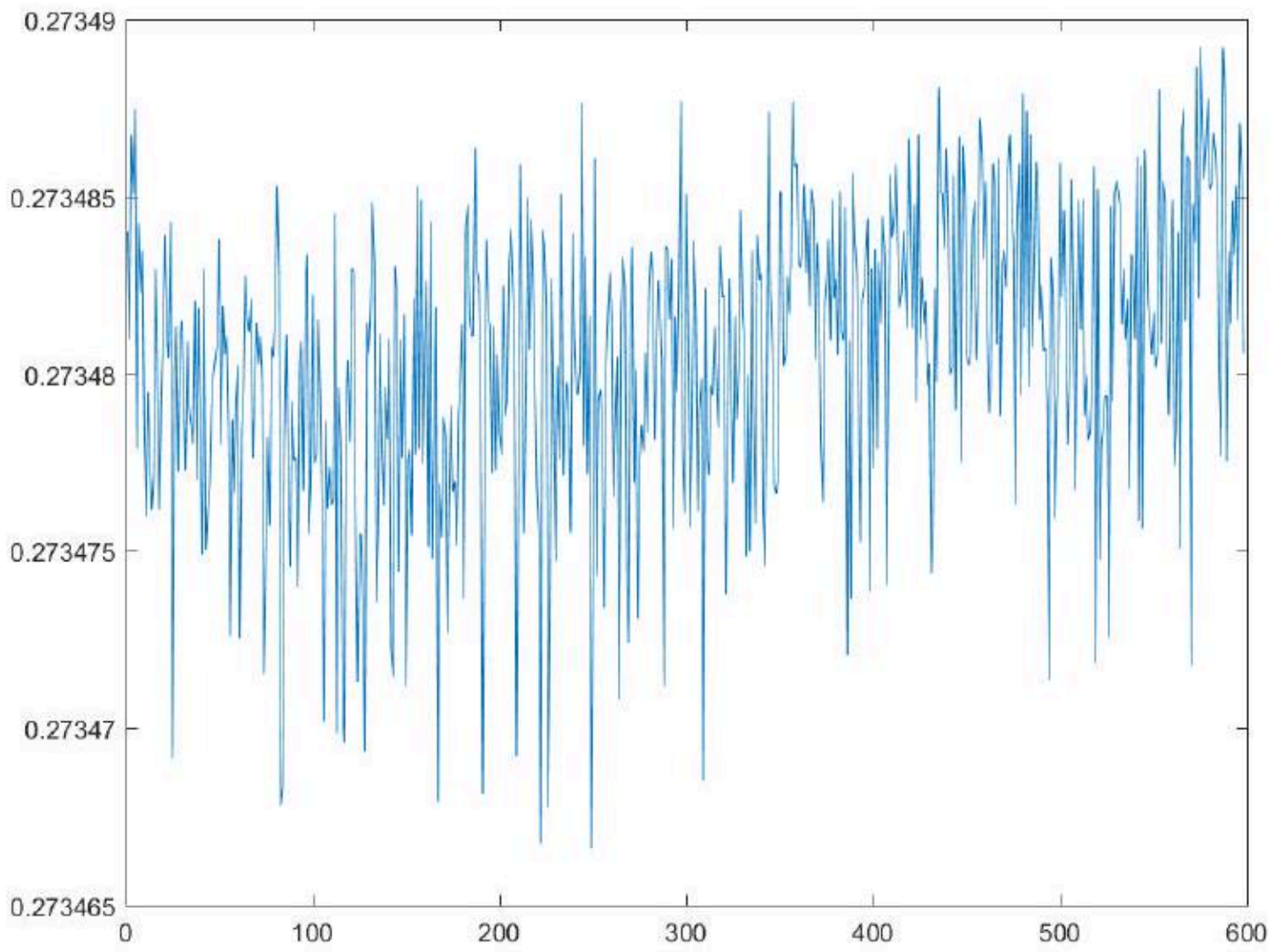



Figure 60: Fig. 59. Graph of field strength over time  $E(T)$ ,  $\Delta t = 10$  s





\captionsetup{labelformat=empty}  
Figure 61: Fig. 61. Graph of field strength over time  $\bar{E}(T)$ ,  $\Delta t = 0.1s$  



\captionsetup{labelformat=empty}  
 Figure 62: Fig. 63. Graph of field strength over time  $\bar{E}(T), \Delta t = 10^{-3}s$  

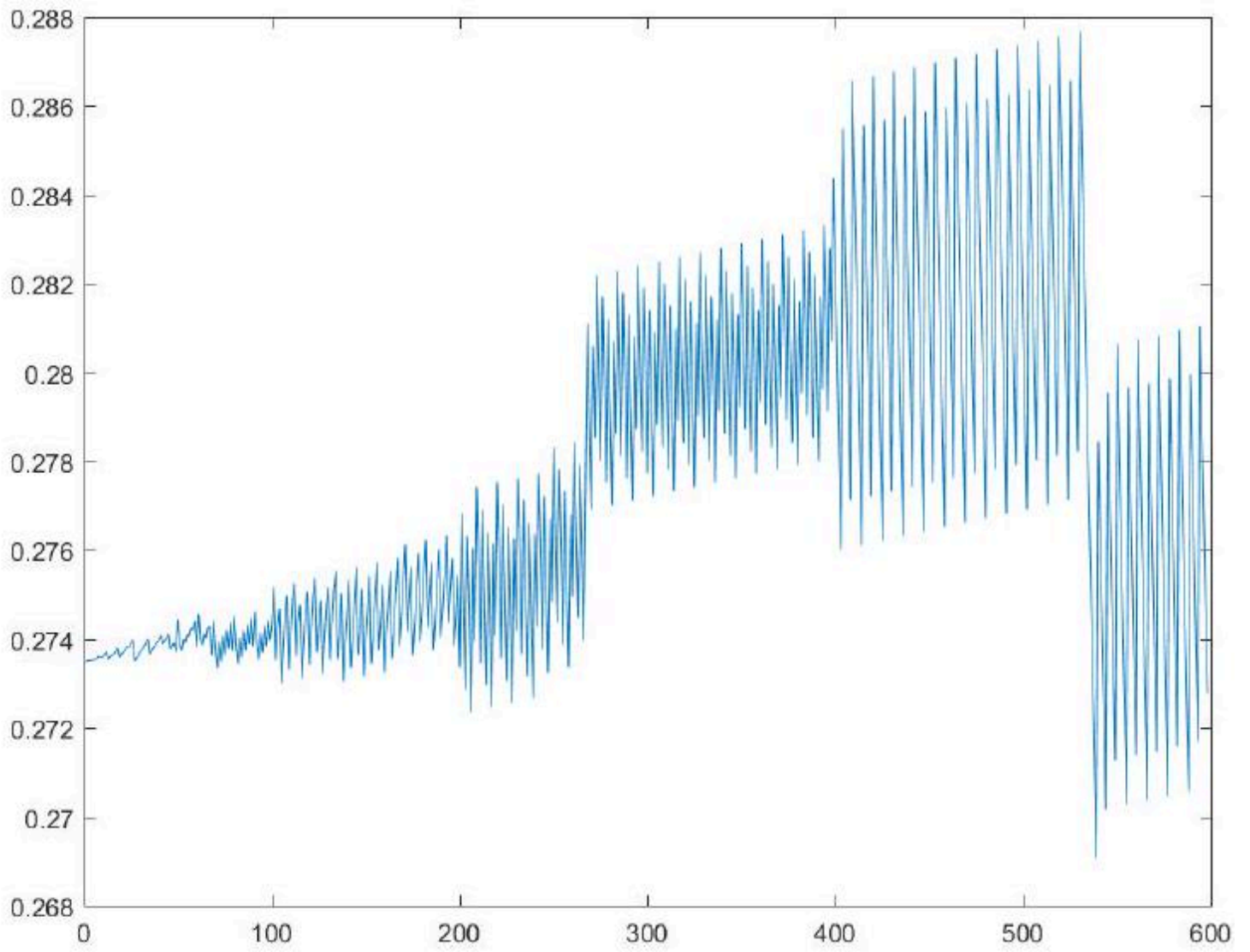
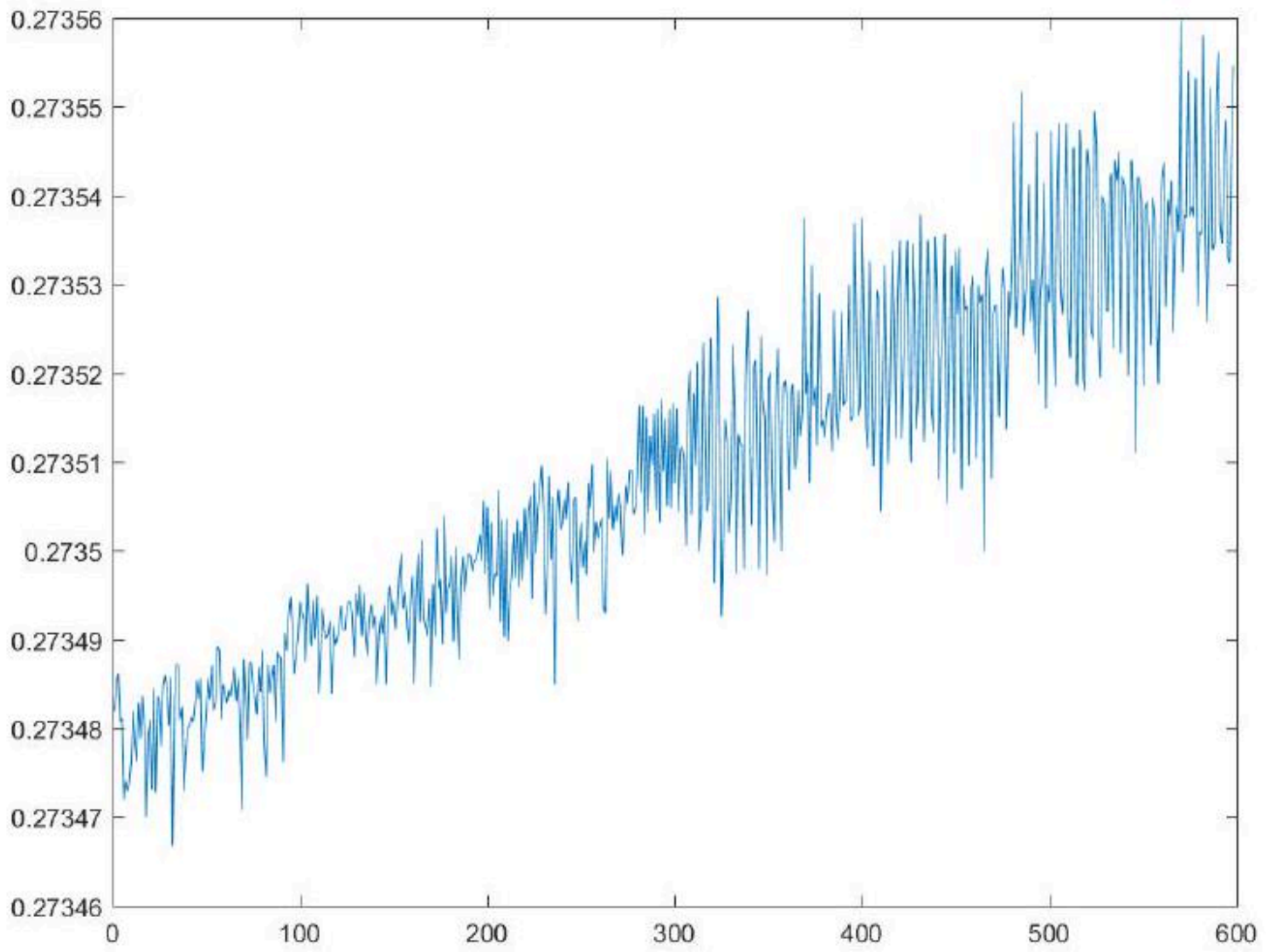

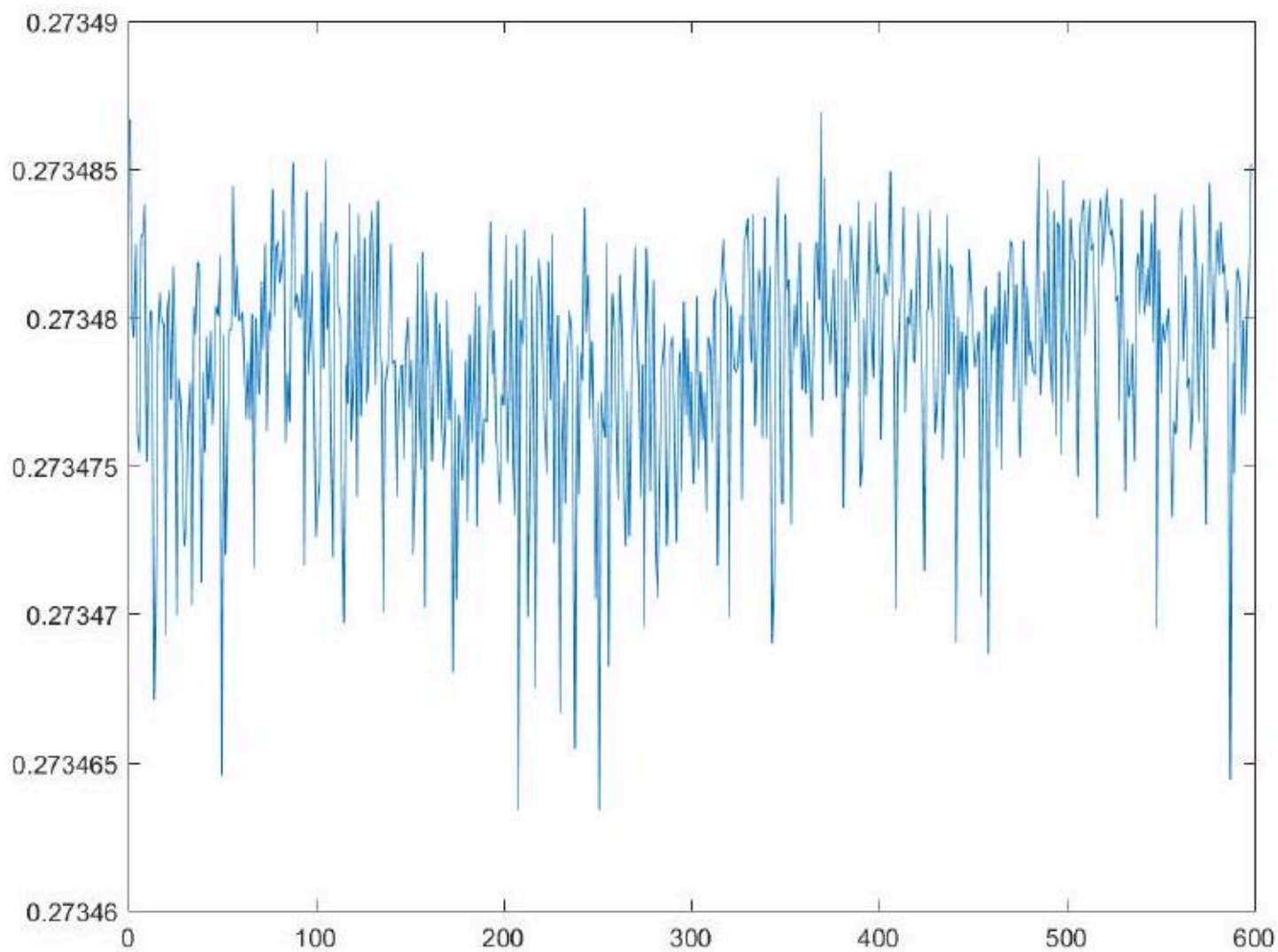


Figure 63: Fig. 60. Graph of field strength over time  $E(T), \Delta t = 1s$

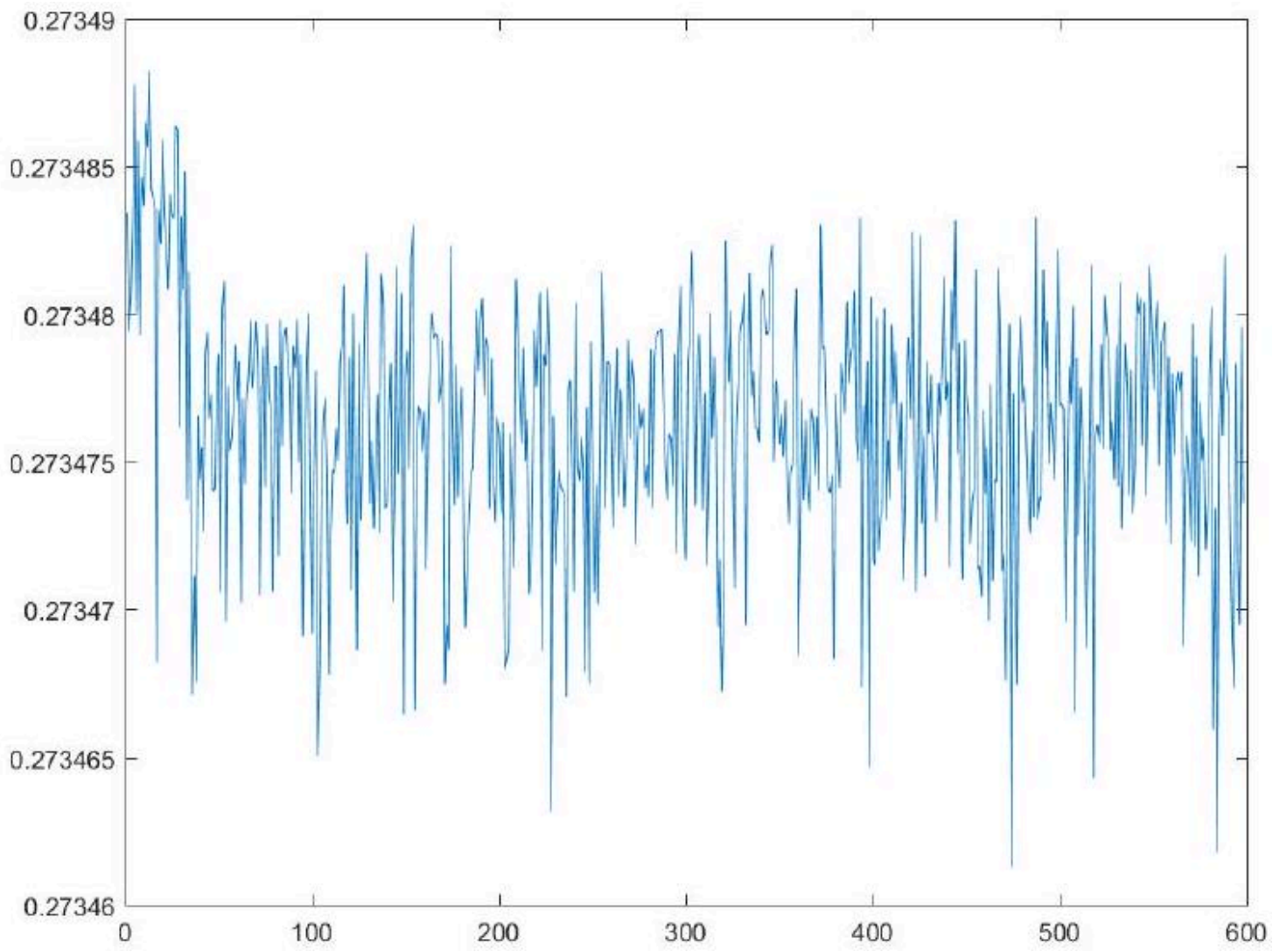





\captionsetup{labelformat=empty}  
Figure 64: Fig. 62. Graph of field strength over time  $E(T)$ ,  $\Delta t = 10^{-2}s$  



\captionsetup{labelformat=empty}  
 Figure 65: Fig. 64. Graph of field strength over time  $E(T)$ ,  $\Delta t = 10^{-4}s$



\captionsetup{labelformat=empty}  
 Figure 66: Fig. 65. Graph of field strength over time  $E(T)$ ,  $\Delta t = 10^{-5}s$  



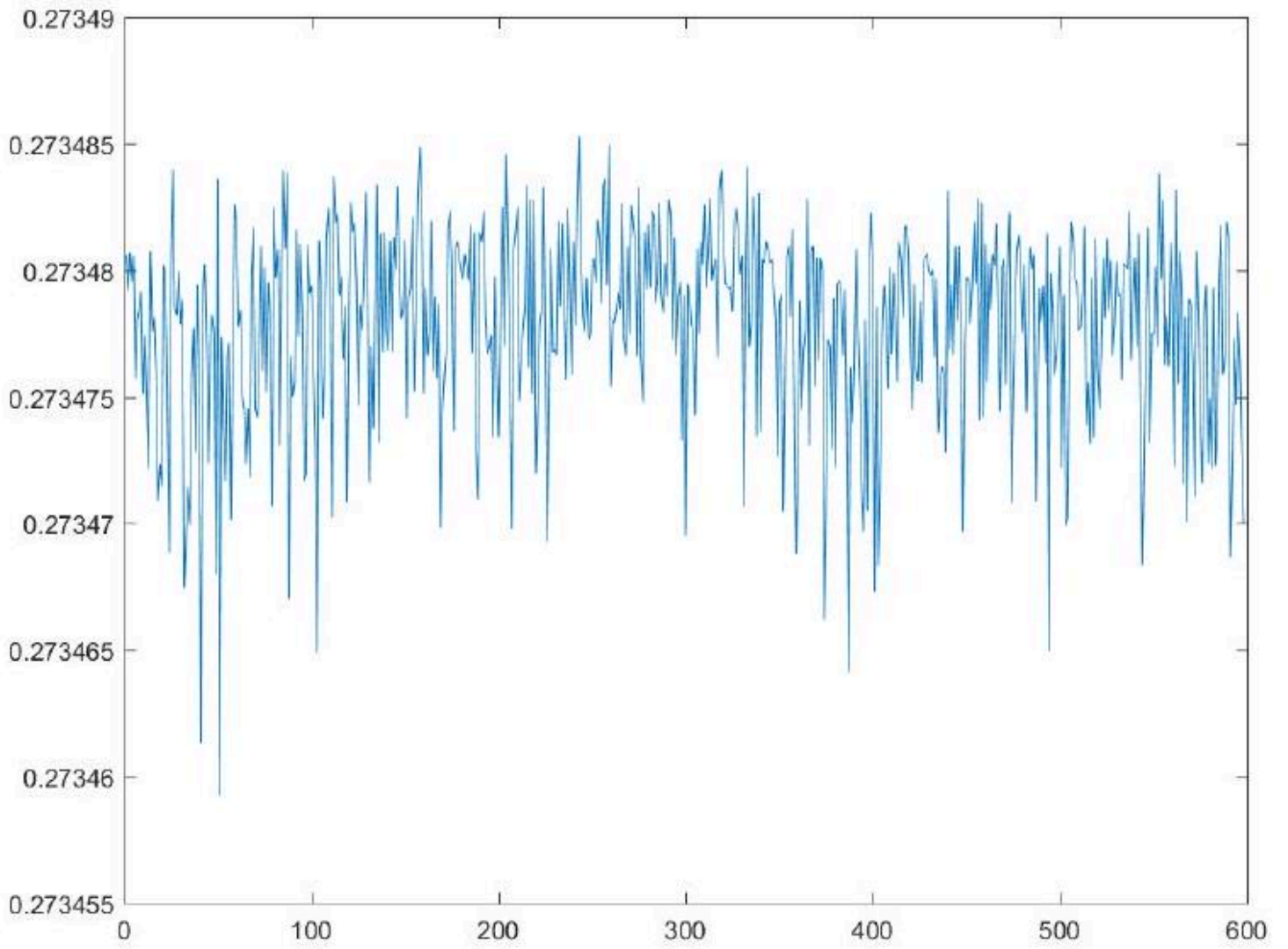
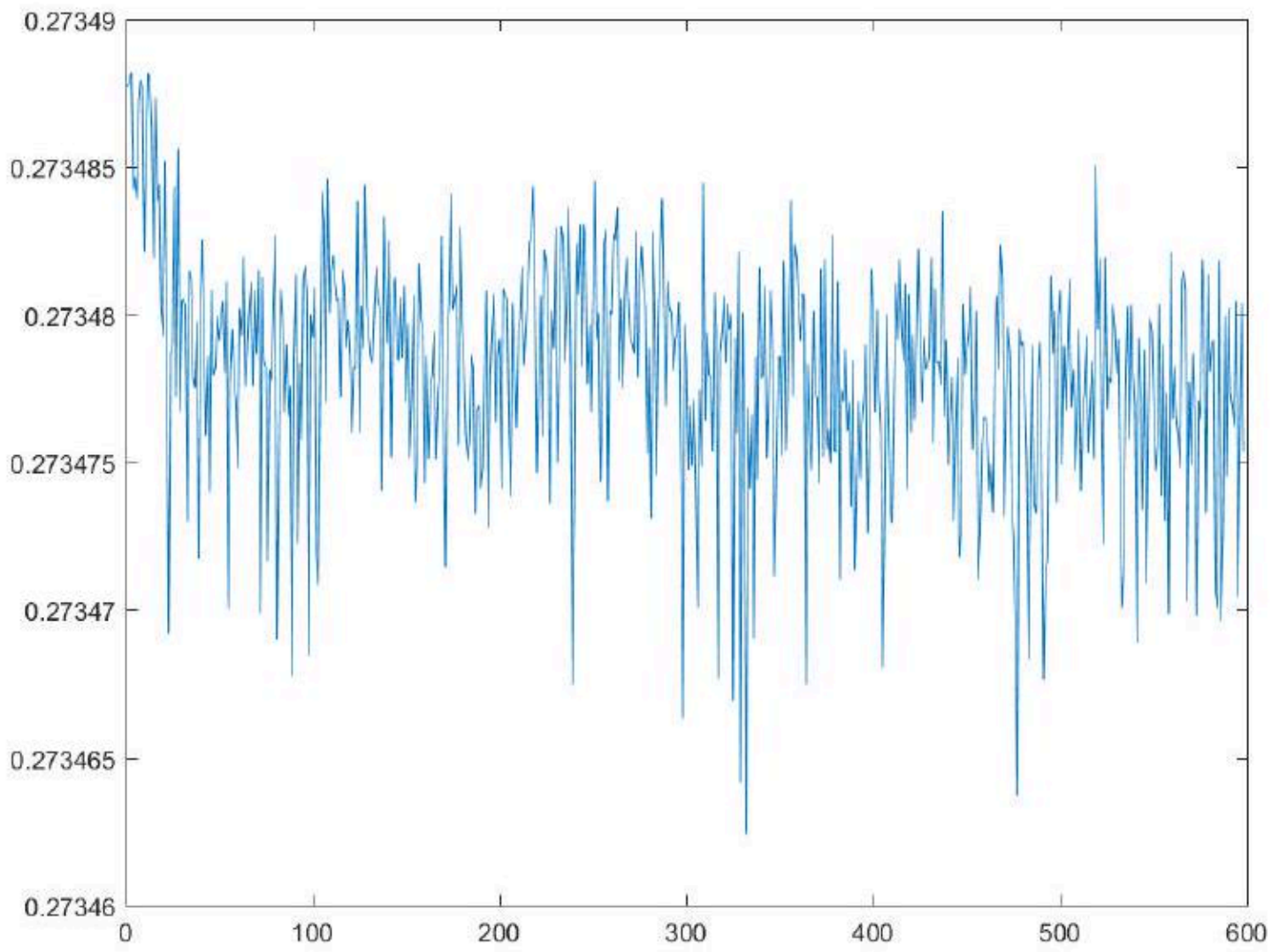


Figure 67: Fig. 67. Graph of field strength over time  $E(T), \Delta t = 10^{-7}s$



\captionsetup{labelformat=empty}  
Figure 68: Fig. 69. Graph of field strength over time  $\bar{E}(T)$ ,  $\Delta t = 10^{-9}s$

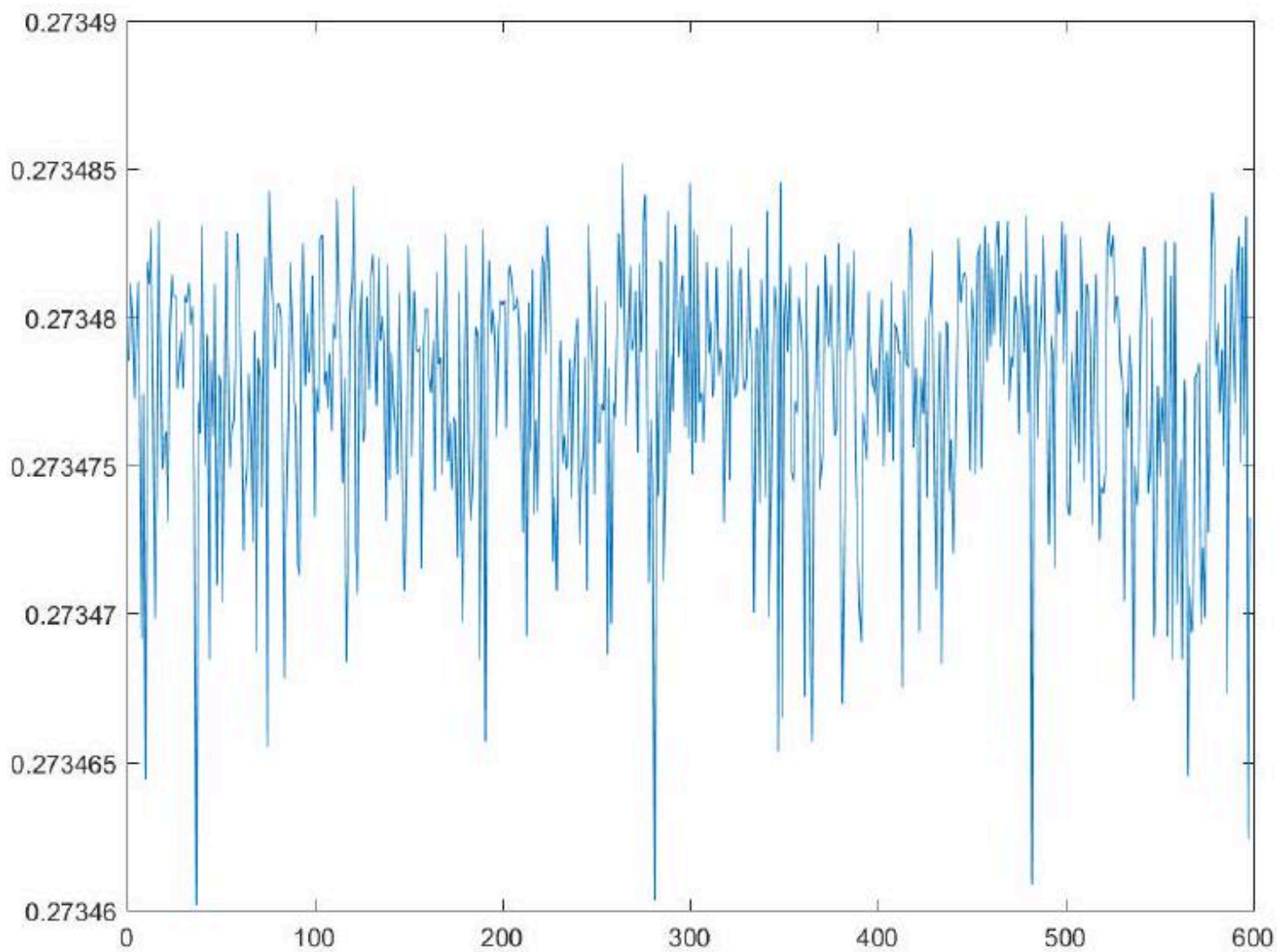
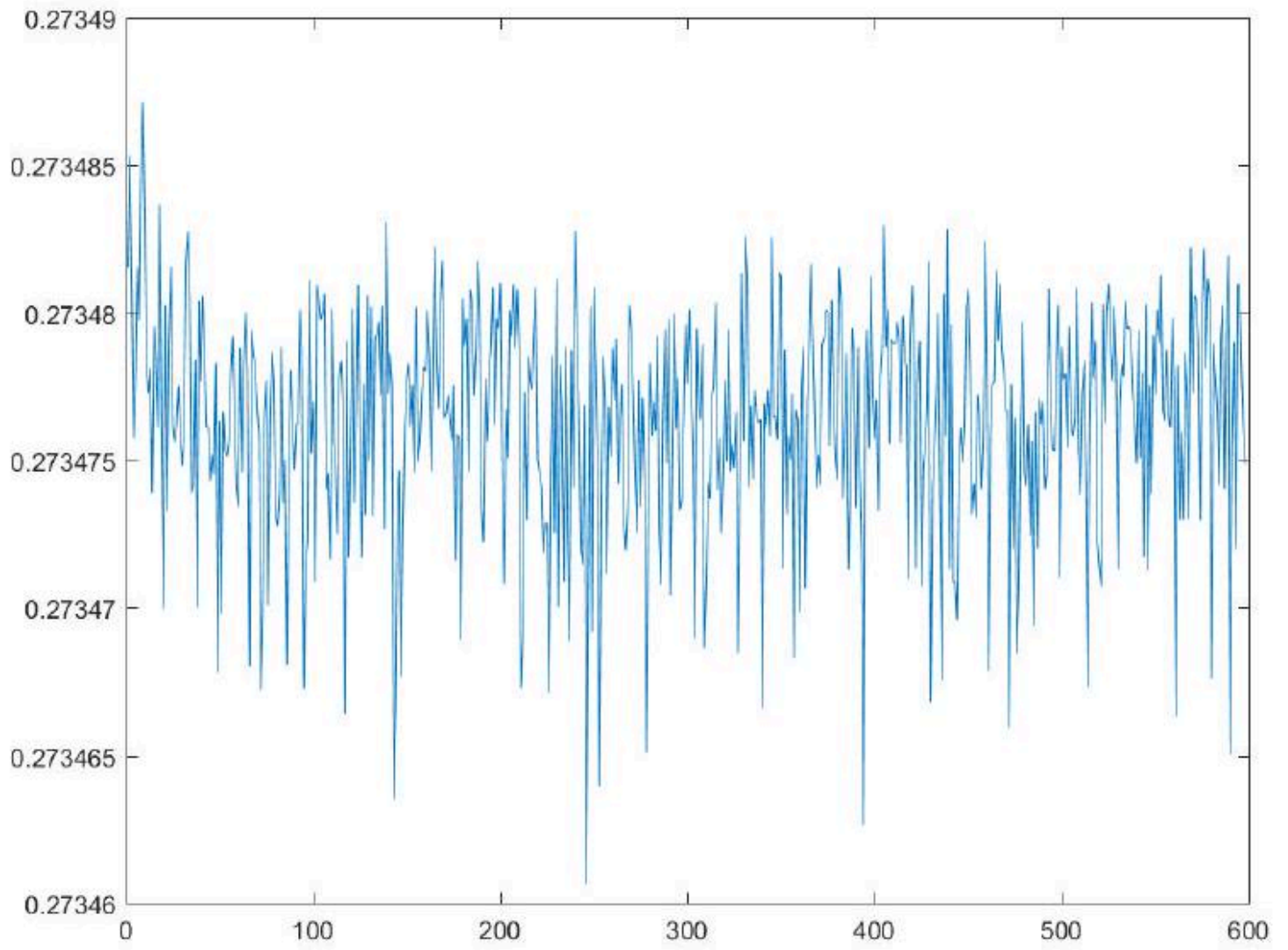


Figure 69: Fig. 66. Graph of field strength over time  $E(T)$ ,  $\Delta t = 10^{-6}s$





\captionsetup{labelformat=empty}  
Figure 70: Fig. 68. Graph of field strength over time  $\bar{E}(T)$ ,  $\Delta t = 10^{-8}s$

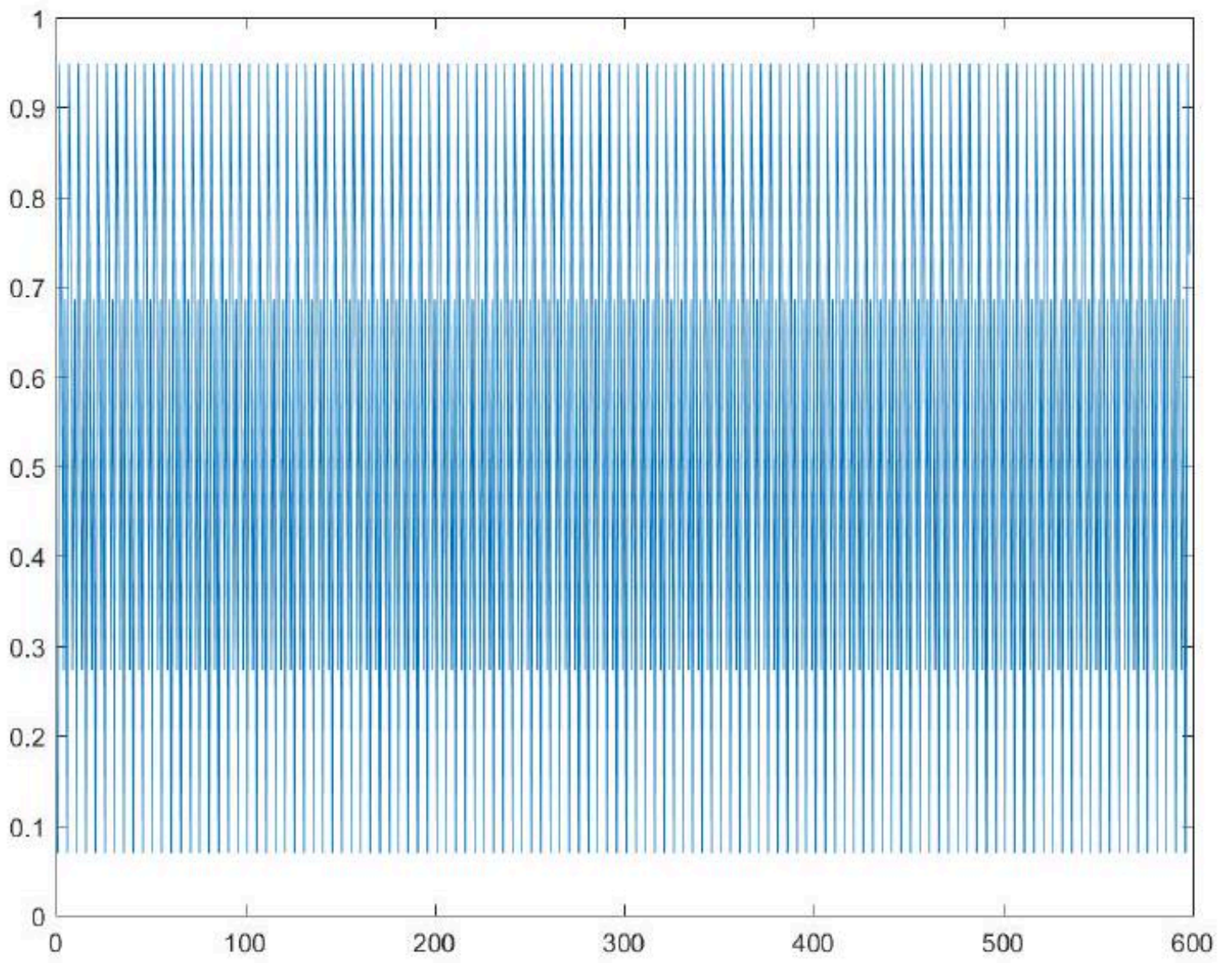


Figure 71: Fig. 70. Graph of field strength over time  $E(T)$ ,  $\Delta t = 10^{-10}s$

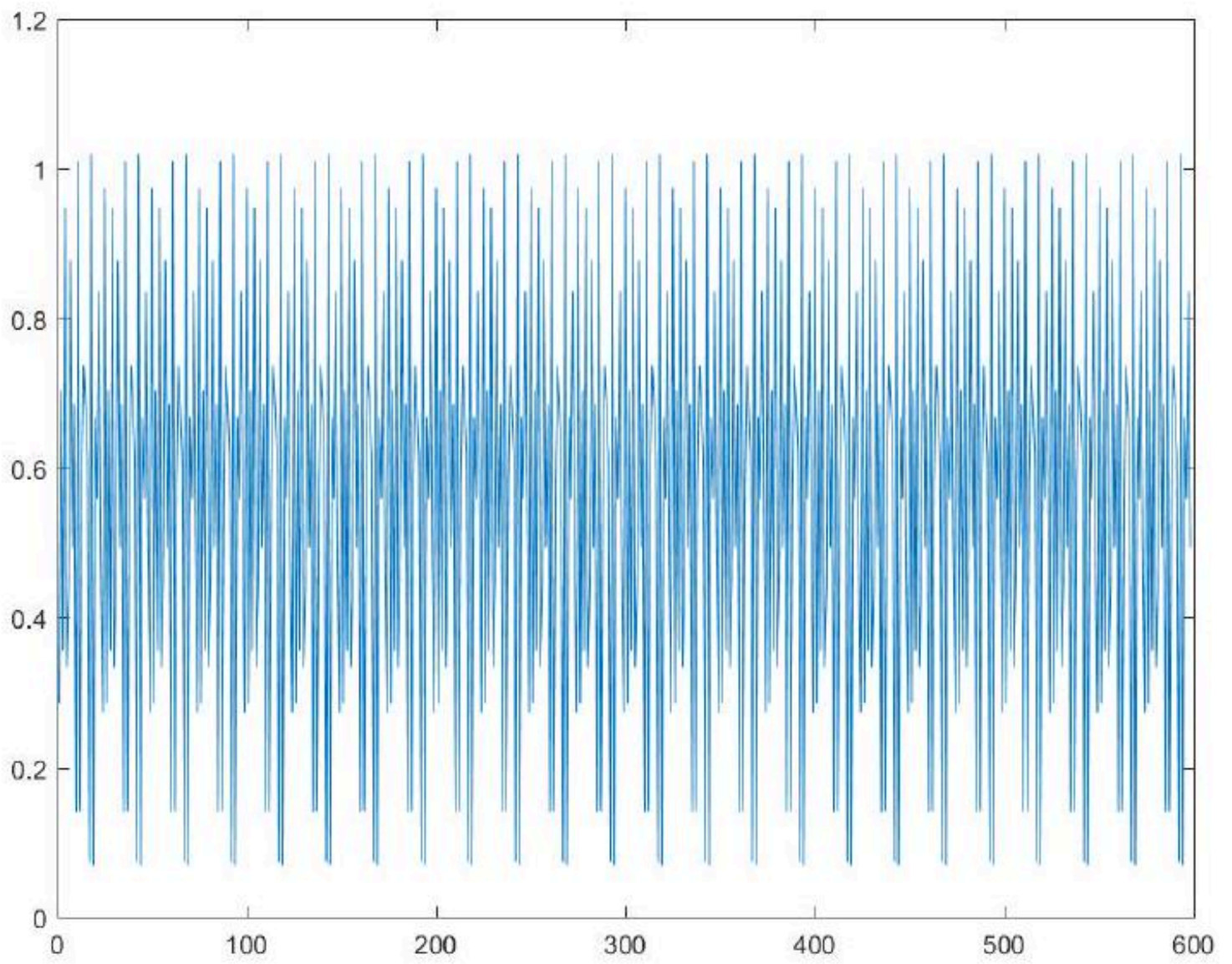


Figure 72: Fig. 71. Graph of field strength over time  $E(T)$ ,  $\Delta t = 10^{-11} s$



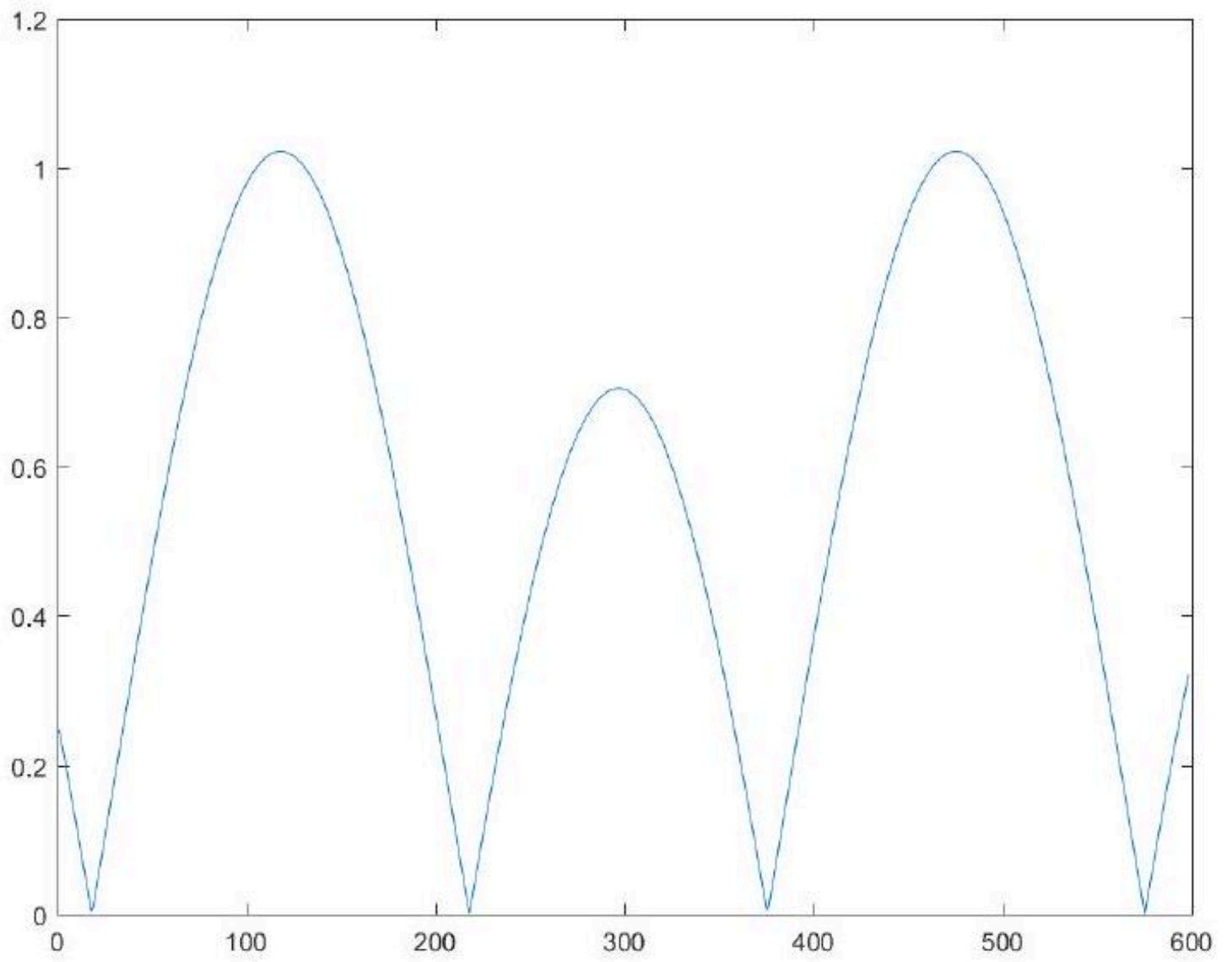
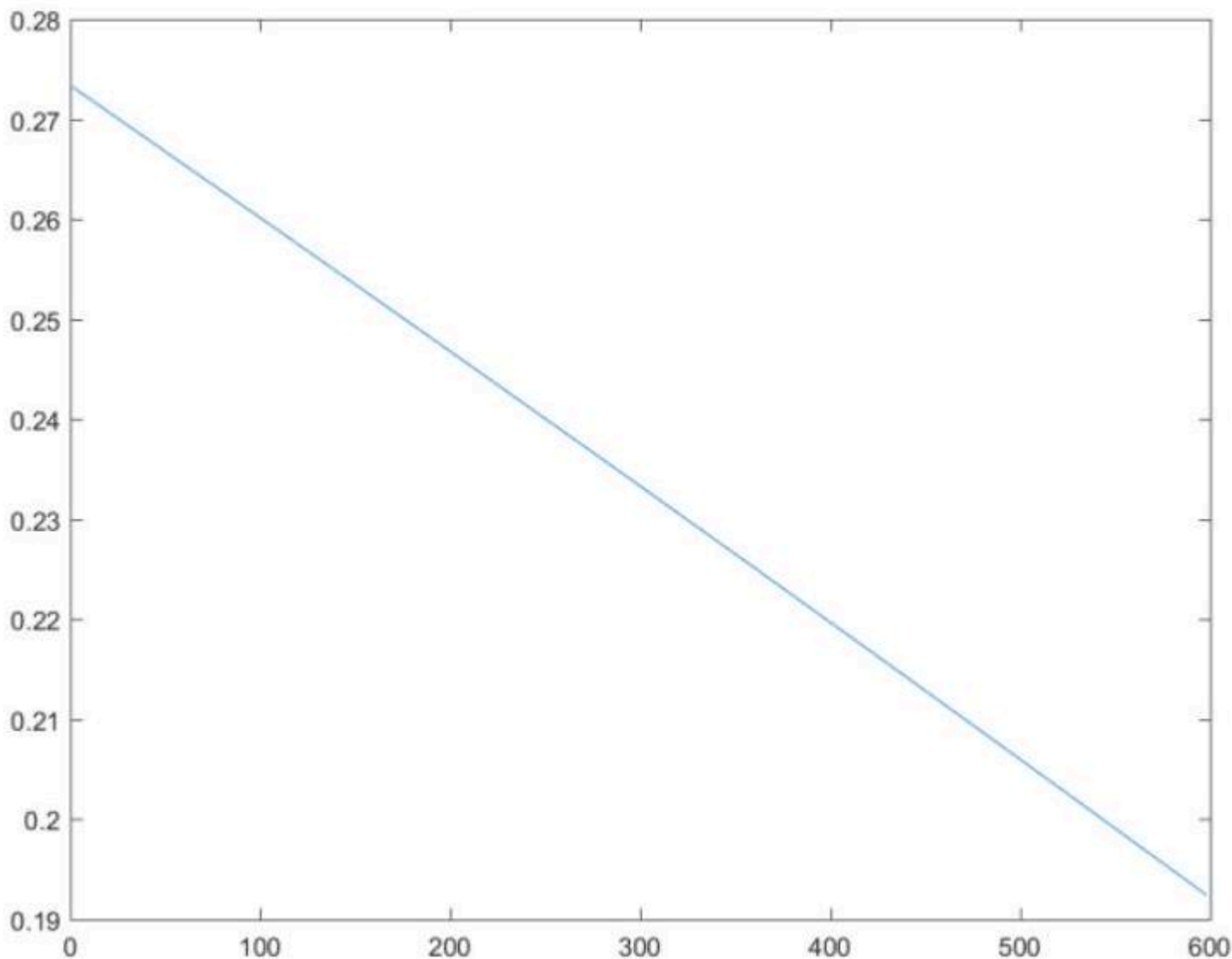
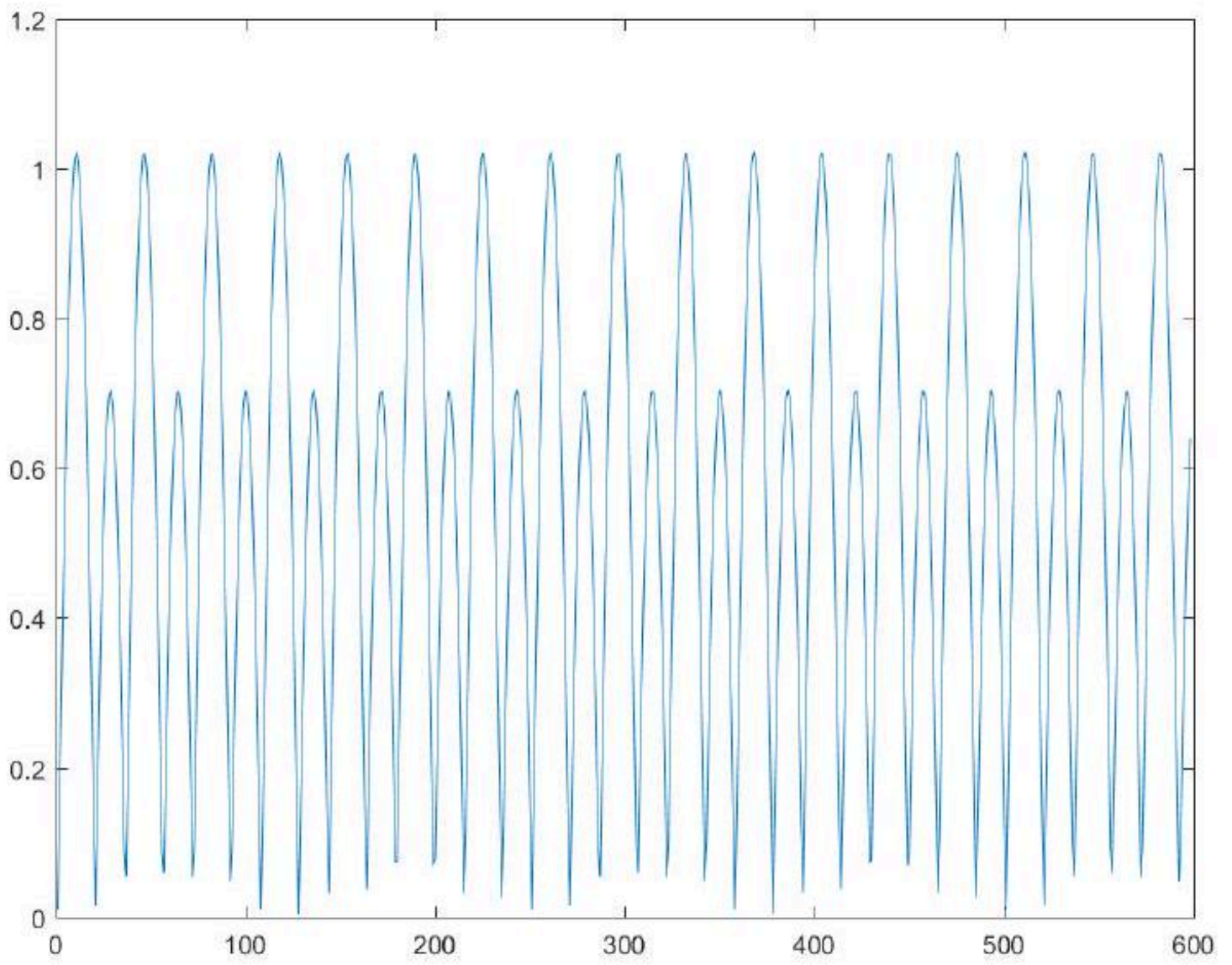


Figure 73: Fig. 73. Graph of field strength over time  $E(T)$ ,  $\Delta t = 10^{-13} s$



\captionsetup{labelformat=empty}  
Figure 74: Fig. 75. Graph of field strength over time  $E(T)$ ,  $\Delta t = 10^{-15} s$



\captionsetup{labelformat=empty}

Figure 75: Fig. 72. Graph of field strength over time  $E(T)$ ,  $\Delta t = 10^{-12}s$ , frequency  $\nu_1 = 6.85\text{GHz}$ , frequency  $\nu_2 = 5.38\text{GHz}$  ☺



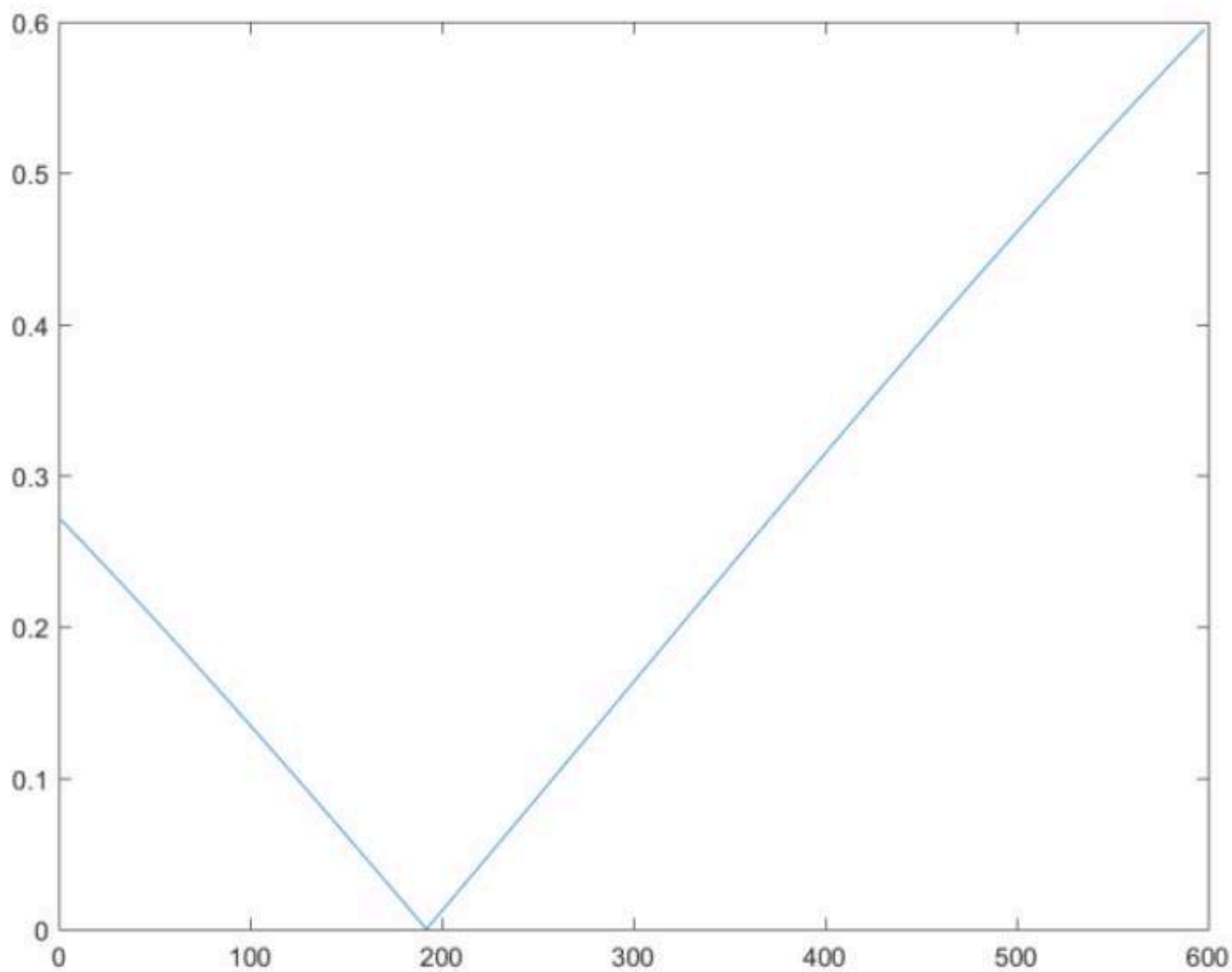


Figure 76: Fig. 74. Graph of field strength over time  $E(T)$ ,  $\Delta t = 10^{-14}s$

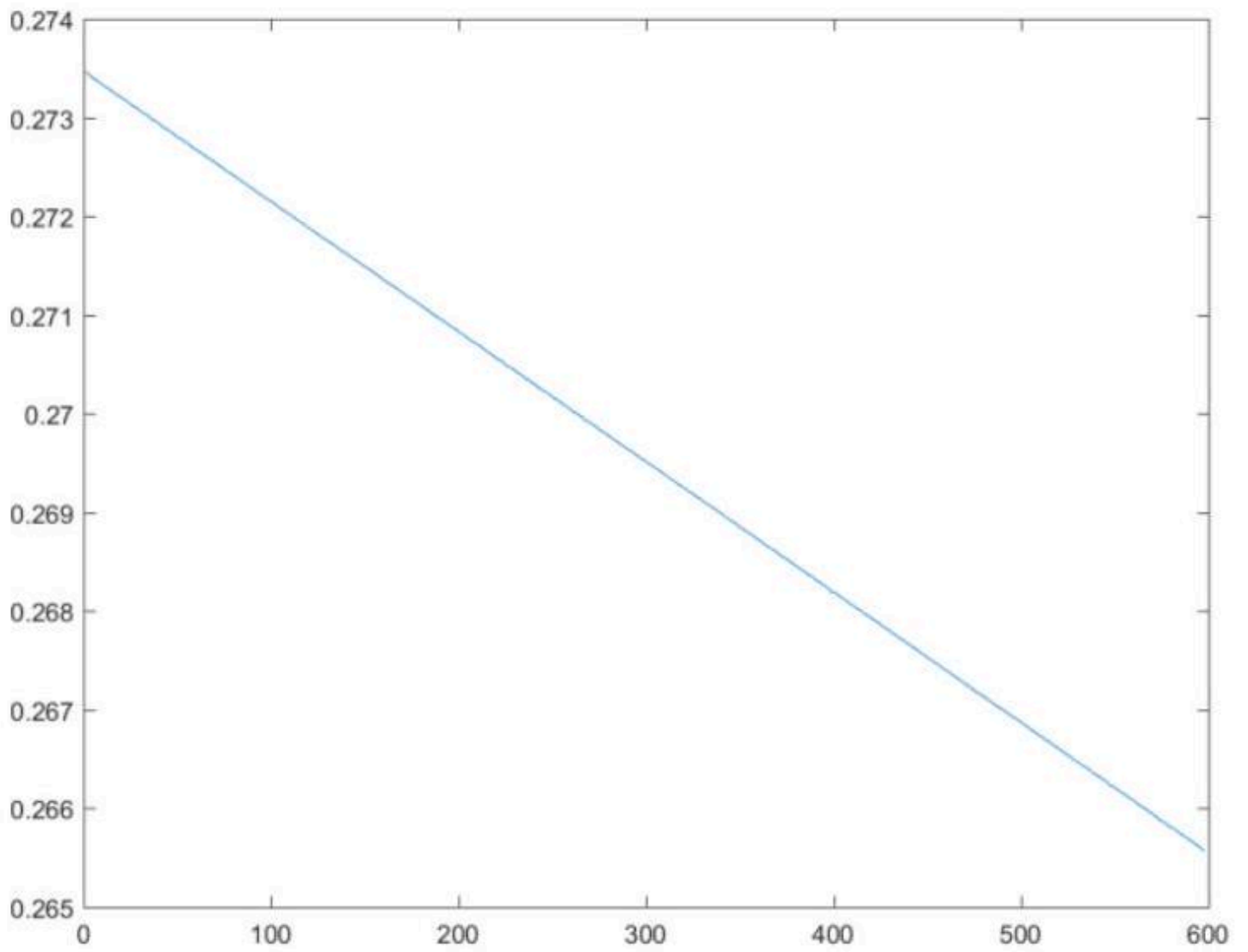


Figure 77: Fig. 76. Graph of field strength over time  $E(T)$ ,  $\Delta t = 10^{-16}_s$

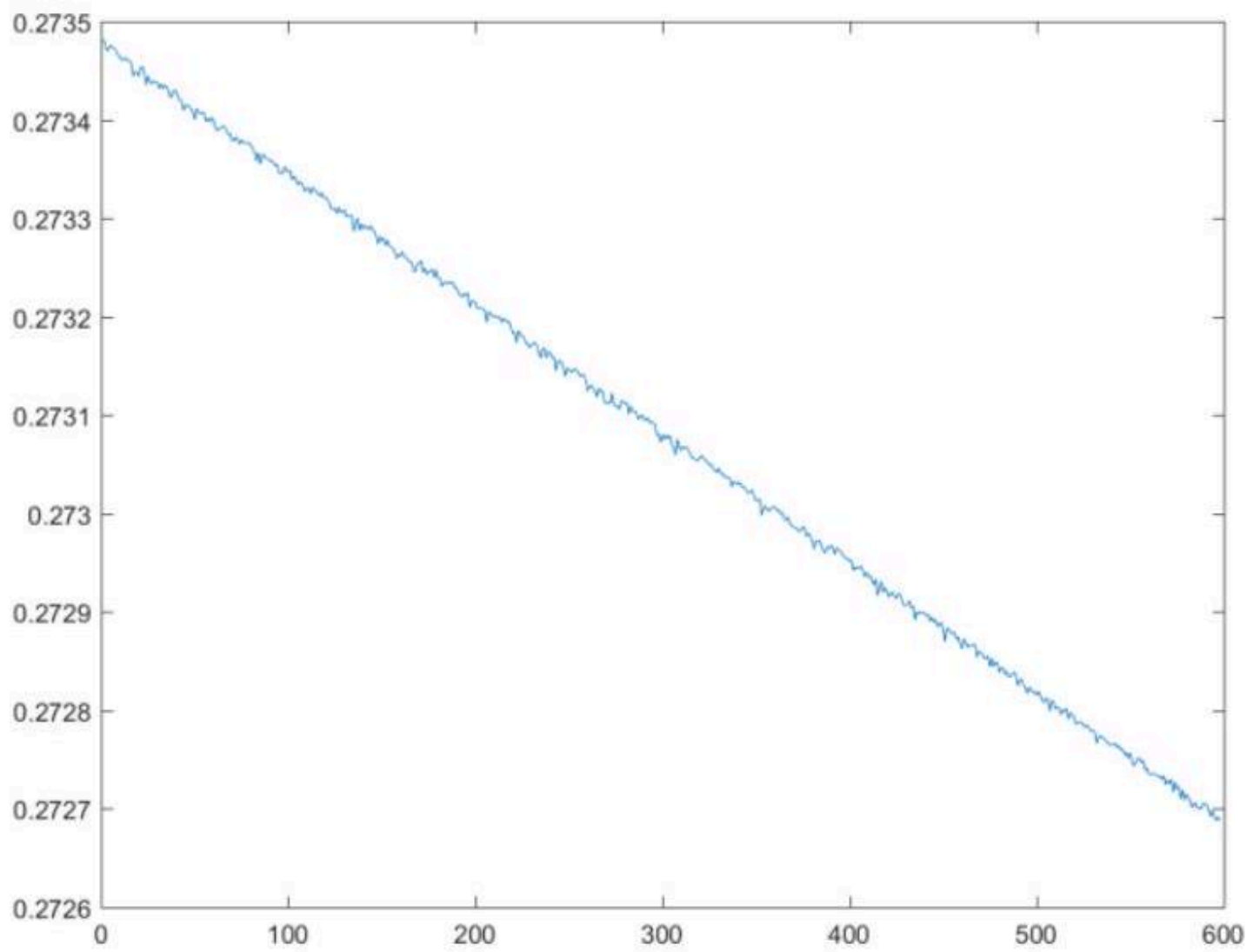


Figure 78: Fig. 77. Graph of field strength over time  $E(T)$ ,  $\Delta t = 10^{-17} s$



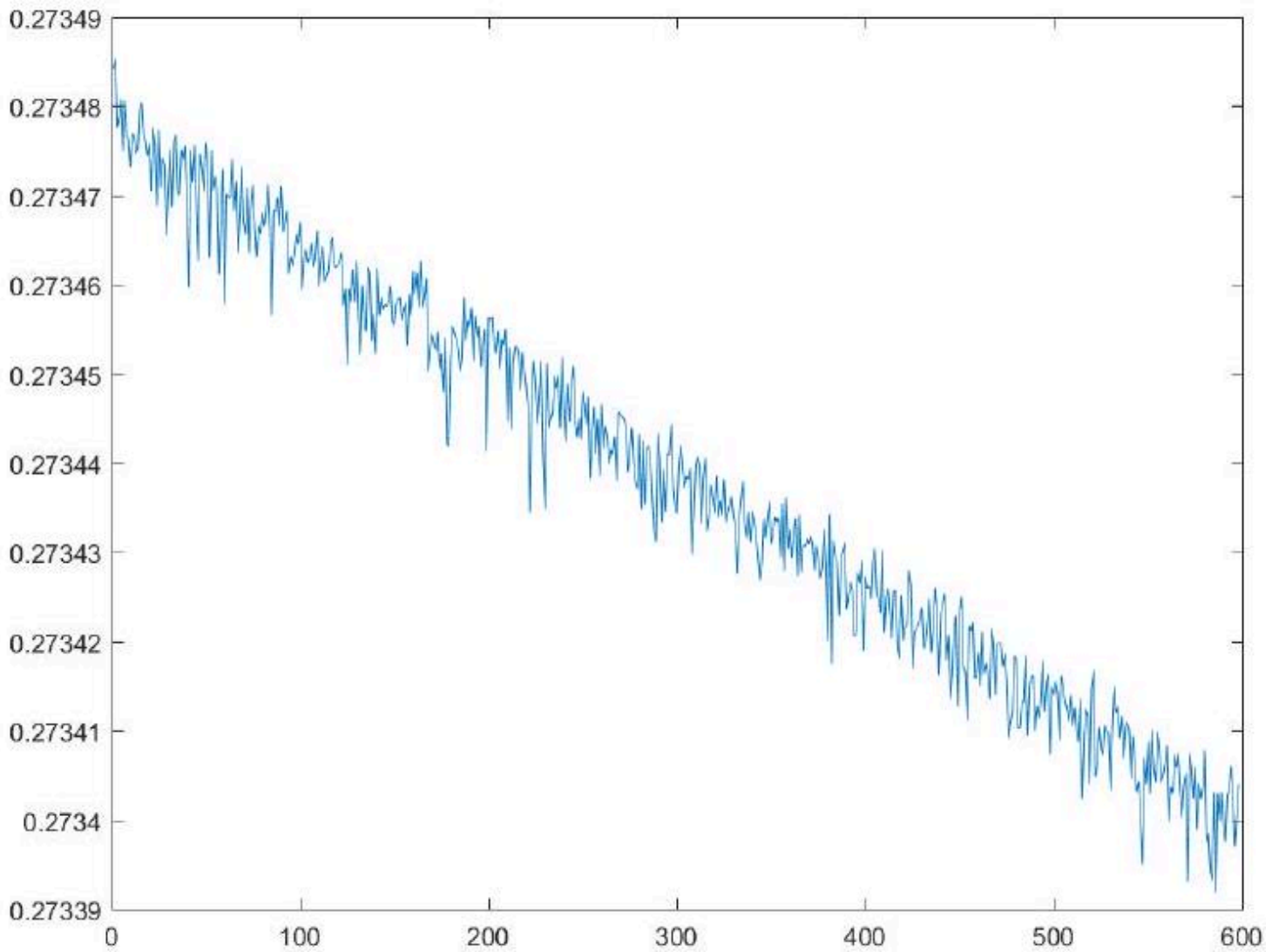


Figure 79: Fig. 78. Graph of field strength over time  $E(T)$ ,  $\Delta t = 10^{-18} s$

As can be seen from the presented graphs (Fig. 53-78), the regularity of the wave response has several levels in the time range with step  $\Delta t = 10^6 s$  to  $10^{-13} s$ . Within this range, a zone is set apart with step  $\Delta t = 10^{-3} s \div 10^{-9} s$ , in which regularity is not observed (Figures 63-69).

When calculating the strength of the electromagnetic field as a function of time,  $E(T)$  with step  $\Delta t = 10^{-12} s$  (Fig. 72), a baseline two-frequency interaction diagram with frequencies  $\nu_1 = 62.5 \text{ GHz}$  and  $\nu_2 = 50 \text{ GHz}$ , which is then projected into the other frequency ranges.

Thus, due to the interaction with the Aires resonator (microprocessor), 28GHz baseline EM radiation increases manifold, which is typical for a diode bridge, and 2 sub-waves arise with frequencies  $\nu_1 = 62.5 \text{ GHz}$  and  $\nu_2 = 50 \text{ GHz}$ . Average frequency  $\nu_{sr} = (\nu_1 + \nu_2)/2 = (62.5 + 50)/2 = 56.25 \sim (28 \times 2) \text{ GHz}$ .

Undoubtedly, this phenomenon associated with the system's discrete step requires additional studies. However, it can be noted that the superposition arising from the Aires resonator (C20S5G) in the form of a stationary field response has a regular character.

The silicon substrate of the Aires resonator (microprocessor) initially has its own electromagnetic superposition, determined by its crystal lattice (n-type monocrystalline silicon substrate with crystallographic plane 100 (Miller index)).

The slit topological pattern formed on the wafer when interacting with incident electromagnetic radiation creates a resonant response over the surface of the resonator in the form of a highly coherent fractal field that interacts with the inherent superposition of the crystal lattice of the silicon substrate, reorganizing the topology of its structural framework according to its own parameters. Thus, based on feedback in the crystal lattice of the substrate, an analog of a stationary fractal pattern arises from a slit matrix deposited on the surface.

Due to the fact that any electromagnetic superposition, according to classical physics, is capable of using feedback to correct the structural organization of the object that initially generates it, we can conjecture with highly probability that a

restructuring of the silicon wafer structure, on which the C20S5G topological slit pattern is applied, is inevitable, and at a certain stage its structural analogue forms with the formation of reference resonators in the form of matching p-n junctions within this pattern, which, apparently, is specifically linked with the point of modification of the object into quantum form. This hypothesis requires additional X-ray structural studies.

Since the parameter of the unit cell of the crystal silicon lattice is  $\sim 5.4\text{\AA}$  (Fig. 79), the accuracy of the characteristics of the corrected superposition of the pattern increases by orders of magnitude.

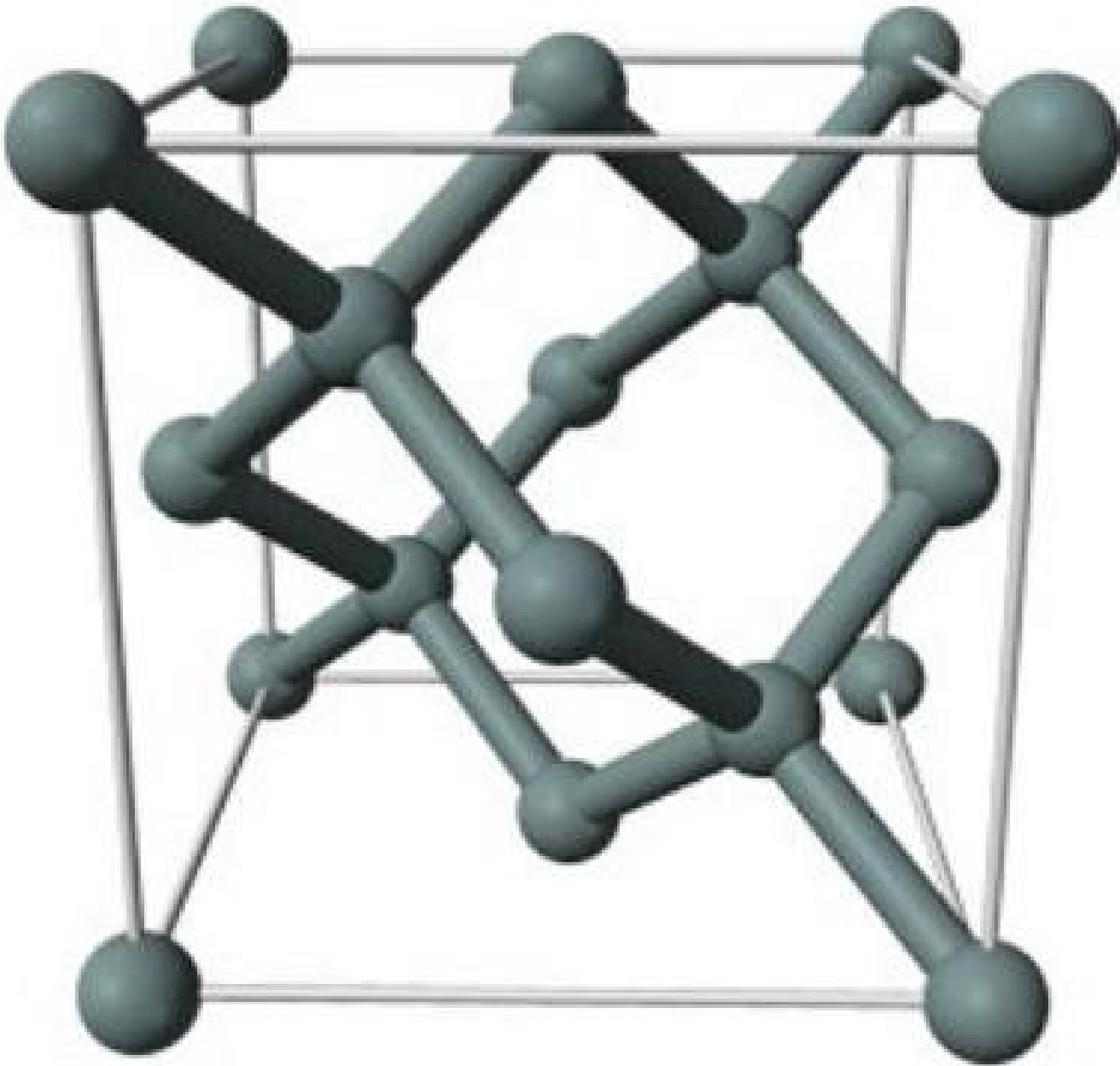


Figure 80: Fig. 79. Silicon crystal lattice

As a result, the wave superposition arising from the modified crystal silicon lattice will be analogous to the fractal pattern formed from the topological slit matrix, which will shift the interaction to the superhighfrequency range with a corresponding increase in field energy.

According to research conducted at Vilnius University [1], the minimum power of the radiation incident on a wafer must be 2 W to activate a resonant response.

As can be seen from the general graph (Fig. 53), over a period of time  $t = 131 \cdot \Delta t = 524 \cdot 10^5 \text{ s}$  (1.66 years), the system reaches the limit and transitions to quantum form, which is accompanied by a sharp collection of potential (vertical line) and then, as shown in the graph (straight line at an angle of  $\sim 58.8^\circ$ ), a subsequent collection of potential leads to further structural self-development of the pattern, i.e. the process becomes completely correlated, since it does not have cyclic modulations. This

suggests that the interaction is harmonized, i.e. the collection of potential and the structural modification take place simultaneously - it's a single process. 🌀

It is necessary to take into account that the pattern was designed for a frequency of 28 GHz and the corresponding power, which is just one fragment of the huge number of wave fronts of different frequency ranges that are in the medium and interact with the pattern. In previous studies on the interaction of a simplified analogue of the pattern with frequencies of 2.4 GHz and 5.5 THz [2-6], the corresponding resonance response was also obtained. In addition, the appearance of a hologram over the pattern (Fig. 8o) suggests that the resonator's pattern creates the corresponding structural response in the optical frequency range. 🌀

Based on the foregoing, it can be argued that when the C20S5G pattern interacts with broadband electromagnetic radiation of various frequencies in real conditions, including very high frequencies carrying the corresponding potential, and power, its transition to a quantum form can occur extremely quickly, even simultaneously, after the initial activation of the pattern, which opens up very broad possibilities for the use of this effect in various fields of application. 🌀

In summary, given external irradiation of the Aires microprocessor, the resonance response is an integral, stationary, highly coherent, symmetric, selfaffine superposition from the interaction of surface waves with annular slits, concentrating the electric potential in them, thus causing them to begin working as waveguides. The points where the rings intersect initiate the phase matching of counter flows, thereby triggering the appearance of a stationary (standing) wave, which is clearly seen in the computer simulation. As a result, the emerging reflex represents a whole complex of corresponding, inter-integrated, fractal (self-similar) interactions. 🌀

The animation (Appendix 3) shows the consecutive responses of the Aires resonator (microprocessor) to the influence of electromagnetic radiation in different sections from the edge of the resonator to its center in the form of a distribution of the strength and energy flux density of the electromagnetic field.

動畫片（附錄 3）顯示了 Aires 諧振器（微處理器）對電磁輻射影響在從諧振器邊緣到中心不同區段的連續響應，以電磁場強度和能量通量密度分佈的形式呈現。

## CONCLUSION 🌀

The simulations showed that given electromagnetic action at a frequency of 28 GHz on an Aires self-affine resonator (microprocessor), the device converts incident electromagnetic radiation into a coherent spatio-temporal selfaffine form (hologram). In particular, over the central region of the resonator, there is a marked increase in both the strength  $E_{\max} = 122.6 \text{ (V/m)}$  ( $\sim 490.4$  times) and the intensity of the electric field  $I_{\max} = 15030.76 \text{ (W/m}^2\text{)}$  ( $\sim 250512.67$  times). 🌀

Further, within the ring of maximum response intensity, a counter resonance forms along its diameters, causing the values of the potentials participating in this process to be multiplied. As a result of counterharmonization with respect to amplitudes, frequencies, phases, and the radiation pattern, there is a maximally neutral zone in the center and, since an active potential always redistributes from zones of maximum amplitude activity to a neutral zone, the potential density at the central point increases sharply, and the amplitude tends to zero, which initiates the singularity phenomenon. According to the first law of thermodynamics (the law of conservation of energy), energy doesn't appear out of nowhere or vanish into nothing - rather it transforms from one state into another, which is what happens in the central point of the circuit as the point of singularity. As a result, the focal point of the vector interaction of all processes with a common potential arises at the center of the circuit:

此外，在最大響應強度的環帶內，沿著其直徑會形成一個反共振，導致參與此過程的電位值被乘增。由於在振幅、頻率、相位與輻射圖形方面發生了相互調和的反向作用，中心出現一個極度中和的區域，而因為活性電位總是從振幅活動最大區向中和區重新分配，中央點的電位密度急劇增加，振幅趨近於零，進而引發奇異現象。根據第一類熱力學定律（能量守恆定律），能量不會憑空出現或消失無蹤——而是從一種狀態轉換為另一種狀態，這正是電路中心作為奇異點時所發生的情況。因此，所有具有共同電位的過程之向量相互作用的焦點便在電路中心產生：

$$(I_{\max})^2 = (15030.76)^2 = 225923746.18 \text{ (W/m}^2\text{)}$$

In addition, the constant inflow of potential from the outside, which strives to fill the circuit's neutral zone, ensures that the emerging superposition is highly stable.

此外，來自外部不斷流入、試圖填充電路中和區的電位，確保了所產生的疊加態具有高度穩定性。

This state of the system is a consequence of the fundamental symmetry principle underlying the fractal topology of the Aires resonators, which is formulated in Noether's theorem, which states that a certain conservation law corresponds to each continuous symmetry of a physical system. 🌀

$$\sum_{i=1}^n \frac{\partial L}{\partial \dot{x}_i} \delta_i = \text{constant}$$

where L is the Lagrangian, functions  $\delta_i$  are random variations.  

The theorem can also be formulated the other way around: conservation laws are a consequence of fundamental symmetry. Thus, the arising stationary wave superposition is a manifestation of fundamental physical laws based on the principle of multilevel symmetry. As a consequence, the stability of the wave pattern, and hence the capacity to accumulate and fix the potential within such a system, goes to a fundamentally different level.  

Thus, the energy of radiation coming from a Wi-Fi source (router) and modern mobile communication equipment (smartphone, telephone, etc.), after interaction with the resonator, is redistributed in space and across frequencies, phases, and the interaction diagram, transforming into a self-affine stationary structure (hologram) corresponding to the self-affine topological lattice of a resonator carrying analogous properties (coherent transformation).  

The field (electromagnetic superposition) (Fig. 80) that results from the AIRES resonator's (microprocessor's) interaction with incident radiation (28 GHz) is self-affine, possess traits of holograms, and, according to the Gabor-Denisyuk theory of holograms, which states that any hologram bears all the same traits as the agent initiating the hologram, becomes a coherent transformer of any waves that interact with it in the corresponding frequency range.  

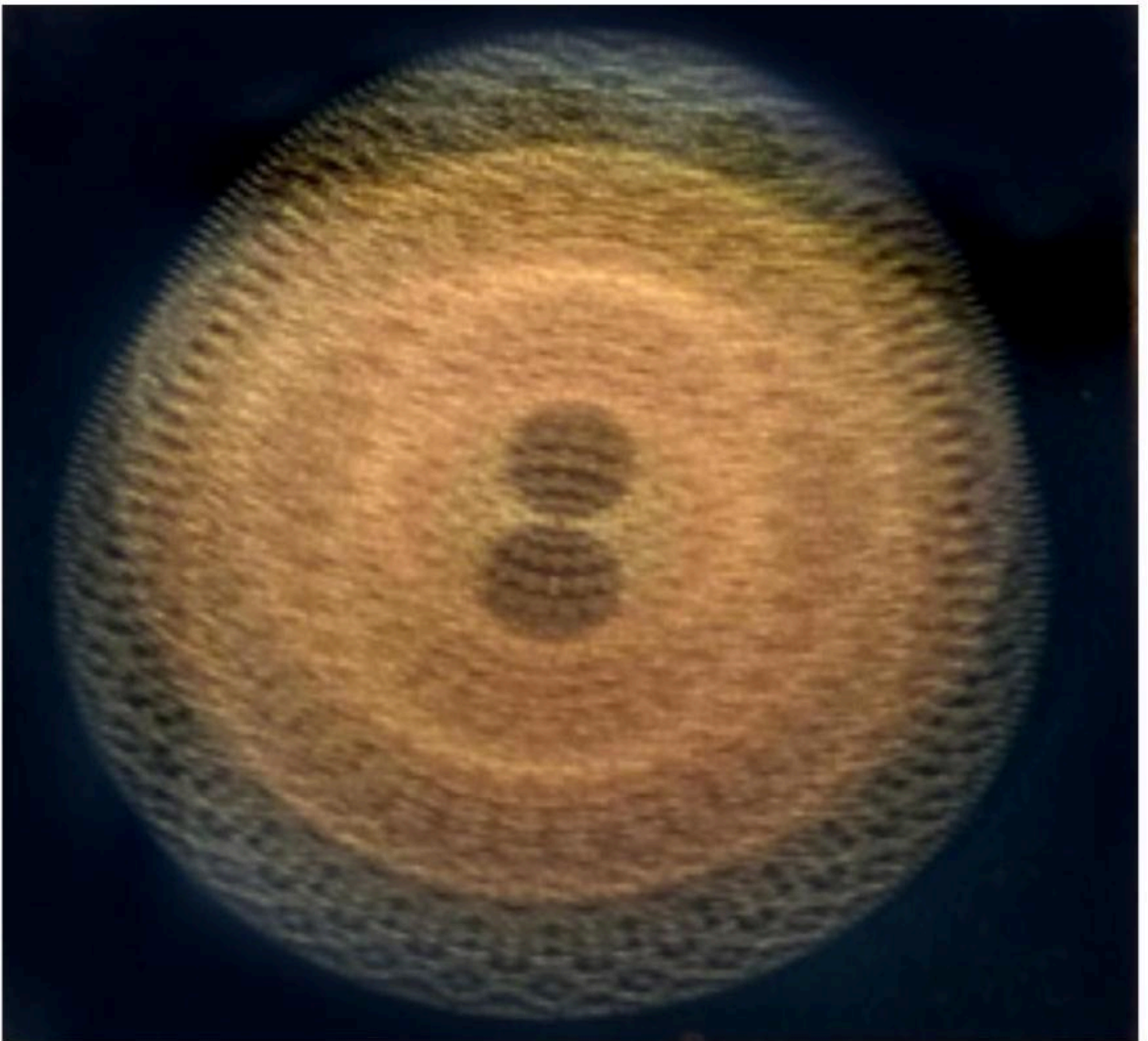


Figure 81: Fig. 80. The photograph of a hologram on the AIRES microprocessor.



The results of the simulation demonstrate the redistribution of the characteristics of the electromagnetic field (strength and energy flux density), which reach their maximum values in the central part of the circuit, with a sharp condensation of the matched potential at its central point, which makes it possible to speak of the resulting stationary, spatial-wave electromagnetic reflex's ability to direct transform into a highly coherent form the electromagnetic radiation that interacts with it if that potential does not exceed the potential of the emerging reflex.

Based on the foregoing, we can state that the AIRES C2oS5G microprocessor used in the Aires Crystal ( 2019 model) is a space-time amplitude-frequency converter (Fourier filter) that converts a dynamic wave pattern ( 28 GHz ) into a stationary electromagnetic field that harmonizes external incident radiation in terms of amplitudes, frequencies, phases and the interaction diagrams and, thus, is a catalyst for coherent transformation of electromagnetic radiation interacting with it in the corresponding range of amplitudes and frequencies.

Consequently, in the presence of this resonator (AIRES microprocessor), the effect of harmonizing the external man-made radiation (28GHz) with a biological organism's inherent radiation will be clearly expressed, which is confirmed by numerous tests with living objects, including the human body.

A comparative analysis of the results of modeling the interaction of electromagnetic radiation at frequencies of 6 GHz [7] and 28 GHz (WiFi 5G) with Aires resonator (microprocessor) C2oS5G revealed the following limiting values of the electromagnetic field strength  $E$  and the intensity  $I$  (tables 2, 3):

Table 2: Table 2  
`\captionsetup{labelformat=empty}`

Aires C2oS5G 6GHz	Min Value	Max Value	Increase (multiple)
E, V/m	0.08	35.34	443.13
I, W/m <sup>2</sup>	0.008	1314.52	164315

Table 3: Table 3  
`\captionsetup{labelformat=empty}`

Aires C2oS5G 28GHz	Min Value	Max Value	Increase (multiple)
E, V/m	0.25	122.6	490.4
I, W/m <sup>2</sup>	0.06	15030.76	250512.67

As can be seen from Tables 2 and 3, during the change of frequency of the radiation incident on the Aires C2oS5G circuit from 6 GHz to 28 GHz , the range of variation of the extreme values of strength  $E$  and intensity  $I$  of the electromagnetic field increases and its degree is: for strength  $E \sim 1.1$  times (490.4/443.13=1.1) and intensity  $I \sim 1.52$  times (250512.67/164315=1.52), respectively.

Based on these calculations, we can state that:

The Aires C2oS5G microprocessor is a wide-band converter of electromagnetic radiation to coherent form (its effectiveness is confirmed at 6 GHz and 28 GHz ); During the Aires C2oS5G microprocessor's interaction with EM radiation at 5 G frequencies ( 6 GHz and 28 GHz ), the microprocessor's effectiveness is significant, despite the increase in the signal frequency and its energy potential and density. Thus, the microprocessor maintains its stated properties that create high-quality protection for the body.

Analysis of changes in the electric field strength  $E$  over the central point of the pattern in time  $T$  showed that after passage of time interval  $T = 524 * 10^5$  s (1.66 years) the dynamic process reaches the limit, where there is a sharp instantaneous surge of strength from  $E = 1.02$  V/m to  $E = 7.98 * 10^{18}$  V/m, which, apparently, is associated with the object's transformation to a quantum form.

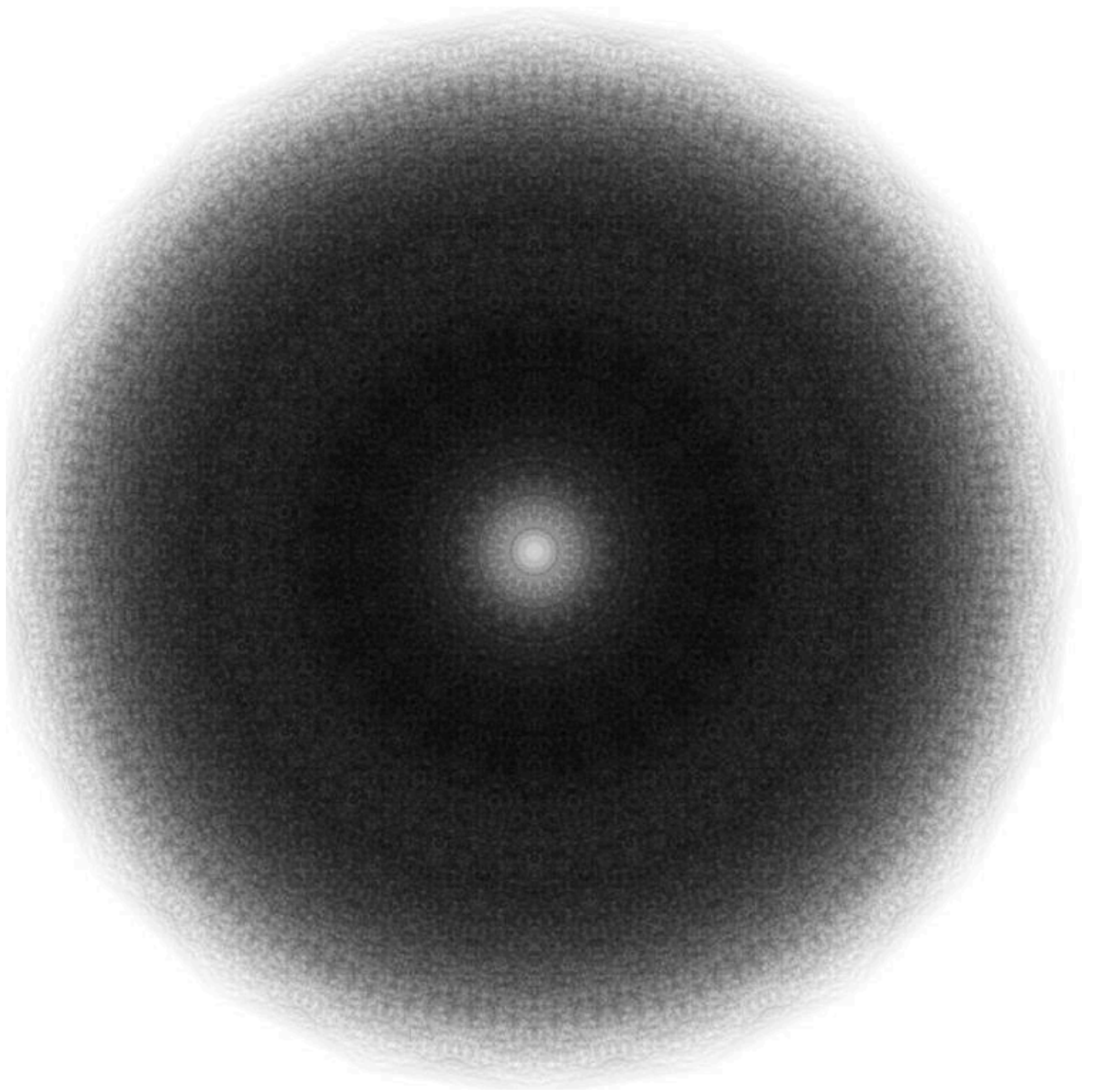
It is necessary to take into account that the pattern was designed for a frequency of 28 GHz and the corresponding power, which is just one fragment of the huge number of wave fronts of different frequency ranges that are in the medium and interact with the pattern.

Thus, when an Aires C2oS5G resonator interacts with broadband electromagnetic radiation of various frequencies in real conditions, its transition to a quantum form can occur extremely quickly, perhaps even simultaneously, which opens up very broad possibilities for using this effect in various fields of application.

## BIBLIOGRAPHY

- A. Jukna Studies of the prototype of the converter-resonator of electromagnetic radiation, Stage report, Vilnius, 2016.
- I.N. Serov, A.V. Kopyltsov, K.A. Korshunov, I.A. Soltovskaya, G.N. Lukyanov Calculation of electric field strength given background electromagnetic radiation's interaction with the AIRES C8 resonator (microprocessor), 2017.
- I. Serov, K. Korshunov, I. Soltovskaya, T. Shamko R&D: Calculation of the strength and intensity of the electromagnetic field in the interaction of electromagnetic radiation at a frequency of 2.4 GHz (WiFi) with an Aires K8 resonator (microprocessor), which is used in the Aires Shield Extreme (2016 model), 2018.
- I. Serov, K. Korshunov, I. Soltovskaya, T. Shamko, A.V. Kopyltsov, A. Jukna R&D: Calculation of the strength and intensity of the electromagnetic field in the interaction of electromagnetic radiation at a frequency of 2.4 GHz (WiFi) with an Aires C16S resonator (microprocessor), which is used in the Aires Shield Pro (2018 model), 2018.
- I. Serov, K. Korshunov, I. Soltovskaya, T. Shamko, A.V. Kopyltsov, A. Jukna R&D: Calculation of the strength and intensity of the electromagnetic field in the interaction of electromagnetic radiation at a frequency of 2.4 GHz (WiFi) with an Aires C28S resonator (microprocessor), which is used in the Aires Defender Pro (2018 model), 2018.
- I. Serov, K. Korshunov, I. Soltovskaya, T. Shamko, A.V. Kopyltsov, A. Jukna R&D: Calculation of the strength and intensity of the electromagnetic field in the interaction of electromagnetic radiation at a frequency of 2.4 GHz (WiFi) with an Aires C32S resonator (microprocessor), which is used in the Aires Guardian (2018 model), 2018.
- I. Serov, K. Korshunov, I. Soltovskaya, T. Shamko, A.V. Kopyltsov, A. Jukna R&D: Calculation of the strength and intensity of the electromagnetic field in the interaction of electromagnetic radiation at a frequency of 6 GHz (WiFi 5G) with an Aires C20S5G resonator (microprocessor), which is used in the Aires Crystal (2019 model), 2018.

## TOPOLOGY OF THE RESONATOR (MICROPROCESSOR) AIRES C20S5G



## Appendix 2

### HARDWARE AND SOFTWARE

#### Hardware:

Server: Supermicro CSE-733TQ-665B  
Processor: Intel Xeon E5-2620 v2 2.1 GHz (6-core) x 2.  
RAM: Kingston DDR3-1600 MHz, 96 GB  
Video card: ASUS GeForce GT 740

#### Software:

[PascalABC.NET](#) v.3.3  
MATHLAB R2015b

## Appendix 3

## ANIMATION

The dynamics of the computer simulation process can be viewed here: <https://yadi.sk/i/9C-9TmISzu87bQ> .